

Calibration Strategies for Robust Causal Estimation: Theoretical and Empirical Insights on Propensity Score Based Estimators

Jan Rabenseifner^{1,2,†}, Sven Klaassen^{2,1}, Jannis Kueck³, and Philipp Bach¹

¹University of Hamburg, Germany

²Economic AI, Germany

³Heinrich Heine University Düsseldorf, Düsseldorf Institute for Competition Economics, Germany

April 2, 2025

Abstract

The partitioning of data for estimation and calibration critically impacts the performance of propensity score based estimators like inverse probability weighting (IPW) and double/debiased machine learning (DML) frameworks. We extend recent advances in calibration techniques for propensity score estimation, improving the robustness of propensity scores in challenging settings such as limited overlap, small sample sizes, or unbalanced data. Our contributions are twofold: First, we provide a theoretical analysis of the properties of calibrated estimators in the context of DML. To this end, we refine existing calibration frameworks for propensity score models, with a particular emphasis on the role of sample-splitting schemes in ensuring valid causal inference. Second, through extensive simulations, we show that calibration reduces variance of inverse-based propensity score estimators while also mitigating bias in IPW, even in small-sample regimes. Notably, calibration improves stability for flexible learners (e.g., gradient boosting) while preserving the doubly robust properties of DML. A key insight is that, even when methods perform well without calibration, incorporating a calibration step does not degrade performance, provided that an appropriate sample-splitting approach is chosen.

1 Introduction

1.1 Motivation

In many settings of the causal inference literature, researchers are interested in the effect of a (binary) treatment $D \in \{0,1\}$ on an outcome $Y \in \mathbb{R}$. If the treatment is not assigned randomly, a common assumption is the so-called unconfoundedness assumption

$$Y(0), Y(1) \perp D \mid X$$

† Corresponding author email: jan.rabenseifner@uni-hamburg.de

assuming that the potential outcomes $Y(1)$ and $Y(0)$ are independent of the actual treatment status D conditional on control variables X . Let

$$m_0(x) := P(D = 1|X = x) = \mathbb{E}[D|X = x]. \quad (1)$$

be the propensity score. As famously shown in [Rosenbaum and Rubin \(1983\)](#) conditioning on the propensity score is sufficient to effectively account for the confounding through X

$$Y(0), Y(1) \perp D \mid m_0(X).$$

Consequently, propensity scores are a cornerstone of modern causal inference for addressing confounding in observational studies. They enable balancing treatment and control groups, allowing for unbiased estimation of treatment effects under unconfoundedness. Commonly, propensity scores are used in methods such as inverse probability weighting (IPW), matching, stratification, Bayesian causal inference and more recently double machine learning (DML). Moreover, effective propensity adjustment requires sufficient overlap for propensity score-based estimators. When overlap between treatment and control groups is limited, or treatment assignment is unbalanced, propensity scores can become extreme (i.e. close to 0 or 1) leading to instability of the causal estimates. In such cases, estimators can suffer from inflated variance as extreme weights in IPW disproportionately amplify small errors in propensity score estimation. Similarly, matching algorithms may struggle to find suitable matches, resulting in biased estimates. These challenges highlight the importance of robust and well-calibrated propensity score models to maintain the reliability of causal estimates.

To mitigate instability, researchers often enforce common support by trimming or bounding propensity scores. For example, observations with propensity scores below a certain threshold or outside a predefined range are excluded from analysis. While this approach can reduce variance, it does so at the expense of bias, as it discards valuable information and reduces sample size. Such trade-offs are particularly problematic in small-sample settings, where the exclusion of even a few observations can significantly impact the precision and validity of treatment effect estimates.

To use the propensity score for balancing, the property

$$m_0(X) = \mathbb{E}[D|m_0(X)] \quad (2)$$

is crucial, e.g. see Theorem 2 in [Rosenbaum and Rubin \(1983\)](#). In the classification literature, Equation (2) is known as the so-called calibration property.¹ Intuitively, a (binary) classifier $\hat{m}(\cdot)$ is well calibrated if the percentage of positive labels ($D = 1$) is approximately m for all instances with $\hat{m}(X) \approx m$. As the true propensity score is the conditional expectation it is calibrated

$$\begin{aligned} m_0(X) &= \mathbb{E}[D|X] \\ &= \mathbb{E}[\mathbb{E}[D|X]|\mathbb{E}[D|X]] \quad (\sigma(\mathbb{E}[D|X]) \subseteq \sigma(X)) \\ &= \mathbb{E}[D|m_0(X)]. \quad P\text{-a.s.} \end{aligned}$$

¹To be precise, this notion of calibration is also referred to as conditional calibration, which is equivalent to probabilistic calibration for binary outcomes ([Gneiting and Ranjan, 2011](#)).

In most settings the true propensity score is not known such that it is typically estimated via some classification algorithm such as logistic regression, random forest, boosting methods or even deep neural networks. Consequently, the resulting estimator $\hat{m}(\cdot)$ of $m_0(\cdot)$ might not be calibrated, e.g. the percentage of treated units with $\hat{m}(X) \approx m$ might differ substantially from m for certain values of $m \in (0, 1)$.

Early work by [Zadrozny and Elkan \(2001\)](#) demonstrates that decision tree-based models can exhibit high bias as they aim for uniformity in their leaves, which shifts observed frequencies toward extreme values. These models also face high variance when leaves rely on small training samples. Predicting overconfident propensity scores close to 0 or 1 blows up the weights of inverse propensity based estimators leading to unstable treatment effect estimation. This holds especially true for boosting algorithms ([Błasiok et al., 2023](#)). Bagging or random forest that average predictions from a base set of learners struggle to predict values near 0 and 1, due to variance in the underlying base learners ([Niculescu-Mizil and Caruana, 2005](#)). [Błasiok et al. \(2023\)](#) show that logistic regression, which is often considered well-calibrated ([Niculescu-Mizil and Caruana, 2005](#); [Johansson et al., 2023](#); [Pedregosa et al., 2018](#)), can also be affected by poor calibration through the linear form restriction. [Bai et al. \(2021\)](#) show that even when logistic regression is correctly specified, it remains inherently overconfident, indicating that calibration error is intrinsic to the model. The calibration error decreases as the sample size grows relative to the number of parameters, but the overconfidence effect persists. This highlights that propensity scores are often not well calibrated, such that the estimated treatment probabilities may not be reliable across subgroups. Even though theoretical and simulation-based studies address the topic of poor calibration, it is often not addressed transparently in applied causal analysis.

Accurately estimating treatment probabilities is crucial for valid causal inference. Inverse propensity score estimators aim to balance covariates between treatment and control groups. This balancing ensures more reliable and unbiased treatment effect estimates by aligning the covariate distributions, improving the comparability of the treatment groups in terms of observable characteristics. Whereas methods like isotonic regression and Platt scaling refer to the calibration of predictions, critical questions remain about the optimal integration of these calibration techniques in causal estimation workflows.

1.2 Related Literature

Recent advances in calibration for propensity score estimation and causal inference emphasize three interconnected themes: the adaptation of machine learning calibration techniques to causal settings, stabilization strategies for inverse probability weighting (IPW), and theoretical insights into finite-sample performance. Initial studies by [Deshpande and Kuleshov \(2023\)](#) showed significant improvements using single split calibration on data with deterministic treatment assignments and complex settings with hidden confounders. They specifically highlight variance reduction properties and analyze the regret of recalibration of propensity scores. Their proofs are independent of the sample size N , as their calibration framework consists of splitting the data into training and calibration sets. This distinction is crucial for our work, as we focus on sample size dependent calibration algorithms.

[Gutman et al. \(2024\)](#) demonstrated that post-processing propensity scores using methods such as Platt scaling, referred to as post-calibration, improves treatment effect estima-

tion by correcting propensity score distortions beyond covariate balancing. Calibration significantly benefits miscalibrated models like tree-based methods (e.g. gradient boosting), while logistic regression, contrary to the findings of [Deshpande and Kuleshov \(2023\)](#), shows minimal gains. This suggests that post-calibration allows flexible learners to retain their predictive accuracy while enhancing robustness to data challenges such as small sample sizes, model misspecification, class imbalance, or limited overlap, thus challenging the conventional trade-off between model complexity and calibration. [Ballinari and Bearth \(2025\)](#) use nested cross-fitting, reserving distinct data folds for propensity estimation and calibration, which is a straightforward application of the double machine learning theory of [Chernozhukov et al. \(2018\)](#). They reported instability in small samples, a limitation attributed to reduced effective sample sizes for both steps. These studies collectively identify a tension between calibration flexibility and stability, particularly in finite-sample regimes. Efforts to address these challenges have taken different paths. For instance, [van der Laan et al. \(2024a\)](#) proposed a stratified calibration for treated and control groups to stabilize IPW weights. In another work, they extended calibration frameworks to estimate heterogeneous treatment effects ([van der Laan et al., 2023](#)). Meanwhile, [van der Laan et al. \(2024b\)](#) extend automatic debiased machine learning (autoDML) ([Chernozhukov et al., 2022, 2024](#)) by calibrating both outcome regression and Riesz representer. They demonstrate that the calibration step yields doubly robust asymptotically linear estimators, reducing nuisance rate requirements.

Theoretical work by [Gamarnik \(1998\)](#), [Mammen and Yu \(2007\)](#) and [Wüthrich and Ziegel \(2023\)](#) established consistency guarantees for isotonic regression, but practical implementations often struggle with convergence rates in small samples, as shown by [Yang and Barber \(2019\)](#). Furthermore, [Yang and Barber \(2019\)](#) established that isotonic projection is non-contractive under the ℓ_∞ norm, exacerbating edge instability in propensity score estimates. This theoretical insight justifies the empirical requirement of clipping extreme probabilities, which explains the unstable treatment effect estimates in [Ballinari and Bearth \(2025\)](#) using isotonic regression under limited overlap.

This paper systematically evaluates how calibration performance depends on data partitioning for propensity estimation and calibration. While existing studies fix specific splitting strategies (e.g., single-split or nested cross-fitting), we show that the choice of partitioning interacts critically with sample size, clipping thresholds, and complexity of the data generating process. For instance, [van der Laan et al. \(2024a\)](#) suggest calibration on the full-sample, which avoids reserving data exclusively for calibration. This approach can mitigate instability without sacrificing theoretical guarantees, a hypothesis we test across multiple data-generating processes (DGP). Similarly, we reconcile the debates about stratified versus pooled calibration by demonstrating that efficient reuse of cross-fitted propensity scores obviates the need for group-specific adjustments in many settings. Further, beyond the work of [Ballinari and Bearth \(2025\)](#), we provide a theoretical extension of the double machine learning theory to allow for different sample-splitting schemes. By synthesizing these insights, our work clarifies when and how calibration improves ATE estimation, providing a bridge between theoretical calibration properties and practical implementation challenges.

Plan of the Paper. The rest of the paper is organized as follows. Section 2 introduces propensity score calibration, highlighting different approaches and providing details on the

properties of isotonic regression. Section 3 proposes calibration algorithms for estimating the average treatment effect and establishes theoretical guarantees under double machine learning (DML), including convergence rates and asymptotic normality. Section 4 demonstrates robustness through simulations across diverse and challenging data-generating processes. Proofs of the theorems can be found in Appendix A, while implementation details for reproducibility, extended simulation results and sensitivity analyses are available in Appendices B and C.

2 Propensity Score Calibration

Let $D \in \{0, 1\}$ be a binary treatment variable with covariates $X \in \mathcal{X} \subseteq \mathbb{R}^d$. The propensity score is defined as

$$m_0(x) := P(D = 1|X = x) = \mathbb{E}[D|X = x].$$

As the propensity score is a conditional expectation it is calibrated

$$m_0(X) = \mathbb{E}[D|m_0(X)]$$

The goal is to achieve a similar balancing property of an estimated version of $m_0(X)$. Given an estimate $\hat{m}(X)$ of $m_0(X)$, we consider popular calibration methods such as isotonic regression. Generally, we consider calibration procedures based on the pseudo-sample

$$((D_1, \hat{m}(X_1)), \dots, (D_N, \hat{m}(X_N))).$$

The calibration algorithm approximates $\mathbb{E}[D|\hat{m}(X)]$ which typically differs from $\mathbb{E}[D|m_0(X)]$. In the following, we denote the calibrated propensity score by

$$\begin{aligned} \tilde{m} : \mathcal{X} &\rightarrow [0, 1] \\ x &\mapsto \tilde{m}(x) \end{aligned}$$

2.1 Rate Comparison $\hat{m}(\cdot)$ and $\tilde{m}(\cdot)$

At first, we will consider the effect of the calibration procedure on the convergence rate and compare $\hat{m}(\cdot)$ and $\tilde{m}(\cdot)$ with respect to $m_0(\cdot)$. For any estimate $\hat{m}(\cdot)$ of $m_0(\cdot)$ the mean-squared-error can be decomposed

$$\|\hat{m}(X) - m_0(X)\|_{p,2} = (\mathbb{E} [\text{Var}(m_0(X)|\hat{m}(X))] + \|\mathbb{E}[m_0(X)|\hat{m}(X)] - \hat{m}(X)\|_{p,2}^2)^{1/2}. \quad (3)$$

Here, the first term denotes the expected precision of $\hat{m}(\cdot)$, whereas the second term can be interpreted as the calibration error. Calibration procedures, which minimize the mean square error in the pseudo-sample, approximate $\mathbb{E}[D|\hat{m}(X)]$, reducing the calibration error. The following assumption bounds the root-mean-squared-error of the calibrated function $\tilde{m}(\cdot)$.

Assumption 1. Let $\tilde{m}(X)$ be an estimator of $\tilde{m}_0(X) := \mathbb{E}[D|\hat{m}(X)]$ with

$$\|\tilde{m}(X) - \tilde{m}_0(X)\|_{P,2} \leq \tilde{\epsilon}_N.$$

Lemma 1. Under Assumption 1 it holds

$$\|\tilde{m}(X) - m_0(X)\|_{P,2} \leq \left(\mathbb{E}[\text{Var}(m_0(X)|\hat{m}(X))]\right)^{1/2} + \tilde{\epsilon}_N. \quad (4)$$

Comparing Equations (3) and (4) highlights the difference in rates. When the calibration error $\|\mathbb{E}[m_0(X)|\hat{m}(X)] - \hat{m}(X)\|_{P,2}^2$ is the dominant term, the estimation rate can be improved, if for example

$$\tilde{\epsilon}_N = o(\|\mathbb{E}[m_0(X)|\hat{m}(X)] - \hat{m}(X)\|_{P,2}).$$

This can become specifically relevant in the double machine learning approach. In standard double machine learning settings, the required estimation rate of the propensity score is often assumed to be

$$\|\hat{m}(X) - m_0(X)\|_{P,2} = o(N^{-1/4}).$$

Consequently, if $\tilde{\epsilon}_N = o(N^{-1/4})$, the rate requirement is also satisfied for $\tilde{m}(\cdot)$ where the rate can be even improved if $\tilde{\epsilon}_N$ converges faster towards zero.

2.2 Calibration Methods

Model calibration has roots in meteorological forecasting to address reliability in probabilistic weather predictions (Toth et al., 2006; Dawid, 2014; Gneiting, 2014). Calibration is often achieved via post-hoc point calibrators that transform $\hat{m}(X)$ into $f(\hat{m}(X))$, balancing two aims: (1) calibration validity, and (2) preservation of predictive sharpness (i.e., $f \circ \hat{m}(X)$ approximates \hat{m} 's discriminative power) (Gneiting et al., 2007; Gupta et al., 2020). Common approaches include parametric methods like Platt scaling, which fits a logistic sigmoid to $f(X)$ (Platt, 1999; COX, 1958); non-parametric methods such as histogram binning, partitioning predictions into fixed intervals (Zadrozny and Elkan, 2001; Gupta and Ramdas, 2021), and isotonic regression, learning a monotonic transform via empirical risk minimization (Zadrozny and Elkan, 2002; Barlow and Brunk, 1972); as well as conformal methods like Venn-Abers predictors, refining calibration through cross-conformal inference (Vovk and Petej, 2014). Isotonic calibration, while distribution-free and tuning parameter-free, achieves asymptotic guarantees with $O_P(N^{-1/3})$ convergence (Zhang, 2002; van der Laan et al., 2023). In contrast, histogram binning requires explicit bin specification and trades flexibility for finite-sample validity (Gupta and Ramdas, 2021). We focus on three common calibration methods, noting that calibration is an active area of research with potential for improvements and new proposals that require further simulation testing.

2.2.1 Isotonic Regression

Isotonic regression is a popular method to calibrate predictions.

Definition 1. Given an estimate $\hat{m}(\cdot)$ of the propensity score, perform an isotonic regression as

$$f = \arg \min_{f \in \mathcal{F}_{\text{iso}}} \sum_{i=1}^N (D_i - (f \circ \hat{m})(X_i))^2$$

with \mathcal{F}_{iso} being the set of non-decreasing functions. The calibrated propensity score is then given by

$$\tilde{m} = f \circ \hat{m}.$$

Especially, the in-sample calibration property

$$\mathbb{E}_n[D|\tilde{m}(X_i)] = \tilde{m}(X_i)$$

for $i \in \{1, \dots, N\}$, seems to be desirable (e.g. [Wüthrich and Ziegel \(2023\)](#)). We consider an estimated propensity score $\hat{m}(\cdot)$ based on a separate sample such that $\hat{m}(\cdot)$ can be considered a fixed function. Let $U := \hat{m}(X)$ and define the pseudo sample as $Z := (D, U)$, where $(Z_i)_{i=1}^N$ are iid. copies of Z . Consider the following assumption

Assumption 2. *The regression function*

$$\tilde{m}_0(u) := \mathbb{E}[D|U = u]$$

is monotone.

Remark 1. *Assumption 2 is substantially weaker than requiring monotonicity in the original covariates X , intuitively only requiring the preliminary propensity score $\hat{m}(\cdot)$ to be monotone "on average". When $\hat{m}(\cdot)$ is not injective, distinct values of X may map to the same U , allowing $\tilde{m}_0(U)$ to average over these X values. This aggregation can smooth out non-monotonic behavior in X , making monotonicity in U easier to satisfy. However, if $\hat{m}(\cdot)$ is bijective, each U uniquely determines X , and monotonicity of $\tilde{m}_0(U)$ becomes equivalent to monotonicity of $\mathbb{E}[D|X = x]$ using the reparameterization $u = \hat{m}(x)$.*

Define \tilde{m} as the estimator obtained by isotonic regression on the sample $(Z_i)_{i=1}^N$.

Lemma 2 (Convergence of Isotonic Regression). *Under Assumption 2, the isotonic regression estimator \tilde{m} satisfies:*

$$\|\tilde{m}(U) - \tilde{m}_0(U)\|_{P,2} = O_P(N^{-1/3}).$$

The rate follows from the bracketing entropy bound in Theorem 2.7.5 of [Vaart and Wellner \(2023\)](#) for monotonic functions. Relying on Lemma 3.4.3 of [Vaart and Wellner \(2023\)](#) gives the desired rate as mentioned in the corresponding Section 3.4.3.2. Earlier work by [Birman and Solomjak \(1967\)](#) and [Geer \(2000\)](#) established foundational approximation and entropy arguments, extended to additive isotonic regression in [Mammen and Yu \(2007\)](#). For detailed convergence properties see e.g. [Zhang \(2002\)](#).

Notably, similar convergence rates hold in settings where the data is not strictly i.i.d., such as when using sample splitting or cross-fitting to estimate $\hat{m}(\cdot)$. Theorem 2 in [van der Laan et al. \(2024a\)](#) demonstrates that under cross-fitting regimes, where $\hat{m}(\cdot)$ is trained on an independent sample and applied to the estimation sample, the pseudo-sample Z is still

sufficiently weakly dependent for the $O_P(N^{-1/3})$ rate to hold. This aligns with the mean squared error (MSE) decomposition in (3), where the $O_P(N^{-1/3})$ $L_2(P)$ convergence rate of isotonic regression (Lemma 2) ensures that the calibration error term $\|\mathbb{E}[m_0(X)|\hat{m}(X)] - \hat{m}(X)\|_{p,2}^2$ decays as $O_P(N^{-2/3})$. Theorem 1 in van der Laan et al. (2024a) further establishes distribution-free calibration guarantees, bounding the calibration error by $O_P(N^{-2/3})$, irrespective of the smoothness of the inverse propensity score or the dimension of the covariates. Together, these results accommodate the calibration algorithms introduced in Section 3.

2.2.2 Venn-Abers Calibration

Venn-Abers predictors (VAPs) (Vovk et al., 2004) provide calibrated probability estimates by considering both possible labels for a test instance and fitting separate isotonic regressions for each case. For binary outcomes (Vovk and Petej, 2014) $D \in \{0, 1\}$, VAPs assign each test unit X_{l+1} two probabilities: $\tilde{m}_0(W)$ and $\tilde{m}_1(W)$, derived from isotonic regression under the assumed labels $D_{l+1} = 0$ and $D_{l+1} = 1$. These estimates are oracle calibrated—the true label’s corresponding probability is valid. While aligning one probability distribution with the true outcome ensures accurate calibration, the “oracle” selector $S = D$ is not known in practice. This means we often need to use heuristic methods, like averaging, to combine information, even though these methods do not come with formal guarantees. Computational expense also arises from refitting isotonic models per test instance.

Inductive Venn-Abers predictors (IVAPs) (Lambrou et al., 2012; Nouretdinov et al., 2018) address these issues by splitting data into a proper training set (to fit a propensity model $\hat{m}(X)$) and a calibration set (to fit isotonic maps \tilde{m}_0, \tilde{m}_1). For square loss, IVAPs combine $p_0 = \tilde{m}_0(\hat{m}(X))$ and $p_1 = \tilde{m}_1(\hat{m}(X))$ into a single probability:

$$p = p_1 + \frac{p_0^2}{2} - \frac{p_1^2}{2}.$$

As Vovk and Petej (2014) point out, this can be rewritten as:

$$p = \bar{p} + (p_1 - p_0) \left(\frac{1}{2} - \bar{p} \right), \quad \bar{p} = \frac{p_0 + p_1}{2}.$$

Thus, p is a regularized version of \bar{p} moving the prediction towards $\frac{1}{2}$. This characteristic is particularly advantageous in mitigating the risk of inflated weights during treatment effect estimation.

2.2.3 Platt Scaling

Platt scaling (Platt, 1999) leverages the robust calibration properties of log-loss. It applies logistic regression, expressed by the function

$$f(\hat{m}(X)) := \frac{1}{1 + \exp(A\hat{m}(X) + B)},$$

to the scores produced by an estimator, using treatment assignment labels as targets for calibration, where $A < 0$ and B are parameters. The parameters A and B are estimated

using a maximum likelihood method on the same training set as the original classifier $m(x)$. To avoid overfitting, a held-out calibration set or cross-validation can be used. Platt also recommends clipping the outputs d to target probabilities in the range

$$\left(\frac{1}{N_0 + 2}, \frac{N_1 + 1}{N_1 + 2} \right),$$

where N_0 is the number of control units and N_1 is the number of treated units in the calibration set. This motivates the testing of additional clipping in small sample sizes, a setting where the parametric form assumption is especially appropriate. Unlike isotonic regression, for which [van der Laan et al. \(2023\)](#) established distribution-free calibration guarantees, Platt scaling lacks universal theoretical guarantees. This limitation is critical in propensity calibration, where treatment assignments can be unbalanced, or propensity scores deviate from logistic normality (e.g., highly skewed or multimodal distributions). Empirical studies further challenge its reliability: [Kumar et al. \(2019\)](#) show that Platt scaling’s apparent calibration is often inflated due to the systematic underestimation of errors in continuous output spaces, where true calibration cannot be verified without uncheckable smoothness assumptions. Recent work by [Li and Sur \(2025\)](#) identifies specific conditions - notably Gaussian-like or light-tailed feature distributions - under which Platt scaling achieves Bregman optimality, minimizing divergences such as log loss or squared error, even in high-dimensional settings.

3 Calibration for Double Machine Learning

The following section combines calibration and double machine learning. The first part focuses on high-level conditions for different double machine learning algorithms, whereas the second part states explicit conditions for particular double machine learning models with isotonic regression.

3.1 Double Machine Learning Theory and Algorithms

In this section, we state conditions which enable a re-estimation step for nuisance estimators in the double machine learning framework if the complexity of the re-estimation procedure is not too large. As in [Chernozhukov et al. \(2018\)](#) we denote $\theta_0 \in \Theta \subset \mathbb{R}$ the parameter of interest. The leading example is the average treatment effect (ATE)

$$\theta_0 = \mathbb{E}[Y(1) - Y(0)].$$

Further, we assume that θ_0 satisfies the moment condition,

$$\mathbb{E}_P[\psi(W; \theta_0, \eta_0)] = 0, \tag{5}$$

where ψ is a known score function, the data W is a random element in $(\mathcal{W}, \mathcal{A}_W)$ with probability measure $P \in \mathcal{P}_N$ and η_0 is the true value of the nuisance parameter $\eta \in T$, where T is the convex subset of a normed vector space with norm $\|\cdot\|_T$.

The previous setting describes the standard double machine learning framework introduced in [Chernozhukov et al. \(2018\)](#). For simplicity, we restrict ourselves to the case of linear score

functions, that is

$$\psi(w; \theta, \eta) = \psi^a(w; \eta)\theta + \psi^b(w; \eta), \quad (6)$$

for all $w \in \mathcal{W}$, $\theta \in \Theta$ and $\eta \in T$. Further, since we would like to consider a scenario with a re-estimation or calibration step, which might not affect all nuisance parameters, we define

$$\eta_0 = (\eta_0^{(1)}, \eta_0^{(2)}),$$

where $\eta_0^{(2)}$ should be re-estimated as for example when $\eta_0^{(2)}$ is a propensity score to be calibrated. Correspondingly define $T = T^{(1)} \times T^{(2)}$.

Algorithm 1 recaps the standard version of the double machine learning algorithm based on cross-fitting (cf. Definition 3.2 in Chernozhukov et al. (2018)).

Let $(W_i)_{i=1}^N$ be iid. copies of W with probability measure P . To simplify notation, assume that N is divisible by K .

Algorithm 1 (uncalibrated) DML 2 Algorithm

- 1: **Input:** Data $(W_i)_{i=1}^N$. A K -fold random partition $(I_k)_{k=1}^K$ of $[N] = \{1, \dots, N\}$ such that each fold I_k is of size $n = N/K$. For each $k \in [K] = \{1, \dots, K\}$, define $I_k^c := \{1, \dots, N\} \setminus I_k$.
- 2: For each $k \in [K]$, fit a machine learning estimator

$$\hat{\eta}_{0,k} = \hat{\eta}_0((W_i)_{i \in I_k^c})$$

of η_0 , where $\hat{\eta}_{0,k}$ is a random element in T , where the randomness only depends on the $(W_i)_{i \in I_k^c}$.

- 3: Construct the estimator $\hat{\theta}_0$ as the solution to

$$\frac{1}{K} \sum_{k=1}^K \mathbb{E}_{n,k}[\psi(W; \hat{\theta}_0, \hat{\eta}_{0,k})] = 0,$$

where $\mathbb{E}_{n,k}[\psi(W)] = n^{-1} \sum_{i \in I_k} \psi(W_i)$ is the empirical expectation over $(W_i)_{i \in I_k}$.

The standard DML 2 algorithm employs cross-fitting to handle the complexity of the estimated nuisance elements $\hat{\eta}_{0,k}$.

Remark 2. Theorem 3.1 in Chernozhukov et al. (2018) shows that the estimator according to Algorithm 1 is asymptotically normally distributed. More specifically, it holds

$$\sqrt{N}\sigma^{-1}(\hat{\theta}_0 - \theta_0) = \frac{1}{N} \sum_{i=1}^N \bar{\psi}(W_i) + O_P(\rho_N) \rightsquigarrow \mathcal{N}(0, 1) \quad (7)$$

uniformly over $P \in \mathcal{P}_N$, where the size of the remainder term obeys

$$\rho_N := N^{-1/2} + r_N + r'_N + N^{1/2}\lambda_N + N^{1/2}\lambda'_N \lesssim \delta_N$$

with $\delta_N \geq N^{-1/2}$. Here, $\bar{\psi}(\cdot) := \sigma^{-1}J_0^{-1}\psi(\cdot; \theta_0, \eta_0)$ is the influence function and the approximate

variance is

$$\sigma^2 := J_0^{-2} \mathbb{E}_P[\psi(W; \theta_0, \eta_0)^2].$$

In Remark 2 it is assumed that $\hat{\eta}_{0,k} = (\hat{\eta}_{0,k}^{(1)}, \hat{\eta}_{0,k}^{(2)}) \in \mathcal{T}_N$ with probability $1 - o(1)$, where \mathcal{T}_N is a suitable nuisance realization set. To enable the re-estimation of nuisance elements $\hat{\eta}_{0,k}^{(2)}$ the algorithm and the nuisance realization set \mathcal{T}_N has to be slightly adapted. A simple and straightforward adaption is presented in Algorithm 2.

Algorithm 2 (nested K -fold cross-fitting calibration) DML 2 Algorithm

- 1: **Input:** Data $(W_i)_{i=1}^N$. A K -fold random partition $(I_k)_{k=1}^K$ of $[N] = \{1, \dots, N\}$ such that each fold I_k is of size $n = N/K$. For each $k \in [K] = \{1, \dots, K\}$ define $I_k^c := \{1, \dots, N\} \setminus I_k$.
- 2: For each $k \in [K]$, fit a machine learning estimator

$$\hat{\eta}_{0,k}^{(1)} = \hat{\eta}_0^{(1)}((W_i)_{i \in I_k^c})$$

of $\eta_0^{(1)}$, where $\hat{\eta}_0^{(1)}$ is a random element in $T^{(1)}$, where the randomness only depends on the $(W_i)_{i \in I_k^c}$.

- 3: For each $k \in [K]$, split the training partition I_k^c into two disjoint samples $I_{k,1}^c$ and $I_{k,2}^c$.
- 4: Use the first subset $I_{k,1}^c$ to fit a machine learning estimator

$$\hat{\eta}_{0,k}^{(2)} = \hat{\eta}_0^{(2)}((W_i)_{i \in I_{k,1}^c})$$

of $\eta_0^{(2)}$, where $\hat{\eta}_0^{(2)}$ is a random element in $T^{(2)}$, where the randomness only depends on the $(W_i)_{i \in I_{k,1}^c}$.

- 5: Use the second subset $I_{k,2}^c$ and the estimated nuisance element $\hat{\eta}_{0,k}^{(2)}$ to fit a re-estimation procedure

$$\tilde{\eta}_{0,k}^{(2)} = \tilde{\eta}_0^{(2)}((W_i)_{i \in I_{k,2}^c}, \hat{\eta}_{0,k}^{(2)})$$

of $\eta_0^{(2)}$, where $\tilde{\eta}_0^{(2)}$ is a random element in $T^{(2)}$, where the randomness only depends on the $(W_i)_{i \in I_k^c}$.

- 6: Construct the estimator $\tilde{\theta}_0$ as the solution to

$$\frac{1}{K} \sum_{k=1}^K \mathbb{E}_{n,k}[\psi(W; \tilde{\theta}_0, (\hat{\eta}_{0,k}^{(1)}, \tilde{\eta}_{0,k}^{(2)}))] = 0,$$

where $\mathbb{E}_{n,k}[\psi(W)] = n^{-1} \sum_{i \in I_k} \psi(W_i)$ is the empirical expectation over $(W_i)_{i \in I_k}$.

As already mentioned, the standard double machine learning procedure in Algorithm 1 uses cross-fitting to handle the complexity of estimated nuisance elements $\hat{\eta}_{0,k}$. Algorithm 2 is a straightforward extension, which leaves the cross-fitting unchanged. The approach just employs a nested sample splitting procedure, such that the calibrated nuisance elements $\tilde{\eta}_{0,k}^{(2)}$ still depend only on the observations of the training sample $(W_i)_{i \in I_k^c}$. As a consequence, only the predictive performance of the calibrated nuisance estimators must be ensured.

Remark 3. Let $\tilde{\theta}_0$ be the estimator according to Algorithm 2. Under the assumptions in Theorem 3.1 in Chernozhukov et al. (2018), Equation (7) in Remark 2 holds analogously for $\tilde{\theta}_0$.

Typically, Assumption 3.2 in Theorem 3.1 in Chernozhukov et al. (2018) requires high-

quality nuisance estimators. In particular, the re-estimation procedure (calibration) has to converge sufficiently fast, i.e.

$$\|\tilde{\eta}_{0,k}^{(2)} - \eta_0^{(2)}\|_{P,2} \lesssim \varepsilon_N = o(N^{-1/4}).$$

Since calibration properties are most important for small samples, further splitting of the training sample for calibration might not be desirable.

Therefore, we state Assumptions 3.1 and 3.2 of Chernozhukov et al. (2018) for an adapted nuisance realization set $\tilde{\mathcal{T}}_N$. It is worth noting that in the following assumption the calibrated nuisance elements $\tilde{\eta}_0^{(2)}((W_i)_{i \in [N]})$ may depend on the full data. This allows us to introduce new estimation algorithms that rely on more sophisticated splitting rules for calibration.

Assumption 3. Let $c_0 > 0$, $c_1 > 0$, and $q \geq 2$ be some finite constants such that $c_0 \leq c_1$, and let $\{\delta_N\}_{N \geq 1}$ and $\{\Delta_N\}_{N \geq 1}$ be some sequences of positive constants converging to zero such that $\delta_N \geq N^{-1/2}$. Also, let $K \geq 2$ be some fixed integer, and let $\{\mathcal{P}_N\}_{N \geq 1}$ be some sequence of sets of probability distributions P of W on W .

Assumption 3.1 (Linear scores with approximate Neyman orthogonality) For all $N \geq 3$ and $P \in \mathcal{P}_N$, the following conditions hold:

- (a) The true parameter value θ_0 obeys (5).
- (b) The score ψ is linear in the sense of (6).
- (c) The map $\eta \mapsto E_P[\psi(W; \theta, \eta)]$ is twice continuously Gateaux-differentiable on T .
- (d) The score ψ obeys the Neyman orthogonality or, more generally, the Neyman λ_N near-orthogonality condition at (θ_0, η_0) with respect to the nuisance realization set $\tilde{\mathcal{T}}_N \subset T$ for

$$\lambda_N := \sup_{\eta \in \tilde{\mathcal{T}}_N} |\partial_\eta \mathbb{E}_P[\psi(W; \theta_0, \eta_0)][\eta - \eta_0]| \leq \delta_N N^{-1/2}.$$

- (e) The identification condition holds; namely, the singular values of the matrix

$$J_0 := \mathbb{E}_P[\psi^a(W; \eta_0)]$$

are between c_0 and c_1 .

Assumption 3.2 (Score regularity and quality of nuisance parameter estimators) For all $N \geq 3$ and $P \in \mathcal{P}_N$, the following conditions hold:

- (a) Given a random subset I of $[N]$ of size $n = N/K$, the nuisance parameter estimator $\tilde{\eta}_0 := (\hat{\eta}_0^{(1)}((W_i)_{i \in I}), \tilde{\eta}_0^{(2)}((W_i)_{i \in [N]}))$ belongs to the realization set $\tilde{\mathcal{T}}_N$ with probability at least $1 - \Delta_N$, where $\tilde{\mathcal{T}}_N = \tilde{\mathcal{T}}_N^{(1)} \times \tilde{\mathcal{T}}_N^{(2)}$ contains η_0 and is constrained by the following conditions.
- (b) The moment conditions hold:

$$m_N := \sup_{\eta \in \tilde{\mathcal{T}}_N} \mathbb{E}_P[|\psi(W; \theta_0, \eta)|^q]^{1/q} \leq c_1;$$

$$m'_N := \sup_{\eta \in \tilde{T}_N} \mathbb{E}_P[|\psi^a(W; \eta)|^q]^{1/q} \leq c_1.$$

(c) The following conditions on the statistical rates r_N , r'_N , and λ'_N hold:

$$r_N := \sup_{\eta \in \tilde{T}_N} |\mathbb{E}_P[\psi^a(W; \eta)] - \mathbb{E}_P[\psi^a(W; \eta_0)]| \leq \delta_N,$$

$$r'_N := \sup_{\eta^{(1)} \in \tilde{T}_N^{(1)}} \left(\mathbb{E}_P \left[\left(\psi(W; \theta_0, (\eta^{(1)}, \eta_0^{(2)})) - \psi(W; \theta_0, (\eta_0^{(1)}, \eta_0^{(2)})) \right)^2 \right] \right)^{1/2} \leq \delta_N,$$

$$\lambda'_N := \sup_{r \in (0,1), \eta \in \tilde{T}_N} |\partial_r^2 \mathbb{E}_P[\psi(W; \theta_0, \eta_0 + r(\eta - \eta_0))]| \leq \delta_N / \sqrt{N}.$$

(d) The variance of the score ψ is non-degenerate:

$$c_0 \leq \mathbb{E}_P[\psi(W; \theta_0, \eta_0)^2].$$

Indeed, if the calibration method is not too complex (see Assumption 4), for example when isotonic regression is used for calibration, the additional sample split in algorithm 2 can be avoided by calibrating the predictions on each “test”-fold I_k which are used to estimate the target parameter θ_0 . This procedure is described in Algorithm 3.

Algorithm 3 (k -fold cross-fitting calibration) DML 2 Algorithm

- 1: **Input:** Data $(W_i)_{i=1}^N$. A K -fold random partition $(I_k)_{k=1}^K$ of $[N] = \{1, \dots, N\}$ such that each fold I_k is of size $n = N/K$. For each $k \in [K] = \{1, \dots, K\}$ define $I_k^c := \{1, \dots, N\} \setminus I_k$.
- 2: For each $k \in [K]$, fit a machine learning estimator

$$\hat{\eta}_{0,k} = \hat{\eta}_0((W_i)_{i \in I_k^c})$$

of η_0 , where $\hat{\eta}_{0,k}$ is a random element in T , where the randomness only depends on the $(W_i)_{i \in I_k^c}$.

- 3: For each $k \in [K]$, rely on estimated nuisance element $\hat{\eta}_{0,k}^{(2)}$ to fit a re-estimation procedure

$$\tilde{\eta}_{0,k}^{(2)} = \tilde{\eta}_0^{(2)}((W_i)_{i \in I_k}, \hat{\eta}_{0,k}^{(2)})$$

of $\eta_0^{(2)}$, where $\tilde{\eta}_{0,k}^{(2)}$ is a random element in $T^{(2)}$.

- 4: Construct the estimator $\tilde{\theta}_0$ as the solution to

$$\frac{1}{K} \sum_{k=1}^K \mathbb{E}_{n,k} [\psi(W; \tilde{\theta}_0, (\hat{\eta}_{0,k}^{(1)}, \tilde{\eta}_{0,k}^{(2)}))] = 0,$$

where $\mathbb{E}_{n,k}[\psi(W)] = n^{-1} \sum_{i \in I_k} \psi(W_i)$ is the empirical expectation over $(W_i)_{i \in I_k}$.

Although the calibrated nuisance estimator depends on the full data in this case, we will show an analog result as in Theorem 3.1 in Chernozhukov et al. (2018) under the Assumptions 3 and 4 in Theorem 1. As a slight modification of Algorithm 3 one can use different K -fold cross-fitting procedures for the estimated nuisance elements. For example, 2-fold cross-fitting as described in Algorithm 4, uses half of the data for nuisance estimation and

the other half for calibration. Consequently, the calibration step might be more stable.

Algorithm 4 (single split cross-fitting calibration) DML 2 Algorithm

- 1: **Input:** Data $(W_i)_{i=1}^N$. A K -fold random partition $(I_k)_{k=1}^K$ of $[N] = \{1, \dots, N\}$ such that each fold I_k is of size $n = N/K$. A 2-fold random partition $\tilde{I}_1 \cup \tilde{I}_2 = \{1, \dots, N\}$ and $\tilde{I}_1 \cap \tilde{I}_2 = \emptyset$. For each $k \in [K] = \{1, \dots, K\}$ define $I_k^c := \{1, \dots, N\} \setminus I_k$ and for $j \in [2] = \{1, 2\}$ define $\tilde{I}_j^c := \{1, \dots, N\} \setminus \tilde{I}_j$.

- 2: For each $k \in [K]$, fit a machine learning estimator

$$\hat{\eta}_{0,k}^{(1)} = \hat{\eta}_0^{(1)}((W_i)_{i \in I_k^c})$$

of $\eta_0^{(1)}$, where $\hat{\eta}_0^{(1)}$ is a random element in $T^{(1)}$, where the randomness only depends on the $(W_i)_{i \in I_k^c}$.

- 3: For each $j \in [2]$, fit a machine learning estimator

$$\hat{\eta}_{0,j}^{(2)} = \hat{\eta}_0^{(2)}((W_i)_{i \in \tilde{I}_j^c})$$

of $\eta_0^{(2)}$, where $\hat{\eta}_0^{(2)}$ is a random element in $T^{(2)}$, where the randomness only depends on the $(W_i)_{i \in \tilde{I}_j^c}$.

- 4: For each $j \in [2]$, rely on estimated nuisance element $\hat{\eta}_{0,j}^{(2)}$ to fit a re-estimation procedure

$$\tilde{\eta}_{0,j}^{(2)} = \tilde{\eta}_0^{(2)}((W_i)_{i \in \tilde{I}_j}, \hat{\eta}_{0,j}^{(2)})$$

of $\eta_0^{(2)}$, where $\tilde{\eta}_0^{(2)}$ is a random element in $T^{(2)}$.

- 5: Construct the estimator $\tilde{\theta}_0$ as the solution to

$$\frac{1}{2K} \sum_{k=1}^K \sum_{j=1}^2 \mathbb{E}_{n,k,j}[\psi(W; \tilde{\theta}_0, (\hat{\eta}_{0,k}^{(1)}, \tilde{\eta}_{0,j}^{(2)}))] = 0,$$

where $\mathbb{E}_{n,k,j}[\psi(W)] = n^{-1} \sum_{i \in I_k \cap \tilde{I}_j} \psi(W_i)$ is the empirical expectation over $(W_i)_{i \in I_k \cap \tilde{I}_j}$.

Another option is to simultaneously calibrate all cross-fitted predictions $\hat{\eta}_0^{(2)}$ as described in Algorithm 5. The main difference between Algorithm 3 and 5 is the dependency structure of the data used to calibrate the nuisance elements. In Algorithm 3 the recalibration is fitted on i.i.d. samples conditional on the corresponding “training”-fold I_k^c , whereas in Algorithm 5 samples used for the calibration step have a complex dependency structure.

Algorithm 5 (full-sample calibration) DML 2 Algorithm

- 1: **Input:** Data $(W_i)_{i=1}^N$. A K -fold random partition $(I_k)_{k=1}^K$ of $[N] = \{1, \dots, N\}$ such that each fold I_k is of size $n = N/K$. For each $k \in [K] = \{1, \dots, K\}$ define $I_k^c := \{1, \dots, N\} \setminus I_k$.
- 2: For each $k \in [K]$, fit a machine learning estimator

$$\hat{\eta}_{0,k} = \hat{\eta}_0((W_i)_{i \in I_k^c})$$

of η_0 , where $\hat{\eta}_{0,k}$ is a random element in T , where the randomness only depends on the $(W_i)_{i \in I_k^c}$.

- 3: Combine all estimated nuisance elements $\hat{\eta}_{0,k}^{(2)}$ to fit a re-estimation procedure

$$\tilde{\eta}_0^{(2)} = \tilde{\eta}_0^{(2)}((W_i)_{i=1}^N, (\hat{\eta}_{0,k}^{(2)})_{k \in [K]})$$

of $\eta_0^{(2)}$, where $\tilde{\eta}_0^{(2)}$ is a random element in $T^{(2)}$.

- 4: Construct the estimator $\tilde{\theta}_0$ as the solution to

$$\frac{1}{K} \sum_{k=1}^K \mathbb{E}_{n,k} [\psi(W; \tilde{\theta}_0, (\hat{\eta}_{0,k}^{(1)}, \tilde{\eta}_0^{(2)}))] = 0,$$

where $\mathbb{E}_{n,k}[\psi(W)] = n^{-1} \sum_{i \in I_k} \psi(W_i)$ is the empirical expectation over $(W_i)_{i \in I_k}$.

Assumption 4 (Calibration Complexity). Let $\{\tilde{r}_N\}_{N \geq 1}$ and $\{\tilde{r}_N^a\}_{N \geq 1}$ be some sequences of positive constants converging to zero. The estimator $\tilde{\eta} = (\hat{\eta}^{(1)}, \hat{\eta}^{(2)})$ is a random element in T with nuisance realization set $\tilde{\mathcal{T}}_N \subseteq \tilde{\mathcal{T}}_N^{(1)} \times \tilde{\mathcal{T}}_N^{(2)}$ such that

- (i) Let $\eta^{(1)}$ is a fixed element in $\tilde{\mathcal{T}}_N^{(1)}$ and define

$$\mathcal{F}_2(\eta^{(1)}) := \left\{ \psi(\cdot; \theta_0, (\eta^{(1)}, \eta^{(2)})) - \psi(\cdot; \theta_0, (\eta^{(1)}, \eta_0^{(2)})) \mid (\eta^{(1)}, \eta^{(2)}) \in \tilde{\mathcal{T}}_N \right\}.$$

Further let $F_2(\eta^{(1)})(\cdot)$ be a measurable envelope for $\mathcal{F}_2(\eta^{(1)})$ such that

$$\sup_{\eta^{(1)} \in \tilde{\mathcal{T}}_N^{(1)}} \|F_2(\eta^{(1)})(W_i)\|_{P,q} \equiv \sup_{\eta^{(1)} \in \tilde{\mathcal{T}}_N^{(1)}} \|F_2(\eta^{(1)})\|_{P,q} \leq V_n$$

for $q > 2$. For each $\eta^{(1)} \in \tilde{\mathcal{T}}_N^{(1)}$ define σ_n^2 as a sequence converging to zero such that

$$\sup_{f \in \mathcal{F}_2(\eta^{(1)})} \mathbb{E}[f^2] \leq \sigma_n^2 \leq \|F_2(\eta^{(1)})\|_{P,2}^2$$

and u_n such that

$$\sup_{\eta^{(1)} \in \tilde{\mathcal{T}}_N^{(1)}} J\left(\sigma_n / \|F_2(\eta^{(1)})\|_{P,2}, \mathcal{F}_2(\eta^{(1)}), F_2(\eta^{(1)})\right) \leq u_n.$$

Finally, assume the following growth condition is satisfied

$$\begin{aligned} & \sup_{\eta^{(1)} \in \tilde{\mathcal{T}}_N^{(1)}} \left(u_n \|F_2(\eta^{(1)})\|_{P,2} + \sigma_n \sqrt{\log(n)} \right. \\ & \left. + n^{1/q-1/2} V_n \left(u_n^2 \frac{\|F_2(\eta^{(1)})\|_{P,2}^2}{\sigma_n^2} \vee \log(n) \right) \right) \lesssim \tilde{r}_N \end{aligned}$$

(ii) It holds

$$\sup_{\eta^{(1)} \in \tilde{\mathcal{T}}_N^{(1)}} \left| \mathbb{E} \left[\psi^a \left(W; (\eta^{(1)}, \eta_0^{(2)}) \right) - \psi^a \left(W; (\eta_0^{(1)}, \eta_0^{(2)}) \right) \right] \right| \leq \tilde{r}_N^a$$

with probability converging to one. Further, the entropy conditions above also need to hold for ψ^a :

Let $\eta^{(1)}$ is a fixed element in $\tilde{\mathcal{T}}_N^{(1)}$ and define

$$\mathcal{F}_2^a(\eta^{(1)}) := \left\{ \psi^a \left(\cdot; (\eta^{(1)}, \eta^{(2)}) \right) - \psi^a \left(\cdot; (\eta^{(1)}, \eta_0^{(2)}) \right) \mid (\eta^{(1)}, \eta^{(2)}) \in \tilde{\mathcal{T}}_N \right\}.$$

Further let $F_2^a(\eta^{(1)})(\cdot)$ be a measurable envelope for $\mathcal{F}_2^a(\eta^{(1)})$ such that

$$\sup_{\eta^{(1)} \in \tilde{\mathcal{T}}_N^{(1)}} \|F_2^a(\eta^{(1)})(W_i)\|_{P,q} \equiv \sup_{\eta^{(1)} \in \tilde{\mathcal{T}}_N^{(1)}} \|F_2^a(\eta^{(1)})\|_{P,q} \leq V_{n,a}$$

for $q > 2$. For each $\eta^{(1)} \in \tilde{\mathcal{T}}_N^{(1)}$ define $\sigma_{n,a}^2$ as a sequence converging to zero such that

$$0 < \sup_{f \in \mathcal{F}_2^a(\eta^{(1)})} \mathbb{E}[f^2] \leq \sigma_{n,a}^2 \leq \|F_2^a(\eta^{(1)})\|_{P,2}^2$$

and $u_{n,a}$ such that

$$\sup_{\eta^{(1)} \in \tilde{\mathcal{T}}_N^{(1)}} J \left(\sigma_{n,a} / \|F_2^a(\eta^{(1)})\|_{P,2}, \mathcal{F}_2^a(\eta^{(1)}), F_2^a(\eta^{(1)}) \right) \leq u_{n,a}.$$

Finally, assume the following growth condition is satisfied

$$\begin{aligned} & u_{n,a} \sup_{\eta^{(1)} \in \tilde{\mathcal{T}}_N^{(1)}} \|F_2^a(\eta^{(1)})\|_{P,2} + \sigma_{n,a} \sqrt{\log(n)} \\ & + n^{1/q-1/2} V_{n,a} \left(u_{n,a}^2 \frac{\sup_{\eta^{(1)} \in \tilde{\mathcal{T}}_N^{(1)}} \|F_2^a(\eta^{(1)})\|_{P,2}^2}{\sigma_{n,a}^2} \vee \log(n) \right) \lesssim \tilde{r}_N^a. \end{aligned}$$

Assumption 4 imposes high-level assumptions on the complexity of the calibration step. Assumption 4 (i) restricts the complexity of the class $\mathcal{F}_2(\eta^{(1)})$ via standard complexity measures. If the function class is suitably measurable and the uniform entropy integral obeys $\log \sup_Q N \left(\epsilon \|F_2(\eta^{(1)})\|_{Q,2}, \mathcal{F}_2(\eta^{(1)}), \|\cdot\|_{Q,2} \right) \leq C$, it holds

$$J \left(\sigma_n / \|F_2(\eta^{(1)})\|_{P,2}, \mathcal{F}_2(\eta^{(1)}), F_2(\eta^{(1)}) \right) \lesssim \sigma_n^{1/2} \|F_2(\eta^{(1)})\|_{P,2}^{-1/2},$$

since

$$\begin{aligned}
& J\left(\delta, \mathcal{F}_2(\eta^{(1)}), F_2(\eta^{(1)})\right) \\
& := \int_0^\delta \sup_Q \sqrt{1 + \log N(\epsilon \|\mathcal{F}_2(\eta^{(1)})\|_{Q,2}, \mathcal{F}_2(\eta^{(1)}), \|\cdot\|_{Q,2})} d\epsilon \\
& \leq \int_0^\delta \sqrt{1 + C\epsilon^{-1}} d\epsilon \leq \delta + \sqrt{C} \int_0^\delta \epsilon^{-1/2} d\epsilon \lesssim \sqrt{\delta}
\end{aligned}$$

for any δ small enough and probability measure Q . The first part of Assumption 4 (ii) imposes a Lipschitz continuity condition on ψ^a which is the first part of the linear score defined in Equation (6). The second part of Assumption 4 (ii) provides similar complexity assumptions as for the function class $\mathcal{F}_2(\eta^{(1)})$ in Assumption 4 (i) and also the required growth rates. Remark that the conditions in Assumption 4 are quite similar to Belloni et al. (2018), but we build upon standard Donsker conditions. Again, it is worth noting that Assumption 4 (ii) depends only on the score ψ^a . In the case of a nonparametric causal model, also known as *interactive regression model* (IRM), considered in Section 3.2.1, the first part of the linear score is given by $\psi^a = -1$, see Equation (10), and therefore $\sigma_{n,a}^2 = 0$. Hence, in the interactive regression model, Theorem 1 below holds with $\tilde{r}_N^a = 0$ and only Assumption 4 (i) is required.

Theorem 1. *Let $\tilde{\theta}_0$ be the estimator according to Algorithm 3 to 5. Assume $\delta_N \geq N^{-1/2}$ for all $N \geq 1$. Under Assumption 3 and 4, equation (7) in Remark 2 holds with updated remainder, that is*

$$\sqrt{N}\sigma^{-1}(\hat{\theta}_0 - \theta_0) = \frac{1}{N} \sum_{i=1}^N \tilde{\psi}(W_i) + O_P(\tilde{\rho}_N) \rightsquigarrow \mathcal{N}(0, 1)$$

uniformly over $P \in \mathcal{P}_N$, where the size of the remainder term obeys

$$\tilde{\rho}_N := \rho_N + \tilde{r}_N + \tilde{r}_N^a = N^{-1/2} + r_N + r'_N + \tilde{r}_N + \tilde{r}_N^a + N^{1/2}\lambda_N + N^{1/2}\lambda'_N \lesssim \delta_N.$$

The crucial difference between Algorithm 3 and 5 lies in the assumptions on the nuisance realization set $\tilde{\mathcal{T}}_N$, which require convergence rates of the recalibration procedure. In Algorithm 3, estimation properties are well known, e.g. for isotonic regression see Section 2.2.1. These proofs heavily rely on the i.i.d. assumption of the samples used for recalibration, which is violated for Algorithm 5. Nevertheless, cross-fitting might result in only weak dependencies between different samples, such that the convergence rates might still be sufficient for the calibration with Algorithm 5. This algorithm closely mirrors the IC-IPW approach described by van der Laan et al. (2024a), where calibration is applied to cross-fitted propensity scores on the full sample, retaining the theoretical guarantees established in van der Laan et al. (2024a) (Theorems 1–2).

3.2 Calibration for Double Machine Learning Models

The results of Section 3 can be applied directly to different regression models and causal parameters of interest. In standard settings, a convergence rate of $\|\hat{m}_0 - m_0\|_{P,2} = o_P(N^{-1/4})$ is assumed. If isotonic regression is used for calibration, Lemma 2 directly implies that the convergence rate of the calibrated propensity score will still satisfy the rate condition $\|\hat{m}_0 -$

$m_0\|_{P,2} = o_P(N^{-1/4})$. Furthermore, we state explicit assumptions to restrict the complexity of the nuisance calibration to avoid additional sample splitting.

3.2.1 Calibration in interactive regression models

Consider the fully heterogeneous or interactive regression model as in Chernozhukov et al. (2018). This nonparametric regression model is often considered when augmented inverse probability weighting (AIPW) is used for estimation. Let $D \in \{0, 1\}$ be a binary treatment variable and $W = (Y, D, X)$, where

$$Y = g_0(D, X) + U, \quad \mathbb{E}[U|D, X] = 0, \quad (8)$$

$$D = m_0(X) + V, \quad \mathbb{E}[V|X] = 0. \quad (9)$$

A common parameter of interest is the average treatment effect

$$\theta_0 := \mathbb{E}[g_0(1, X) - g_0(0, X)].$$

Let

$$\begin{aligned} \psi(W; \theta, \eta) := & (g(1, X) - g(0, X)) + \frac{D}{m(X)}(Y - g(1, X)) - \frac{1-D}{1-m(X)}(Y - g(0, X)) \\ & - \theta \end{aligned} \quad (10)$$

be the considered score function, corresponding to the augmented inverse probability weighted estimator, where $\eta = (g, m)$ denotes the nuisance functions for the outcome regression $g_0(D, X) = E[Y|D, X]$ and propensity score $m_0(X) = E[D|X]$.

Assumption 5 (cf. Assumption 5.1 in Chernozhukov et al. (2018)). Let $(\delta_N)_{n=1}^\infty$ and $(\Delta_N)_{n=1}^\infty$ be sequences of positive constants approaching 0. Also, let c, ϵ, C and q be fixed strictly positive constants such that $q > 4$, and let $K \geq 2$ be a fixed integer. Moreover, for any $\eta = (\eta_1, \dots, \eta_\ell)$, denote $\|\eta\|_{P,q} = \max_{1 \leq j \leq \ell} \|\eta_j\|_{P,q}$. For simplicity, assume that N/K is an integer. For all probability laws $P \in \mathcal{P}$ for the triple (Y, D, X) , the following conditions hold:

(a) Equations (8) and (9) hold

(b) $\|Y\|_{P,q} \leq C$

(c) $P(\epsilon \leq m_0(X) \leq 1 - \epsilon) = 1$

(d) $\|U\|_{P,2} \geq c$

(e) $\|\mathbb{E}_P[U^2 | X]\|_{P,\infty} \leq C$

(f) Given a random subset I of $[N]$ of size $n = N/K$, the nuisance parameter estimator $\hat{\eta}_0 = \hat{\eta}_0((W_i)_{i \in I^\epsilon})$ obeys the following conditions. With P -probability no less than $1 - \Delta_N$,

(i) $\|\hat{\eta}_0 - \eta_0\|_{P,2} \leq \delta_N$ and $\|\hat{\eta}_0 - \eta_0\|_{P,q} \leq C$

(ii) $\|\hat{m}_0 - m_0\|_{P,2} \times \|\hat{g}_0 - g_0\|_{P,2} \leq \delta_N N^{-1/2}$, $\|\hat{g}_0 - g_0\|_{P,\infty} \leq C$ and $\|\hat{m}_0 - 1/2\|_{P,\infty} \leq 1/2 - \epsilon$.

Under Assumption 5, Remark 2 holds (cf. Theorem 5.1 in Chernozhukov et al. (2018)). Remark that Assumption 5 is slightly stronger than Assumption 5.1 in Chernozhukov et al. (2018), as we require larger moment bounds ($q > 4$ instead of $q > 2$). To apply Theorem 1 using a calibrated propensity score, Assumption 4 has to be satisfied. To this end, we introduce the following Assumption 6.

Assumption 6 (Calibration rate and complexity). *We assume*

(i) *The following convergence rates hold with P -probability no less than $1 - \Delta_N$,*

$$\|\tilde{m}(X) - m_0(X)\|_{P,2} \lesssim \varepsilon_N \leq \log^{-1/2}(N),$$

such that

$$\varepsilon_N \cdot \|\hat{g}_0 - g_0\|_{P,2} \leq \delta_N N^{-1/2}.$$

Further, the predictions are well separated from zero and one,

$$\|\tilde{m}(X) - 1/2\|_{P,\infty} \leq 1/2 - \epsilon.$$

(ii) *Let $\tilde{m}(\cdot) \in \mathcal{M}$, such that the covering numbers obey*

$$\sup_Q N(\epsilon, \mathcal{M}, L_2(Q)) \leq C\epsilon^{-1}$$

Assumption 6 imposes mild conditions on the calibration procedure. Assumption 6(i) ensures that the convergence rate of the calibrated propensity score $\tilde{m}(\cdot)$ is still sufficiently fast, while Assumption 6(ii) restricts the complexity of calibration, so that additional cross-fitting can be avoided.

Theorem 2. *Under Assumptions 5 and 6(i) Remark 3 is valid. If additionally Assumption 6(ii) is satisfied, Theorem 1 holds.*

The proof of Theorem 2 is given in the appendix. As mentioned in the beginning of Section 3.2, often convergence rates of $\|\hat{m}_0 - m_0\|_{P,2} = o_P(N^{-1/4})$ and $\|\hat{g}_0 - g_0\|_{P,2} = o_P(N^{-1/4})$ are assumed implying the conditions of Assumption 5(f)(ii). Considering Lemma 2 this immediately implies Assumption 6 if isotonic regression is used for calibration as the convergence rate of the calibrated propensity score is given by $\|\tilde{m}_0 - m_0\|_{P,2} = o_P(N^{-1/4})$ and the complexity of monotone functions satisfies Assumption 6(ii).

3.2.2 Calibration in partially linear regression models

Consider the partially linear regression model as in Chernozhukov et al. (2018). Let $D \in \{0, 1\}$ be a binary treatment variable and $W = (Y, D, X)$, where

$$Y = \theta_0 D + g_0(X) + U, \quad \mathbb{E}[U|D, X] = 0, \quad (11)$$

$$D = m_0(X) + V, \quad \mathbb{E}[V|X] = 0, \quad (12)$$

with θ_0 being the parameter of interest. Let

$$\psi(W; \theta, \eta) := (Y - l(X) - \theta(D - m(X)))(D - m(X))$$

be the “partialling-out” score function, where $\eta = (l, m)$ denotes the nuisance functions for the outcome regression $l_0(X) = \mathbb{E}[Y|X]$ and propensity score $m_0(X) = \mathbb{E}[D|X]$.

Assumption 7 (cf. Assumption 4.1 in [Chernozhukov et al. \(2018\)](#)). Let $(\delta_N)_{n=1}^\infty$ and $(\Delta_N)_{n=1}^\infty$ be sequences of positive constants approaching 0 as before. Also, let c, C and q be fixed strictly positive constants such that $q > 4$, and let $K \geq 2$ be a fixed integer. Moreover, for any $\eta = (\eta_1, \eta_2)$, where η_1 and η_2 are functions mapping the support of X to \mathbb{R} , denote $\|\eta\|_{p,q} = \|\eta_1\|_{p,q} \vee \|\eta_2\|_{p,q}$. For simplicity, assume that N/K is an integer. For all probability laws $P \in \mathcal{P}$ for the triple (Y, D, X) , the following conditions hold:

- (a) Equations (11) and (12) hold
- (b) $\|Y\|_{P,q} + \|D\|_{P,q} \leq C$
- (c) $\|UV\|_{P,2} \geq c^2$ and $\mathbb{E}_P[V^2] \geq c$
- (d) $\|\mathbb{E}_P[U^2 | X]\|_{P,\infty} \leq C$ and $\|\mathbb{E}_P[V^2 | X]\|_{P,\infty} \leq C$
- (e) Given a random subset I of $[N]$ of size $n = N/K$, the nuisance parameter estimator $\hat{\eta}_0 = ((W_i)_{i \in I^c})$ obeys the following conditions for all $N \geq 1$. With P -probability no less than $1 - \Delta_N$,
 - (i) $\|\hat{\eta}_0 - \eta_0\|_{P,q} \leq C$ and $\|\hat{\eta}_0 - \eta_0\|_{P,2} \leq \delta_N$
 - (ii) $\|\hat{m}_0 - m_0\|_{P,2} \times \left(\|\hat{m}_0 - m_0\|_{P,2} + \|\hat{\ell}_0 - \ell_0\|_{P,2} \right) \leq \delta_N N^{-1/2}$.

Under Assumption 7, Remark 2 holds (cf. Theorem 4.1 in [Chernozhukov et al. \(2018\)](#)). To apply Theorem 1 using a calibrated propensity score estimator, Assumption 4 has to be satisfied. To this end, we introduce the following Assumption 8.

Assumption 8 (Calibration rate and complexity). Let $\tilde{m}(X)$ be an estimator of $\tilde{m}_0(X) := \mathbb{E}[D|\hat{m}(X)]$. We assume

- (i) The following convergence rates hold with P -probability no less than $1 - \Delta_N$,

$$\|\tilde{m}(X) - \tilde{m}_0(X)\|_{P,2} \lesssim \varepsilon_N,$$

such that

$$\varepsilon_N \cdot \left(\varepsilon_N + \|\hat{\ell}_0 - \ell_0\|_{P,2} \right) \leq \delta_N N^{-1/2}.$$

- (ii) Let $\tilde{m}(\cdot) \in \mathcal{M}$, such that the covering numbers obey

$$\sup_Q N(\varepsilon, \mathcal{M}, L_2(Q)) \leq C\varepsilon^{-1}.$$

It is worth noting that this calibration assumption does not necessarily require D to be binary.

Theorem 3. *Under Assumptions 7 and 8(i) Remark 3 is valid. If additionally Assumption 8(ii) is satisfied, Theorem 1 holds.*

The proof of Theorem 3 is similar to the proof of Theorem 2 and is therefore left out. It just needs an additional complexity argument to verify Assumption 4 (ii) based on Assumption 8(ii).

4 Simulation

In this section, we investigate the introduced calibrated propensity score models from Section 3.2 through an extensive simulation study². We evaluate the impact of calibration methods (Venn-ABERS, Platt scaling, isotonic regression) on the performance of causal estimators (IPW, DML), supplemented by analyses of weight normalization and a comparison to covariate-balancing reweighting estimators (e.g., entropy balancing). These methods are tested under diverse data-generating processes (DGPs) that systematically vary in challenges such as overlap violations, treatment assignment imbalance, nuisance model misspecification, and varying signal-to-noise ratios. Performance is assessed using calibration diagnostics (e.g., calibration plots, expected calibration error) and causal estimation metrics (RMSE, MAE, and variance) to unravel the interplay between robustness, forecast accuracy, and covariate balance.

4.1 Set-up of the Simulation Study

To assess the contribution of potentially miss-calibrated propensity scores, we briefly introduce the causal estimators considered. The inverse probability weighting (IPW) estimator uses estimates of the propensity scores $\hat{m}(D = 1|X)$ directly. Here, an estimate $\hat{\theta}$ of the ATE is computed as

$$\frac{1}{n} \sum_{i=1}^n \left(\frac{D^{(i)}Y^{(i)}}{\hat{m}(D = 1|X^{(i)})} - \frac{(1 - D^{(i)})Y^{(i)}}{1 - \hat{m}(D = 1|X^{(i)})} \right).$$

Especially treated units with low propensity scores and non-treated units with high propensity scores have extreme contributions. This can be critical if the underlying propensity score model is misspecified or overconfident.

The interactive regression model (IRM, Section 3.2.1) allows for heterogeneous treatment effects without strong form assumptions. Contrary, the partially linear regression model (PLR, Section 3.2.2) imposes an additive structure³. One obstacle in evaluating causal ATE models is that the true value of the causal parameter θ_0 is not observed in observational studies. For a fair evaluation, we have selected four external sources for the data generating processes (DGPs), each proposing different challenges for the models. The DGPs are characterized by varying levels of noise, different dimensionality of observed covariates, and underlying nonlinearities or unbalancedness. The DGPs satisfy the unconfoundedness assumption, $Y(d) \perp D \mid X$, with $Y(d)$ indicating the potential outcome under treat-

²The code for the simulation study is available at the following link: <https://github.com/JanRabenseifner/Causal-Propensity-Calibration.git>. The simulation is executed on an HPC cluster in parallel, using different seeds for the DGPs.

³Both, the IRM and PLR model, are implemented via the `DoubleML` package (Bach et al., 2022, 2024).

ment $D = d$. Hence, these settings allow for identification of the average treatment effect, $\theta_0 = \mathbb{E}[Y(d = 1) - Y(d = 0)]$.

4.2 DGPs

In our first DGP, data units were generated following [Belloni et al. \(2017\)](#)⁴:

$$d_i = 1 \left\{ \frac{\exp(c_D X_i' \beta)}{1 + \exp(c_D X_i' \beta)} > V_i \right\}, \quad V_i \sim \mathcal{U}(0, 1),$$

$$y_i = \theta D_i + c_Y X_i' \beta D_i + \zeta_i, \quad \zeta_i \sim \mathcal{N}(0, 1),$$

where $v_i \sim U(0, 1)$, $\zeta_i \sim N(0, 1)$, V_i and ζ_i are independent, $p = \dim(X_i)$, the covariates $X_i \sim N(0, \Sigma)$ with $\Sigma_{kj} = (0.5)^{|j-k|}$. β is a $p \times 1$ vector with elements set as $\beta_{1,j} = (1/j)^2$ for $j = 1, \dots, p$. c_D and c_Y are scalars given by

$$c_Y = \sqrt{\frac{R_Y^2}{(1 - R_Y^2)\beta' \Sigma \beta}}, \quad c_D = \sqrt{\frac{(\pi^2/3)R_D^2}{(1 - R_D^2)\beta' \Sigma \beta}}.$$

that control the strength of the relationship between the controls, the outcome, and the treatment variable. The underlying treatment effect is heterogeneous. Hence, to accurately model the interaction effects between treatment and covariates, the IRM should be considered. Simple propensity score weighting in the IPW, as well as the additive structural form assumptions for the treatment effect of the PLR, should be inconsistent for this DGP.

Table 1: Overview of the DGPs

DGP	Covariates	Description of $D \mid X$	Description of $g_0(D, X)$
1	$X_i \sim N(0, \Sigma)$ with $\Sigma_{kj} = (0.5)^{ j-k }$	Sigmoid function combined with Uniform indicator. D is exogenous conditional on X .	Heterogeneous treatment effect, linear with simple interaction, $\epsilon_i \stackrel{\text{iid}}{\sim} \mathcal{N}(0, 1)$
2	$X_1 \sim \text{Bin}(1, 0.5)$, $X_2 \mid X_1 \sim \Gamma$, $X_3 \mid X_2 \sim \text{Beta}$	Highly nonlinear, tree-based via conditions, $D \sim \text{Bin}(1, m_0(X))$	Homogeneous treatment effect, Poisson with simple linear combination of covariates
3	$X \sim \text{Unif}[-1, 1]^4$	Expit function combined with $D \sim \text{Bin}(1, m_0(X))$	Heterogeneous treatment effect, nonlinear transformations of the covariates, $\epsilon_i \stackrel{\text{iid}}{\sim} \mathcal{N}(0, 1)$
4	$X \sim \text{Unif}[0, 1]^{20}$	Unbalanced and nonlinear $m_0(X) = \alpha(1 + \beta_{2,4}(\min(X_1, X_2)))$, $D \sim \text{Bin}(1, m_0(X))$	Heterogeneous treatment effect, scaled Friedman function for $g_0(X)$ and simple interaction of D and X , $\epsilon_i \stackrel{\text{iid}}{\sim} \mathcal{N}(0, 1)$

A detailed description of DGP 2-4 is given in [Appendix B](#).

DGP 2 is adapted from [Deshpande and Kuleshov \(2023\)](#). Three covariates are simulated: gender (X_1), age (X_2), and disease severity (X_3), while treatment (D) corresponds to the

⁴This DGP is available at [DoubleMLIRMDData](#).

administration of a drug. The outcome Y is the time taken for the recovery of a patient. In addition to the original setting, we introduced non-deterministic treatment assignments to ensure positivity. The function for the treatment assignment resembles the approach of tree-based models, favoring the IRM and PLR in combination with LGBM and random forest.

For a complicated nonlinear outcome regression, we implemented DGP 3 (van der Laan et al., 2023). The included transformations make it difficult for linear models as well as tree-based classifiers through the local linearity. Given the nonlinear and heterogeneous influence of the treatment on the outcome, we expect the IRM model to outperform the PLR. However, the treatment assignment itself can be modeled consistently, favoring the IPW.

The unbalanced treatment assignment DGP 4 follows Ballinari (2024) and is adapted from Nie and Wager (2020). Three settings of the share of treated $\mathbb{E}[D]$ are tested: $\mathbb{E}[D] \in \{0.05, 0.1, 0.2\}$. To address positivity violations, we tested three clipping thresholds for the propensity scores: $1e-12$, 0.01, and 0.1. Given the majority non-treatment class, a lower threshold is sufficient to limit the contribution of a single observation.

Table 2: Overview of Simulated Settings per DGP

DGP	Parameter	Values
1	n	[100, 200, 500, 1000, 2000]
	p	[5, 20, 50, 100, 200]
	R_a^2	[0.2, 0.5, 0.8]
	Clip	[1e-12, 0.01, 0.1]
2	n	[200, 500, 1000, 2000, 4000]
	p	3
	Overlap	[0.1, 0.5, 0.9]
3	Clip	[1e-12, 0.01, 0.1]
	n	[200, 500, 1000, 2000, 4000]
	p	4
4	Clip	[1e-12, 0.01, 0.1]
	n	[2000, 4000, 6000, 8000]
	p	20
	$\mathbb{E}[D]$	[0.05, 0.1, 0.2]
	Clip	[1e-12, 0.01, 0.1]

4.3 Learners and Calibration Methods

We test different learners for the outcome regression and the propensity score estimation. For the outcome regression, we consider a simple linear regression along with the tree-based Machine Learning algorithms LightGBM (LGBM) (Ke et al., 2017) and random forest. Both are flexible machine learning algorithms that perform well across a wide variety of datasets. For the propensity score estimation, we consider logistic regression, LGBM classifier, and random forest classifier. All models are employed within their default settings. Employing different fine-tuning schemes could benefit either approach and distort the comparison.

For propensity calibration, we consider the three approaches introduced in 2.2. First, we utilize `IsotonicRegression` from the `scikit-learn` package (Pedregosa et al., 2011). In addition, we employ the Inductive Venn-ABERS predictor (VAP) introduced by Vovk et al. (2015) and available at Petej (2024). VAP builds on the groupings in the outcome space made by isotonic regression. It utilizes potential labels to fit separate isotonic regressions. Thus, simple Isotonic Regression receives a coarser partitioning of the outcome space. Lastly, we incorporate Platt scaling, implemented via the `CalibratedClassifierCV` in the

scikit-learn package.

4.4 Calibration Metrics

For binary classification, the ℓ_p Expected Calibration Error (ECE) (Naeini et al., 2015; Sun et al., 2024), for $p \geq 1$, is defined as:

$$\text{ECE}_p := \mathbb{E} [\mathbb{E} [\|D - m(X)\|^p \mid m(X)]]^{\frac{1}{p}}.$$

To approximate the expected calibration error (ECE), the estimated propensity scores $\hat{m}(X)$ are divided across the probabilistic output range $[0, 1]$ into equally spaced intervals (Naeini et al., 2015) $\{I_0, I_1, \dots, I_M\}$ or quantiles (Nguyen and O'Connor, 2015) of $\hat{m}(x)$. This allows us to generate buckets $\{B_i\}_{i=1}^M$, where $B_i = \{(X, D) \mid m(D = 1 \mid X) \in I_i\}$. Each predicted probability is assigned to the appropriate bin. The calibration error is then defined as the difference between the fraction of correct predictions (accuracy) and the mean predicted probability (confidence) within each bin:

$$\text{ECE}_p = \sum_{i=1}^M \frac{n_i}{N} \|\text{acc}_i(B_i) - \text{conf}_i(B_i)\|_p,$$

where $\text{acc}_i(B_i) = \frac{1}{|B_i|} \sum_{j=1}^{|B_i|} D_j$ and $\text{conf}_i(B_i) = \frac{1}{|B_i|} \sum_{j=1}^{|B_i|} m(D = 1 \mid X_j)$. Commonly employed are the L1-Norm and L2-Norm. (Nixon et al., 2020) suggests using either the L2-norm or adaptive intervals, as the L1-norm is highly susceptible to the decision on the number of intervals.

To assess subpopulations with extreme propensity scores, the maximum calibration error (MCE) (Naeini et al., 2015) can be used. MCE is defined as the maximum deviation across all bins, given by:

$$\max_{i \in \{1, \dots, M\}} |\text{acc}_i(B_i) - \text{conf}_i(B_i)|.$$

This error reflects the worst-case deviation between predicted and actual values across all intervals.

All calibration metrics are visualized with respect to the observation size and the underlying propensity learner in Appendix C. In Figure 1, we can observe that the uncalibrated Algorithm 1, as well as the nested k-fold cross-fit Algorithm 2 are poorly calibrated for small sample sizes. Additionally, a version of Algorithm 1 clipped at the one percent level is included. This helps neglect some of the miscalibration, but still performs worse than Algorithms 4 and 5 for all sample sizes.

In propensity weighting, severe deviations in the middle of the propensity score distribution are not particularly critical. However, deviations at the boundaries are crucial because they can lead to exploding weights. Therefore, it is generally advisable to include visualizations to assess both the overlap in propensity scores and their calibration properties. The overlap ratio plot, based on the reliability diagram, splits the probability space into equal parts. For each propensity bin, the plot displays the actual proportion of treated and untreated units separately.

No clear violation of the overlap assumption can be seen for the true underlying propensities displayed in the left panel of Figure 2. The black dotted lines represent perfect cali-

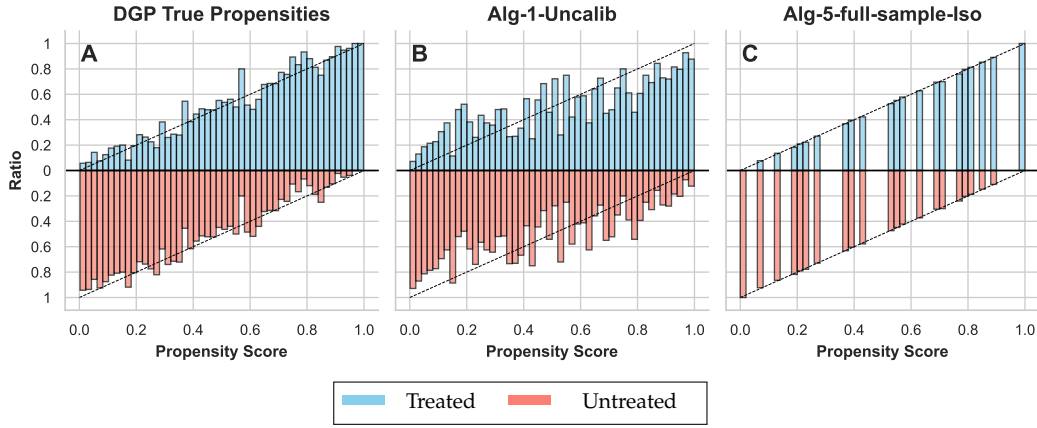


Figure 2: Overlap Ratios, DGP 1, $n = 2000$, $p = 20$, $m = \text{LGBM}$

bration. The ratios illustrate the deviations for both the treated and untreated groups in the uncalibrated Algorithm 1 in the middle panel. Notably critical are the substantial proportions of treated observations with estimated propensity scores near zero and untreated observations with propensities close to one. In contrast, the perfect calibration property of Algorithm 5 is displayed in the right panel.

4.5 Results

4.5.1 General findings

As expected, the nested cross-fitting Algorithm 2 faces stability challenges in small sample size settings. Venn-Abers calibration relies on isotonic regression combined with sample splitting. Consequently, Algorithm 3, when used with Venn-Abers, encountered similar instability. Additionally, the two-fold calibration Algorithm 4, combined with isotonic regression, required clipping at the 1-percent level to maintain stability. This instability arises from the known limitation of isotonic regression, which is prone to overfitting, especially with small calibration sets (van der Laan and Alaa, 2024).

To ensure a fair comparison, the uncalibrated Algorithm 1 is presented both unclipped and with a restriction at the 1-percent threshold (Alg-1-Clipped). All other algorithms were only clipped at a threshold of 10^{-12} . Given the sample sizes, such violations seem unlikely. This serves more as a general recommendation, as the added clipping bias is negligible.

Table 3 provides a summary of the results across all treatment models and the algorithms discussed, in combination with isotonic regression. Detailed results for individual models are included in the Appendices: Table 5 for IPW, Table 6 for IRM, and Table 7 for the PLR model, as presented in Appendix C.

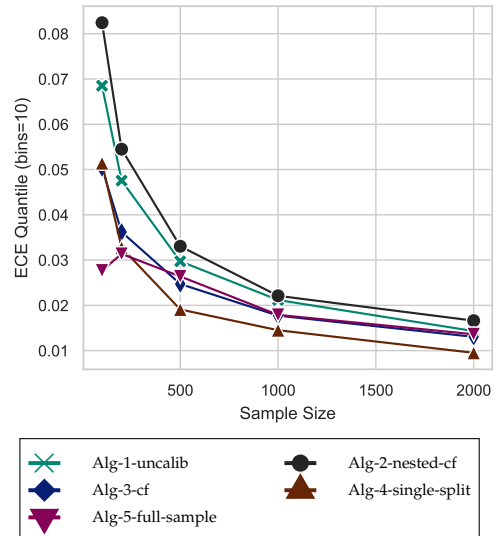


Figure 1: Quantile ECE, DGP 1, $m = \text{LGBM}$, $n = 2000$, $p = 20$

Table 3: Results Overview

DGP	Model	Method	m = Logit			m = Random Forest			m = LGBM		
			MAE	RMSE	Std. dev.	MAE	RMSE	Std. dev.	MAE	RMSE	Std. dev.
1	IRM	Alg-1-Clipped	0.07	0.10	0.10	0.06	0.08	0.07	0.22	0.27	0.24
	IRM	Alg-1-Uncalib	0.08	0.13	0.13	1.85e+06	1.85e+07	1.84e+07	0.48	0.60	0.54
	IRM	Alg-2-nested-cf-Iso	0.12	0.15	0.14	0.10	0.12	0.12	0.10	0.12	0.12
	IRM	Alg-3-cf-Iso	0.06	0.08	0.07	0.06	0.08	0.08	0.06	0.08	0.07
	IRM	Alg-4-single-split-Iso	0.10	0.13	0.12	0.07	0.08	0.06	0.07	0.09	0.06
	IRM	Alg-5-full-sample-Iso	0.06	0.08	0.08	0.06	0.08	0.07	0.07	0.08	0.08
	IPW	Alg-1-Clipped	0.08	0.11	0.11	0.18	0.19	0.06	0.94	0.98	0.31
	IPW	Alg-1-Uncalib	0.10	0.16	0.16	1.09e+06	1.09e+07	1.09e+07	1.57	1.77	0.83
	IPW	Alg-5-full-sample	0.07	0.09	0.08	0.12	0.14	0.06	0.14	0.16	0.07
	PLR	Alg-1-Clipped	0.05	0.06	0.06	0.05	0.06	0.06	0.05	0.06	0.06
	PLR	Alg-1-Uncalib	0.05	0.06	0.06	0.05	0.06	0.06	0.05	0.06	0.06
	PLR	Alg-5-full-sample	0.05	0.06	0.06	0.05	0.06	0.06	0.05	0.07	0.07
2	IRM	Alg-1-Clipped	0.09	0.11	0.11	0.31	0.39	0.39	0.20	0.26	0.26
	IRM	Alg-1-Uncalib	0.09	0.11	0.11	2.22e+09	2.89e+09	2.86e+09	0.24	0.32	0.32
	IRM	Alg-2-nested-cf-Iso	0.18	0.23	0.22	0.16	0.22	0.22	0.19	0.24	0.24
	IRM	Alg-3-cf-Iso	0.09	0.11	0.11	0.09	0.12	0.12	0.10	0.12	0.12
	IRM	Alg-4-single-split-Iso	0.15	0.20	0.20	0.09	0.11	0.11	0.09	0.11	0.11
	IRM	Alg-5-full-sample-Iso	0.09	0.11	0.11	0.09	0.11	0.11	0.09	0.12	0.12
	IPW	Alg-1-Clipped	0.09	0.12	0.11	4.45	4.59	1.11	2.67	2.74	0.61
	IPW	Alg-1-Uncalib	0.09	0.12	0.11	1.17e+10	1.37e+10	7.23e+09	2.86	2.98	0.81
	IPW	Alg-5-full-sample-Iso	0.09	0.11	0.11	0.20	0.23	0.10	0.18	0.20	0.10
	PLR	Alg-1-Clipped	0.09	0.11	0.10	0.12	0.14	0.10	0.10	0.11	0.10
	PLR	Alg-1-Uncalib	0.09	0.11	0.10	0.12	0.14	0.10	0.10	0.11	0.10
	PLR	Alg-5-full-sample-Iso	0.09	0.11	0.10	0.09	0.11	0.10	0.09	0.10	0.10
3	IRM	Alg-1-Clipped	0.05	0.07	0.07	0.08	0.10	0.10	0.11	0.13	0.13
	IRM	Alg-1-Uncalib	0.05	0.07	0.07	9.97e+07	2.74e+08	2.73e+08	0.11	0.14	0.14
	IRM	Alg-2-nested-cf-Iso	0.10	0.13	0.12	0.08	0.10	0.10	0.10	0.13	0.13
	IRM	Alg-3-cf-Iso	0.05	0.07	0.07	0.06	0.07	0.07	0.05	0.07	0.06
	IRM	Alg-4-single-split-Iso	0.10	0.12	0.11	0.05	0.07	0.06	0.05	0.07	0.06
	IRM	Alg-5-full-sample-Iso	0.05	0.07	0.07	0.06	0.07	0.07	0.05	0.07	0.07
	IPW	Alg-1-Clipped	0.06	0.08	0.08	0.54	0.58	0.21	2.00	2.02	0.31
	IPW	Alg-1-Uncalib	0.06	0.08	0.08	3.07e+08	8.49e+08	7.91e+08	2.05	2.07	0.34
	IPW	Alg-5-full-sample-Iso	0.06	0.08	0.08	0.37	0.37	0.07	0.42	0.43	0.07
	PLR	Alg-1-Clipped	0.06	0.08	0.08	0.06	0.07	0.07	0.08	0.10	0.07
	PLR	Alg-1-Uncalib	0.06	0.08	0.08	0.06	0.07	0.07	0.08	0.10	0.07
	PLR	Alg-5-full-sample-Iso	0.07	0.09	0.08	0.06	0.07	0.07	0.06	0.07	0.07
4	IRM	Alg-1-Clipped	0.04	0.06	0.06	0.07	0.09	0.09	0.17	0.21	0.20
	IRM	Alg-1-Uncalib	0.04	0.06	0.06	1.74e+08	2.70e+08	2.68e+08	0.36	0.46	0.43
	IRM	Alg-2-nested-cf-Iso	0.05	0.07	0.07	0.05	0.07	0.07	0.06	0.07	0.07
	IRM	Alg-3-cf-Iso	0.04	0.06	0.06	0.05	0.06	0.06	0.05	0.06	0.06
	IRM	Alg-4-single-split-Iso	0.05	0.06	0.06	0.05	0.06	0.06	0.04	0.06	0.06
	IRM	Alg-5-full-sample-Iso	0.04	0.06	0.06	0.05	0.06	0.06	0.04	0.06	0.06
	IPW	Alg-1-Clipped	0.13	0.15	0.06	0.54	0.55	0.13	6.14	6.17	0.52
	IPW	Alg-1-Uncalib	0.13	0.15	0.06	4.64e+08	6.89e+08	5.11e+08	8.37	8.45	1.21
	IPW	Alg-5-full-sample-Iso	0.07	0.08	0.05	0.11	0.12	0.05	0.10	0.11	0.06
	PLR	Alg-1-Clipped	0.08	0.09	0.06	0.05	0.06	0.05	0.05	0.06	0.05
	PLR	Alg-1-Uncalib	0.08	0.09	0.06	0.05	0.06	0.05	0.05	0.06	0.05
	PLR	Alg-5-full-sample-Iso	0.08	0.09	0.06	0.07	0.09	0.05	0.08	0.09	0.05

For all DGPs: $g = \text{LGBM}$, and for Algorithms 2 - 5: Calibration = Isotonic Regression;

DGP 1: $n = 2000$, $p = 20$, $R2.d = 0.5$; DGP 2: $n = 2000$, $p = 3$, $\text{overlap} = 0.5$;

DGP 3: $n = 2000$, $p = 4$; DGP 4: $n = 4000$, $p = 20$, $\text{share treated} = 0.1$

Across all DGPs and settings, we can observe that calibration improves the inverse propensity-based IPW and IRM especially in combination with the tree-based propensity learners. The PLR model produces stable results across all settings, with minimal improvement from clipping or calibration for most DGPs. In general, the doubly-robust calibrated IRM and the PLR outperform the IPW. Algorithm (4) is biased in the PLR model for the tree-based methods random forest and LGBM in combination with VAP or isotonic regression⁵. This bias appears to persist regardless of the sample size, as demonstrated on the right-hand

⁵For more details on the influence of sample size on the proposed Algorithms, we refer to Appendix C, Figures 35, 37, 39, 41. Figures 36, 38, 40, and 42 display the effects of varying sample sizes with different calibration methods in combination with Algorithm 3.

side of Figure 3⁶.

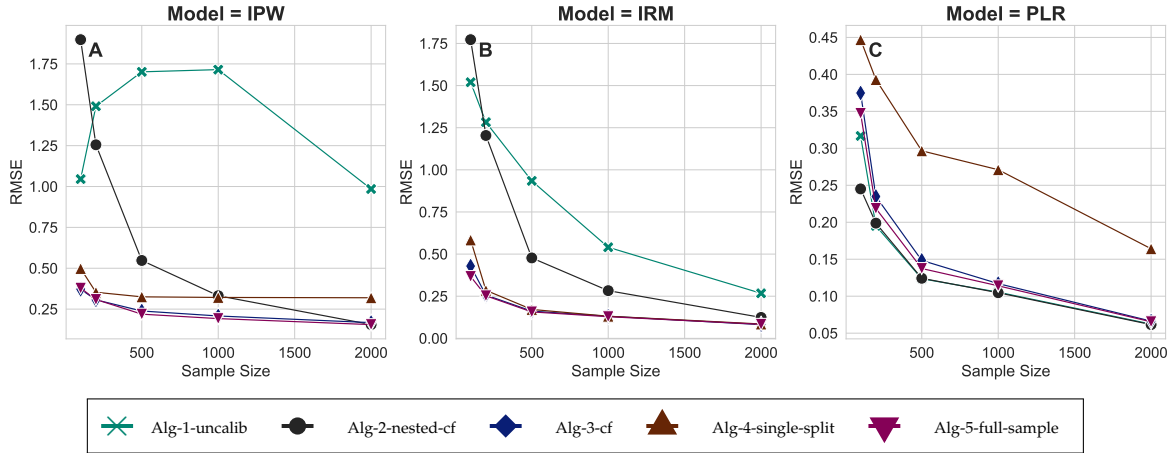


Figure 3: DGP 1, $n = 2000$, $p = 20$, $R2D = 0.5$, $m = \text{LGBM}$, $g = \text{LGBM}$

The impact of calibration is strongly dependent on the underlying propensity score learner. In contrast to [Błasiok et al. \(2023\)](#), we generally observe good calibration properties for logistic regression and the least improvements through calibration.

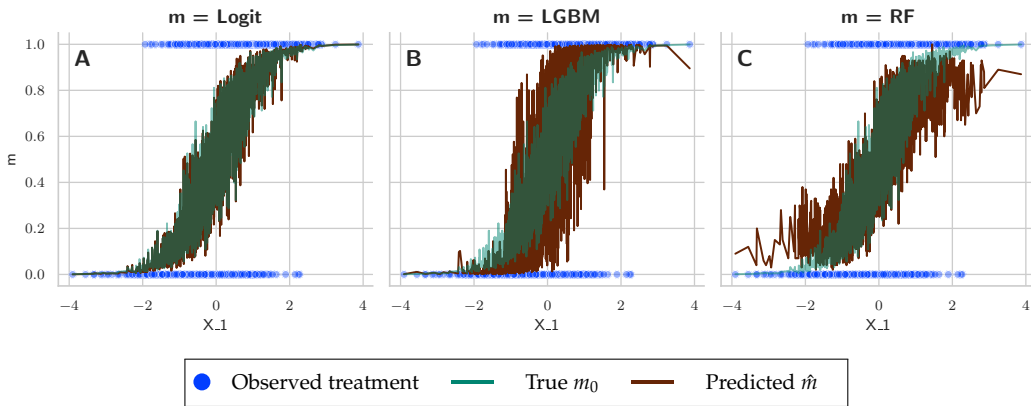


Figure 4: DGP 1, $n = 2000$, $p = 20$, $R2D = 0.5$

Random forest can be both under-confident, as seen in Figure 4 for DGP 1, and over-confident for DGPs 2 and 3.⁷ As shown by [Johansson et al. \(2023\)](#), random forest tends to be under-confident for the minority class in unbalanced settings (DGP 4, Figure 10 in Appendix C). In general, the combination of random forest with calibration performs well across various settings.

On the other hand, boosting-based methods, such as LGBM, tend to be over-confident. Figure 5 displays the distribution of ATE estimates for different propensity score learners under the IRM across 100 repetitions with different seeds in DGP 1. Calibration can correct for both under-confident and over-confident learners. However, the impact appears strongest for over-confident learners. For more details, we refer to Appendix C, where the robustness of our algorithms is tested with respect to the propensity and outcome learners, different clipping thresholds, and various levels of signal-to-noise ratio (DGP 1), overlap (DGP 2), and share of treated units (DGP 4).

⁶For better visualization, Algorithms 1, 2, and 4 are clipped at the 1-percent level.

⁷The corresponding figures are located in Appendix C, Figures 8 and 9.

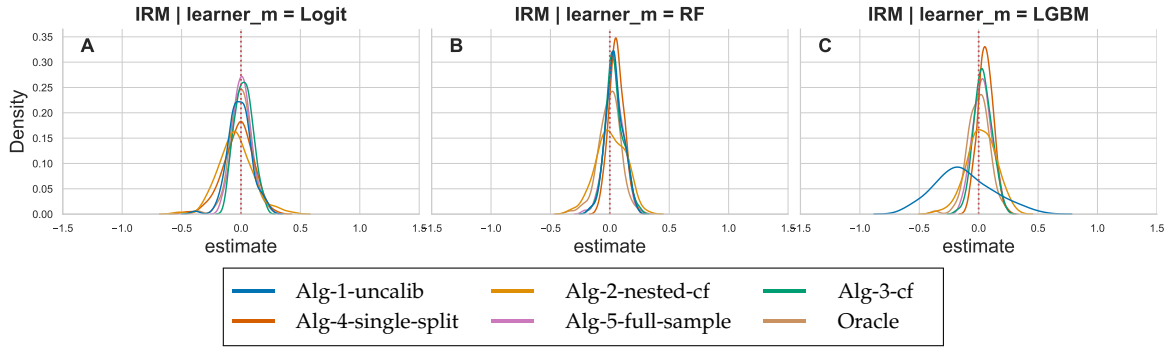


Figure 5: DGP 1, $n = 2000$, $p = 20$, $R2D = 0.5$, $m = \text{LGBM}$, $g = \text{LGBM}$

4.5.2 Findings related to previous work

We extended and adapted some of the simulation settings to gain further insights from the studies implemented by [Deshpande and Kuleshov \(2023\)](#), [Gutman et al. \(2024\)](#), [Ballinari \(2024\)](#), and [van der Laan et al. \(2024a\)](#). In our simulation study, our objective was to determine whether calibration works and to explore the best methods to achieve effective calibration.

[Deshpande and Kuleshov \(2023\)](#) employ a non-cross-fitted version of Algorithm 4, where the data is split for calibration only. They achieve significant improvements, even in logistic regression, through calibration. This result seems counterintuitive. However, given their deterministic propensity scores in the drug effectiveness DGP, it is unsurprising that logistic regression is miscalibrated. In our adapted version, DGP 2, with non-deterministic propensity scores, such large improvements are not observed. In particular, Algorithm 4 without clipping, or in combination with PLR, is not recommended based on our findings.

[Ballinari \(2024\)](#) implements the nested cross-fitting Algorithm 2. As demonstrated, nested cross-fitting combined with isotonic regression is effective only when clipping is applied. Generally, Algorithm 2 shows poor calibration properties and is not recommended for small sample sizes, where calibration has the most significant impact. The unbalanced and non-linear settings labeled “difficult” and “extreme” for DGPs 4 and 5 by [Ballinari \(2024\)](#) were tested under DGP 4 in this study. We show that either using a larger share of observations for calibration or adding 1-percent clipping allows isotonic regression to lower RMSEs for boosting-based methods and remain stable for other learners.

The instability observed in the results of [Ballinari \(2024\)](#) was also addressed by [van der Laan et al. \(2024a\)](#). The authors concluded that, in a discretized version, it is important to calibrate the treated and untreated observations separately. However, as we demonstrate, the instability of isotonic regression is more likely due to small sample size issues. Our calibration algorithms, 3 and 5, are both stable without clipping or separate calibration for treated and untreated units. The latter follows [van der Laan et al. \(2024a\)](#)’s recommendation to calibrate on the full sample using cross-fitted propensity scores.

Desirable Properties

Modern causal inference methods using weighting estimators address two core challenges: (1) achieving covariate balance, where the weighted covariate distributions satisfy $\mathbb{E}[w\mathbf{X} \mid D = 1] = \mathbb{E}[w\mathbf{X} \mid D = 0]$ for treatment $D \in \{0, 1\}$ and covariates \mathbf{X} , and (2) ensuring

normalization $\sum_{i:D_i=1} w_i = 1$ and $\sum_{i:D_i=0} w_i = 1$ to stabilize weights (Busso et al., 2014). Covariate balance is quantified via standardized mean differences (SMD):

$$\text{SMD}_k = \frac{\bar{X}_{k,D=1}^w - \bar{X}_{k,D=0}^w}{\sqrt{(s_{k,D=1}^w)^2 + (s_{k,D=0}^w)^2 / 2}},$$

where $\bar{X}_{k,D}^w$ and $s_{k,D}^w$, with $D \in \{0,1\}$, are the weighted means and standard deviations of X_k in the treated and control groups, respectively. The SMD expresses an imbalance in standard deviation units, with $|\text{SMD}_k| < 0.1$ indicating an adequate balance (Austin and Stuart, 2015). Figure 6 demonstrates SMD reduction across methods. Entropy balancing (EBAL) minimizes KL/ Rényi divergence from uniform weights $q_i = 1/n$ under balance constraints $\sum_{i:D_i=0} w_i \phi(\mathbf{X}_i) = \frac{1}{n_1} \sum_{i:D_i=1} \phi(\mathbf{X}_i)$ (Hainmueller, 2012).

OptimWeight solves $\min_w \sum_{i:D_i=0} (w_i - 1/n_0)^2$ with ℓ_∞ -norm balance constraints $\|\frac{1}{n_1} \sum_{i:D_i=1} \mathbf{X}_i - \sum_{i:D_i=0} w_i \mathbf{X}_i\|_\infty \leq \delta$ (Zubizarreta, 2015). Covariate balancing propensity score (CBPS) estimates the propensity score $m(\mathbf{X}_i; \beta) = \text{expit}(\mathbf{X}_i^T \beta)$ via GMM, combining score equations $\sum_{i=1}^n [D_i - m(\mathbf{X}_i; \beta)] \mathbf{X}_i = 0$ with balancing moments Imai and Ratkovic (2014). Inverse probability tilting (IPT) solves dual-moment conditions for normalization $\sum D_i / m(\mathbf{X}_i; \theta) = n$ and balance $\sum D_i \mathbf{X}_i / m(\mathbf{X}_i; \theta) = \sum (1 - D_i) \mathbf{X}_i / (1 - m(\mathbf{X}_i; \theta))$ (Graham et al., 2012). GLM uses $m(\mathbf{X}_i) = \text{expit}(\mathbf{X}_i^T \hat{\beta}_{\text{MLE}})$ with normalized IPW weights. To ensure a fair comparison, only first-order moments were rebalanced in the setup of the outcome equation for the weightit approaches. Similarly, Alg-3-cf and Alg-5-full-sample used a linear outcome function without further fine-tuning, as excessive fine-tuning could bias the comparison. This means the outcome equation is misspecified for all methods. Figure 6 shows that methods from the R package weightit (Greifer, 2025) (EBAL, OptWeight, CBPS, GLM, IPT) as well as the full-sample calibrated IRM model achieve covariate balance, unlike the unadjusted IRM model. Table 4 compares performance metrics and normalization.

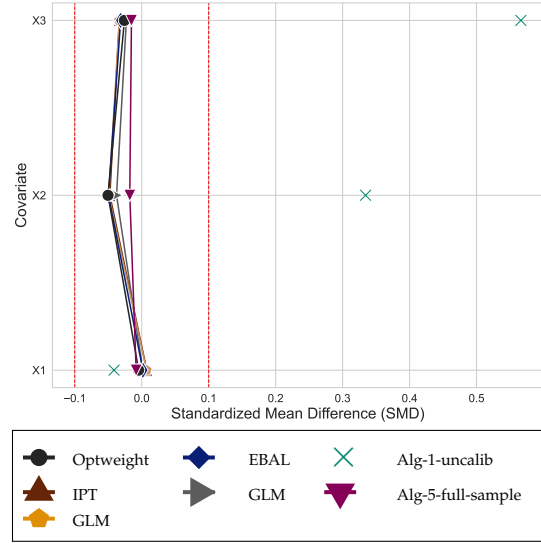


Figure 6: SMD across covariates for DGP 2. Dashed line indicates $|\text{SMD}| = 0.1$.

Table 4: Comparison under covariate balance

Method	m	Coverage	CI Length	Norm $D = 1$	Norm $D = 0$	RMSE	Std. dev.	MAE	
Alg-3-cf	isotonic	Logit	0.960	0.413	0.996	0.987	0.098	0.097	0.077
Alg-3-cf	isotonic	RF	0.960	0.389	0.997	0.994	0.096	0.094	0.075
Alg-3-cf	platt	Logit	0.960	0.388	1.003	0.984	0.094	0.093	0.075
Alg-3-cf	platt	RF	0.940	0.358	0.984	0.961	0.092	0.091	0.072
Alg-5-full-sample	isotonic	Logit	0.970	0.404	0.999	0.998	0.097	0.095	0.077
Alg-5-full-sample	isotonic	RF	0.940	0.386	1.000	1.000	0.095	0.094	0.075
Alg-5-full-sample	platt	Logit	0.960	0.397	1.003	0.996	0.094	0.093	0.075
Alg-5-full-sample	platt	RF	0.950	0.373	0.998	0.988	0.094	0.093	0.074
Cbps	weighted	Logit	0.950	0.371	1.000	1.000	0.094	0.093	0.074
Ebal	weighted	-	0.950	0.376	1.000	1.000	0.094	0.093	0.074
Glm	weighted	Logit	0.950	0.371	1.000	1.000	0.094	0.093	0.075
lpt	weighted	Logit	0.950	0.371	1.000	1.000	0.094	0.093	0.075
Optweight	weighted	-	0.960	0.376	1.000	1.000	0.093	0.092	0.074

DGP 2: $n = 2000$, $p = 3$, overlap = 0.5, Clip = $1e-12$ g = Linear

All weighting methods enforce exact normalization via $\mathbb{E}[D/m(\mathbf{X})] = 1$ and $\mathbb{E}[(1 - D)/(1 - m(\mathbf{X}))] = 1$ (columns ‘Norm $D = 1$ ’ and ‘Norm $D = 0$ ’), ensuring weight stability. Full-sample calibration achieves higher levels of normalization compared to their cross-fitted counterparts. However, the remaining small deviations from optimally normalized weights do not deteriorate performance.

5 Acknowledgment

This work was partly funded by the Bavarian Joint Research Program (BayVFP) – Digitization (Funding reference: DIK0294/01). Economic AI kindly thanks the the VDI/VDE-IT Munich for the organization and the Free State of Bavaria for the financial support.

References

- P. C. Austin and E. A. Stuart. Moving towards best practice when using inverse probability of treatment weighting (iptw) using the propensity score to estimate causal treatment effects in observational studies. *Statistics in Medicine*, 34(28):3661–3679, 2015. doi: <https://doi.org/10.1002/sim.6607>. URL <https://onlinelibrary.wiley.com/doi/abs/10.1002/sim.6607>.
- P. Bach, V. Chernozhukov, M. S. Kurz, and M. Spindler. DoubleML – An object-oriented implementation of double machine learning in Python. *Journal of Machine Learning Research*, 23(53):1–6, 2022. URL <http://jmlr.org/papers/v23/21-0862.html>.
- P. Bach, M. S. Kurz, V. Chernozhukov, M. Spindler, and S. Klaassen. DoubleML: An object-oriented implementation of double machine learning in R. *Journal of Statistical Software*, 108(3):1–56, 2024. doi: 10.18637/jss.v108.i03. arXiv:2103.09603 [stat.ML].
- Y. Bai, S. Mei, H. Wang, and C. Xiong. Don’t just blame over-parametrization for over-confidence: Theoretical analysis of calibration in binary classification, 2021. URL <https://arxiv.org/abs/2102.07856>.
- D. Ballinari. Calibrating doubly-robust estimators with unbalanced treatment assignment, 2024.

- D. Ballinari and N. Bearth. Improving the finite sample estimation of average treatment effects using double/debiased machine learning with propensity score calibration, 2025. URL <https://arxiv.org/abs/2409.04874>.
- R. E. Barlow and H. D. Brunk. The isotonic regression problem and its dual. *Journal of the American Statistical Association*, 67(337):140–147, 1972. ISSN 01621459, 1537274X. URL <http://www.jstor.org/stable/2284712>.
- A. Belloni, V. Chernozhukov, I. Fernández-Val, and C. Hansen. Program evaluation and causal inference with high-dimensional data. *Econometrica*, 85(1):233–298, 2017.
- A. Belloni, V. Chernozhukov, D. Chetverikov, and Y. Wei. Uniformly valid post-regularization confidence regions for many functional parameters in z-estimation framework. *Annals of statistics*, 46(6B):3643, 2018.
- M. S. Birman and M. Z. Solomjak. Piecewise-polynomial approximations of functions of the classes w_p^α . *Matematicheskii Sbornik*, 73 (115)(3):295–317, 1967.
- M. Busso, J. DiNardo, and J. McCrary. New evidence on the finite sample properties of propensity score reweighting and matching estimators. *The Review of Economics and Statistics*, 96(5):885–897, 2014. ISSN 00346535, 15309142. URL <http://www.jstor.org/stable/43554965>.
- J. Blasiok, P. Gopalan, L. Hu, and P. Nakkiran. When does optimizing a proper loss yield calibration?, 2023. URL <https://arxiv.org/abs/2305.18764>.
- V. Chernozhukov, D. Chetverikov, and K. Kato. Gaussian approximation of suprema of empirical processes. *The Annals of Statistics*, 42(4):1564 – 1597, 2014. doi: 10.1214/14-AOS1230. URL <https://doi.org/10.1214/14-AOS1230>.
- V. Chernozhukov, D. Chetverikov, M. Demirer, E. Duflo, C. Hansen, W. Newey, and J. Robins. Double/debiased machine learning for treatment and structural parameters. *The Econometrics Journal*, 21(1):C1–C68, 2018. doi: <https://doi.org/10.1111/ectj.12097>.
- V. Chernozhukov, W. K. Newey, and R. Singh. Automatic Debiased Machine Learning of Causal and Structural Effects. *Econometrica*, 90(3):967–1027, May 2022. doi: 10.3982/ECTA18515.
- V. Chernozhukov, W. K. Newey, V. Quintas-Martinez, and V. Syrgkanis. Automatic debiased machine learning via riesz regression, 2024. URL <https://arxiv.org/abs/2104.14737>.
- D. R. COX. Two further applications of a model for binary regression. *Biometrika*, 45(3-4): 562–565, 12 1958. ISSN 0006-3444. doi: 10.1093/biomet/45.3-4.562. URL <https://doi.org/10.1093/biomet/45.3-4.562>.
- A. P. Dawid. *Probability Forecasting*. John Wiley & Sons, Ltd, 2014. ISBN 9781118445112. doi: <https://doi.org/10.1002/9781118445112.stat02978>. URL <https://onlinelibrary.wiley.com/doi/abs/10.1002/9781118445112.stat02978>.
- S. Deshpande and V. Kuleshov. Calibrated propensity scores for causal effect estimation. *arXiv preprint arXiv:2306.00382*, 2023.

- J. H. Friedman. Multivariate adaptive regression splines. *The Annals of Statistics*, 19(1):1–67, 1991.
- D. Gamarnik. Efficient learning of monotone concepts via quadratic optimization. In *Proceedings of the eleventh annual conference on computational learning theory*, pages 134–143, 1998.
- S. A. Geer. *Empirical Processes in M-estimation*, volume 6. Cambridge university press, 2000.
- T. Gneiting. Calibration of medium-range weather forecasts, 03/2014 2014. URL <https://www.ecmwf.int/node/9607>.
- T. Gneiting and R. Ranjan. Combining predictive distributions. *Electronic Journal of Statistics*, 7, 06 2011. doi: 10.1214/13-EJS823.
- T. Gneiting, F. Balabdaoui, and A. E. Raftery. Probabilistic forecasts, calibration and sharpness. *Journal of the Royal Statistical Society: Series B (Statistical Methodology)*, 69(2):243–268, 2007. doi: <https://doi.org/10.1111/j.1467-9868.2007.00587.x>. URL <https://rss.onlinelibrary.wiley.com/doi/abs/10.1111/j.1467-9868.2007.00587.x>.
- B. S. Graham, C. C. De Xavier Pinto, and D. Egel. Inverse probability tilting for moment condition models with missing data. *The Review of Economic Studies*, 79(3):1053–1079, 04 2012. ISSN 0034-6527. doi: 10.1093/restud/rdr047. URL <https://doi.org/10.1093/restud/rdr047>.
- N. Greifer. *WeightIt: Weighting for Covariate Balance in Observational Studies*, 2025. URL <https://ngreifer.github.io/WeightIt/>. R package version 1.4.0, <https://github.com/ngreifer/WeightIt>.
- C. Gupta and A. K. Ramdas. Distribution-free calibration guarantees for histogram binning without sample splitting, 2021. URL <https://arxiv.org/abs/2105.04656>.
- C. Gupta, A. Podkopaev, and A. Ramdas. Distribution-free binary classification: prediction sets, confidence intervals and calibration. In H. Larochelle, M. Ranzato, R. Hadsell, M. Balcan, and H. Lin, editors, *Advances in Neural Information Processing Systems*, volume 33, pages 3711–3723. Curran Associates, Inc., 2020. URL https://proceedings.neurips.cc/paper_files/paper/2020/file/26d88423fc6da243ffddf161ca712757-Paper.pdf.
- R. Gutman, E. Karavani, and Y. Shimoni. Improving inverse probability weighting by post-calibrating its propensity scores. *Epidemiology*, 35(4):473–480, Apr. 2024. ISSN 1044-3983. doi: 10.1097/ede.0000000000001733. URL <http://dx.doi.org/10.1097/EDE.0000000000001733>.
- J. Hainmueller. Entropy balancing for causal effects: A multivariate reweighting method to produce balanced samples in observational studies. *Political Analysis*, 20(1):25–46, 2012. doi: 10.1093/pan/mpr025.
- K. Imai and M. Ratkovic. Covariate balancing propensity score. *Journal of the Royal Statistical Society Series B*, 76(1):243–263, 2014.

- G. Imbens. Nonparametric estimation of average treatment effects under exogeneity: A review. *The Review of Economics and Statistics*, 86:4–29, 02 2004. doi: 10.1162/003465304323023651.
- U. Johansson, T. Lofström, and C. Sönströd. Well-calibrated probabilistic predictive maintenance using venn-abers, 2023. URL <https://arxiv.org/abs/2306.06642>.
- G. Ke, Q. Meng, T. Finley, T. Wang, W. Chen, W. Ma, Q. Ye, and T.-Y. Liu. Lightgbm: A highly efficient gradient boosting decision tree. *Advances in neural information processing systems*, 30:3146–3154, 2017.
- A. Kumar, P. S. Liang, and T. Ma. Verified uncertainty calibration. In H. Wallach, H. Larochelle, A. Beygelzimer, F. d'Alché-Buc, E. Fox, and R. Garnett, editors, *Advances in Neural Information Processing Systems*, volume 32. Curran Associates, Inc., 2019. URL https://proceedings.neurips.cc/paper_files/paper/2019/file/f8c0c968632845cd133308b1a494967f-Paper.pdf.
- S. R. Künzel, J. S. Sekhon, P. J. Bickel, and B. Yu. Metalearners for estimating heterogeneous treatment effects using machine learning. *Proceedings of the National Academy of Sciences*, 116(10):4156–4165, Feb. 2019. ISSN 1091-6490. doi: 10.1073/pnas.1804597116. URL <http://dx.doi.org/10.1073/pnas.1804597116>.
- A. Lambrou, H. Papadopoulos, I. Nourtdinov, and A. Gammerman. Reliable probability estimates based on support vector machines for large multiclass datasets. *IFIP Advances in Information and Communication Technology*, 382:182–191, 09 2012. doi: 10.1007/978-3-642-33412-2_19.
- Y. Li and P. Sur. Optimal and provable calibration in high-dimensional binary classification: Angular calibration and platt scaling, 2025. URL <https://arxiv.org/abs/2502.15131>.
- E. Mammen and K. Yu. Additive isotone regression. *Lecture Notes-Monograph Series*, pages 179–195, 2007.
- P. M. Naeni, G. Cooper, and M. Hauskrecht. Obtaining well calibrated probabilities using bayesian binning. *Proceedings of the ... AAAI Conference on Artificial Intelligence. AAAI Conference on Artificial Intelligence*, 2015:2901–2907, 04 2015. doi: 10.1609/aaai.v29i1.9602.
- K. Nguyen and B. O'Connor. Posterior calibration and exploratory analysis for natural language processing models. *arXiv preprint arXiv:1508.05154*, 2015.
- A. Niculescu-Mizil and R. Caruana. Predicting good probabilities with supervised learning. In *Proceedings of the 22nd International Conference on Machine Learning, ICML '05*, page 625–632, New York, NY, USA, 2005. Association for Computing Machinery. ISBN 1595931805. doi: 10.1145/1102351.1102430. URL <https://doi.org/10.1145/1102351.1102430>.
- X. Nie and S. Wager. Quasi-oracle estimation of heterogeneous treatment effects. *Biometrika*, 108(2):299–319, 2020. ISSN 0006-3444.

- J. Nixon, M. Dusenberry, G. Jerfel, T. Nguyen, J. Liu, L. Zhang, and D. Tran. Measuring calibration in deep learning, 2020. URL <https://arxiv.org/abs/1904.01685>.
- I. Nouretdinov, D. Volkhonskiy, P. Lim, P. Toccaceli, and A. Gammerman. Inductive Venn-Abers predictive distribution. In A. Gammerman, V. Vovk, Z. Luo, E. Smirnov, and R. Peeters, editors, *Proceedings of the Seventh Workshop on Conformal and Probabilistic Prediction and Applications*, volume 91 of *Proceedings of Machine Learning Research*, pages 15–36. PMLR, 11–13 Jun 2018. URL <https://proceedings.mlr.press/v91/nouretdinov18a.html>.
- F. Pedregosa, G. Varoquaux, A. Gramfort, V. Michel, B. Thirion, O. Grisel, M. Blondel, P. Prettenhofer, R. Weiss, V. Dubourg, J. Vanderplas, A. Passos, D. Cournapeau, M. Brucher, M. Perrot, and E. Duchesnay. Scikit-learn: Machine learning in Python. *Journal of Machine Learning Research*, 12:2825–2830, 2011.
- F. Pedregosa, G. Varoquaux, A. Gramfort, V. Michel, B. Thirion, O. Grisel, M. Blondel, A. Müller, J. Nothman, G. Louppe, P. Prettenhofer, R. Weiss, V. Dubourg, J. Vanderplas, A. Passos, D. Cournapeau, M. Brucher, M. Perrot, and Édouard Duchesnay. Scikit-learn: Machine learning in python, 2018. URL <https://arxiv.org/abs/1201.0490>.
- I. Petej. venn-abers. <https://github.com/ip200/venn-abers>, 2024.
- J. Platt. Probabilistic outputs for support vector machines and comparisons to regularized likelihood methods. *Advances in large margin classifiers*, 10(3):61–74, 1999.
- P. R. Rosenbaum and D. B. Rubin. The central role of the propensity score in observational studies for causal effects. *Biometrika*, 70(1):41–55, 1983.
- Y. Sun, P. Chaudhari, I. J. Barnett, and E. Dobriban. A confidence interval for the ℓ_2 expected calibration error, 2024. URL <https://arxiv.org/abs/2408.08998>.
- Z. Toth, O. Talagrand, and Y. Zhu. *The attributes of forecast systems: a general framework for the evaluation and calibration of weather forecasts*, page 584–595. Cambridge University Press, 2006.
- A. v. d. Vaart and J. A. Wellner. Empirical processes. In *Weak Convergence and Empirical Processes: With Applications to Statistics*, pages 127–384. Springer, 2023.
- L. van der Laan and A. M. Alaa. Self-calibrating conformal prediction, 2024. URL <https://arxiv.org/abs/2402.07307>.
- L. van der Laan, E. Ulloa-Perez, M. Carone, and A. Luedtke. Causal isotonic calibration for heterogeneous treatment effects. In A. Krause, E. Brunskill, K. Cho, B. Engelhardt, S. Sabato, and J. Scarlett, editors, *Proceedings of the 40th International Conference on Machine Learning*, volume 202 of *Proceedings of Machine Learning Research*, pages 34831–34854. PMLR, 23–29 Jul 2023. URL <https://proceedings.mlr.press/v202/van-der-laan23a.html>.
- L. van der Laan, Z. Lin, M. Carone, and A. Luedtke. Stabilized inverse probability weighting via isotonic calibration, 2024a. URL <https://arxiv.org/abs/2411.06342>.

- L. van der Laan, A. Luedtke, and M. Carone. Automatic doubly robust inference for linear functionals via calibrated debiased machine learning, 2024b. URL <https://arxiv.org/abs/2411.02771>.
- V. Vovk and I. Petej. Venn-abers predictors, 2014. URL <https://arxiv.org/abs/1211.0025>.
- V. Vovk, G. Shafer, and I. Nourtdinov. Self-calibrating probability forecasting. In *Advances in Neural Information Processing Systems 16 - Proceedings of the 2003 Conference, NIPS 2003*, Advances in Neural Information Processing Systems. Neural information processing systems foundation, 2004. ISBN 0262201526. 17th Annual Conference on Neural Information Processing Systems, NIPS 2003 ; Conference date: 08-12-2003 Through 13-12-2003.
- V. Vovk, I. Petej, and V. Fedorova. Large-scale probabilistic predictors with and without guarantees of validity. *CoRR*, abs/1511.00213, 2015.
- M. V. Wüthrich and J. Ziegel. Isotonic recalibration under a low signal-to-noise ratio. *arXiv preprint arXiv:2301.02692*, 2023.
- F. Yang and R. F. Barber. Contraction and uniform convergence of isotonic regression, 2019. URL <https://doi.org/10.1214/18-EJS1520>.
- B. Zadrozny and C. Elkan. Obtaining calibrated probability estimates from decision trees and naive bayesian classifiers. *ICML*, 1, 05 2001.
- B. Zadrozny and C. Elkan. Transforming classifier scores into accurate multiclass probability estimates. In *Proceedings of the Eighth ACM SIGKDD International Conference on Knowledge Discovery and Data Mining, KDD '02*, page 694–699, New York, NY, USA, 2002. Association for Computing Machinery. ISBN 158113567X. doi: 10.1145/775047.775151. URL <https://doi.org/10.1145/775047.775151>.
- C.-H. Zhang. Risk bounds in isotonic regression. *The Annals of Statistics*, 30(2):528 – 555, 2002. doi: 10.1214/aos/1021379864. URL <https://doi.org/10.1214/aos/1021379864>.
- J. R. Zubizarreta. Stable weights that balance covariates for estimation with incomplete outcome data. *Journal of the American Statistical Association*, 110(511):910–922, 2015. doi: 10.1080/01621459.2015.1023805. URL <https://doi.org/10.1080/01621459.2015.1023805>.

A Proofs

A.1 Proofs for Section 2

It holds

$$\begin{aligned}
& \|\hat{m}(X) - m_0(X)\|_{P,2}^2 \\
&= \mathbb{E} \left[(m_0(X) - \mathbb{E}[m_0(X)|\hat{m}(X)] + \mathbb{E}[m_0(X)|\hat{m}(X)] - \hat{m}(X))^2 \right] \\
&= \mathbb{E} \left[\mathbb{E} \left[(m_0(X) - \mathbb{E}[m_0(X)|\hat{m}(X)] + \mathbb{E}[m_0(X)|\hat{m}(X)] - \hat{m}(X))^2 | \hat{m}(X) \right] \right] \\
&= \mathbb{E} \left[\text{Var}(m_0(X)|\hat{m}(X)) \right] + \|\mathbb{E}[m_0(X)|\hat{m}(X)] - \hat{m}(X)\|_{P,2}^2 \\
&\quad + 2\mathbb{E} \left[\left(\mathbb{E}[m_0(X)|\hat{m}(X)] - \hat{m}(X) \right) \underbrace{\mathbb{E} \left[(m_0(X) - \mathbb{E}[m_0(X)|\hat{m}(X)]) | \hat{m}(X) \right]}_{=0} \right]
\end{aligned}$$

such that

$$\|\hat{m}(X) - m_0(X)\|_{P,2} = \left(\mathbb{E} \left[\text{Var}(m_0(X)|\hat{m}(X)) \right] + \|\mathbb{E}[m_0(X)|\hat{m}(X)] - \hat{m}(X)\|_{P,2}^2 \right)^{1/2}.$$

Proof of Lemma 1.

Under Assumption 1 we can decompose the root-mean-squared-error as follows

$$\begin{aligned}
\|\tilde{m}(X) - m_0(X)\|_{P,2} &\leq \underbrace{\|\tilde{m}(X) - \mathbb{E}[D|\hat{m}(X)]\|_{P,2}}_{\leq \tilde{\epsilon}_N} + \|\mathbb{E}[D|\hat{m}(X)] - m_0(X)\|_{P,2} \\
&\leq \left(\mathbb{E} \left[\text{Var}(m_0(X)|\hat{m}(X)) \right] \right)^{1/2} + \tilde{\epsilon}_N
\end{aligned}$$

due to

$$\begin{aligned}
\|\mathbb{E}[D|\hat{m}(X)] - m_0(X)\|_{P,2}^2 &= \|\mathbb{E}[m_0(X)|\hat{m}(X)] - m_0(X)\|_{P,2}^2 \\
&= \mathbb{E} \left[\mathbb{E} \left[(m_0(X) - \mathbb{E}[m_0(X)|\hat{m}(X)])^2 | \hat{m}(X) \right] \right] \\
&= \mathbb{E} \left[\text{Var}(m_0(X)|\hat{m}(X)) \right].
\end{aligned}$$

Here, we used that

$$\sigma(\hat{m}(X)) \subseteq \sigma(X),$$

such that

$$\mathbb{E}[m_0(X)|\hat{m}(X)] = \mathbb{E}[\mathbb{E}[D|X]|\hat{m}(X)] = \mathbb{E}[D|\hat{m}(X)].$$

□

A.2 Proofs for Section 3

For any $k \in \{1, \dots, K\}$, we use the following empirical process notation

$$\mathbf{G}_{n,k}[\phi(W)] = \frac{1}{\sqrt{n}} \sum_{i \in I_k} \left(\phi(W_i) - \int \phi(w) dP_N \right)$$

for any P_N -integrable function ϕ on \mathcal{W} .

Proof of Theorem 1.

This proof adjusts the proof of Theorem 3.1 in Chernozhukov et al. (2018). Upon inspecting the Step 1 (DML2 case) of the proof of Theorem 3.1 in Chernozhukov et al. (2018), it is worth noting that the only terms which are affected by the calibration are

$$\begin{aligned} \tilde{R}_{N,1} &:= \frac{1}{K} \sum_{k=1}^K \mathbb{E}_{n,k} \left[\psi^a \left(W; (\hat{\eta}_{0,k}^{(1)}, \tilde{\eta}_{0,k}^{(2)}) \right) \right] - \mathbb{E} \left[\psi^a \left(W; (\eta_{0,k}^{(1)}, \eta_{0,k}^{(2)}) \right) \right] \\ \tilde{R}_{N,2} &:= \frac{1}{K} \sum_{k=1}^K \mathbb{E}_{n,k} \left[\psi \left(W; \theta_0, (\hat{\eta}_{0,k}^{(1)}, \tilde{\eta}_{0,k}^{(2)}) \right) \right] - \frac{1}{N} \sum_{i=1}^N \psi \left(W; \theta_0, (\eta_{0,k}^{(1)}, \eta_{0,k}^{(2)}) \right) \end{aligned}$$

as the other terms do not depend on the calibrated element $\tilde{\eta}_{0,k}^{(2)}$. First, we focus on the term $\tilde{R}_{N,2}$. Following Step 3 of the proof of Theorem 3.1, we obtain by triangle inequality

$$\left| \mathbb{E}_{n,k} \left[\psi \left(W; \theta_0, (\hat{\eta}_{0,k}^{(1)}, \tilde{\eta}_{0,k}^{(2)}) \right) \right] - \frac{1}{n} \sum_{i \in I_k} \psi \left(W; \theta_0, (\eta_{0,k}^{(1)}, \eta_{0,k}^{(2)}) \right) \right| \leq \frac{\mathcal{I}_{3,k} + \mathcal{I}_{4,k}}{\sqrt{n}},$$

where

$$\begin{aligned} \mathcal{I}_{3,k} &:= \left| \mathbf{G}_{n,k} \left[\psi \left(W; \theta_0, (\hat{\eta}_{0,k}^{(1)}, \tilde{\eta}_{0,k}^{(2)}) \right) \right] - \mathbf{G}_{n,k} \left[\psi \left(W; \theta_0, (\eta_{0,k}^{(1)}, \eta_{0,k}^{(2)}) \right) \right] \right| \\ \mathcal{I}_{4,k} &:= \sqrt{n} \left| \mathbb{E} \left[\psi \left(W; \theta_0, (\hat{\eta}_{0,k}^{(1)}, \tilde{\eta}_{0,k}^{(2)}) \right) \mid (W_i)_{i \in I_k^c} \right] - \mathbb{E} \left[\psi \left(W; \theta_0, (\eta_{0,k}^{(1)}, \eta_{0,k}^{(2)}) \right) \right] \right|. \end{aligned}$$

Due to Assumption 3 it holds $(\hat{\eta}_{0,k}^{(1)}, \tilde{\eta}_{0,k}^{(2)}) \in \tilde{\mathcal{T}}_N$ with probability $\geq 1 - \Delta_N$. Define \mathcal{E}_N as the event that $(\hat{\eta}_{0,k}^{(1)}, \tilde{\eta}_{0,k}^{(2)}) \in \tilde{\mathcal{T}}_N$ for all $k \in [K]$. Therefore, $P(\mathcal{E}_N) \geq 1 - K\Delta_N$. Consequently, the whole argument of Chernozhukov et al. (2018) is still valid which implies

$$\mathcal{I}_{4,k} = O_{P_N}(\sqrt{n}(\lambda_N + \lambda'_N)).$$

Next, due to the triangle inequality

$$\begin{aligned} \mathcal{I}_{3,k} &\leq \left| \mathbf{G}_{n,k} \left[\psi \left(W; \theta_0, (\hat{\eta}_{0,k}^{(1)}, \tilde{\eta}_{0,k}^{(2)}) \right) \right] - \mathbf{G}_{n,k} \left[\psi \left(W; \theta_0, (\hat{\eta}_{0,k}^{(1)}, \eta_{0,k}^{(2)}) \right) \right] \right| \\ &\quad + \left| \mathbf{G}_{n,k} \left[\psi \left(W; \theta_0, (\hat{\eta}_{0,k}^{(1)}, \eta_{0,k}^{(2)}) \right) \right] - \mathbf{G}_{n,k} \left[\psi \left(W; \theta_0, (\eta_{0,k}^{(1)}, \eta_{0,k}^{(2)}) \right) \right] \right| \\ &=: \mathcal{I}_{3,k}^{(1)} + \mathcal{I}_{3,k}^{(2)}, \end{aligned}$$

where $\mathcal{I}_{3,k}^{(2)} = O_{P_N}(r'_N)$ by Assumption 3.2, see Chernozhukov et al. (2018). To bound $\mathcal{I}_{3,k}^{(1)}$, we rely on classical empirical process theory. Since conditionally on $(W_i)_{i \in I_k^c}$ the $\hat{\eta}_{0,k}^{(1)}$ is non-

stochastic, remark that

$$\begin{aligned}
& \mathbb{E} \left[\mathcal{I}_{3,k}^{(1)} | (W_i)_{i \in I_k^c} \right] \\
&= \mathbb{E} \left[\left| \mathbf{G}_{n,k} \left[\psi \left(W; \theta_0, (\hat{\eta}_{0,k}^{(1)}, \tilde{\eta}_{0,k}^{(2)}) \right) \right] - \mathbf{G}_{n,k} \left[\psi \left(W; \theta_0, (\hat{\eta}_{0,k}^{(1)}, \eta_{0,k}^{(2)}) \right) \right] \right| \middle| (W_i)_{i \in I_k^c} \right] \\
&\leq \sup_{\eta^{(1)} \in \tilde{\mathcal{T}}_N^{(1)}} \mathbb{E} \left[\sup_{\eta^{(2)}: (\eta^{(1)}, \eta^{(2)}) \in \tilde{\mathcal{T}}_N} \left| \mathbf{G}_{n,k} \left[\psi \left(W; \theta_0, (\eta^{(1)}, \eta^{(2)}) \right) \right] \right. \right. \\
&\quad \left. \left. - \mathbf{G}_{n,k} \left[\psi \left(W; \theta_0, (\eta^{(1)}, \eta_{0,k}^{(2)}) \right) \right] \right| \middle| (W_i)_{i \in I_k^c} \right] \\
&\leq \sup_{\eta^{(1)} \in \tilde{\mathcal{T}}_N^{(1)}} \mathbb{E} \left[\sup_{f \in \mathcal{F}_2(\eta^{(1)})} |\mathbf{G}_{n,k}(f)| \middle| (W_i)_{i \in I_k^c} \right] \\
&\leq \sup_{\eta^{(1)} \in \tilde{\mathcal{T}}_N^{(1)}} \mathbb{E} \left[\sup_{f \in \mathcal{F}_2(\eta^{(1)})} |\mathbf{G}_{n,k}(f)| \right] \\
&= \sup_{\eta^{(1)} \in \tilde{\mathcal{T}}_N^{(1)}} \|\mathbf{G}_{n,k}\|_{\mathcal{F}_2(\eta^{(1)})}
\end{aligned}$$

where \mathcal{F}_2 is defined in Assumption 4. Let $\eta^{(1)}$ be a any element of $\tilde{\mathcal{T}}_N^{(1)}$. Relying on Theorem 5.2 of Chernozhukov et al. (2014), it holds

$$\begin{aligned}
\mathbb{E} \left[\|\mathbf{G}_{n,k}\|_{\mathcal{F}_2(\eta^{(1)})} \right] &\lesssim J \left(\delta_n, \mathcal{F}_2(\eta^{(1)}), F_2(\eta^{(1)}) \right) \|F_2(\eta^{(1)})\|_{P,2} \\
&\quad + \frac{\|M\|_{P,2} J^2 \left(\delta_n, \mathcal{F}_2(\eta^{(1)}), F_2(\eta^{(1)}) \right)}{\delta_n^2 \sqrt{n}}
\end{aligned}$$

with $\delta_n = \sigma_n / \|F_2(\eta^{(1)})\|_{P,2}$, $M = \max_{1 \leq i \leq n} F_2(\eta^{(1)})(W_i)$, where $\sup_{f \in \mathcal{F}_2(\eta^{(1)})} \mathbb{E}[f^2] \leq \sigma_n^2 \leq \|F_2(\eta^{(1)})\|_{P,2}^2$. Under Assumption 4(i) and using $\|M\|_{P,q} \leq n^{1/q} \|F_2(\eta^{(1)})\|_{P,q}$ this implies

$$\mathbb{E} \left[\|\mathbf{G}_{n,k}\|_{\mathcal{F}_2(\eta^{(1)})} \right] \lesssim u_n \|F_2(\eta^{(1)})\|_{P,2} + n^{1/q-1/2} V_n u_n^2 \frac{\|F_2(\eta^{(1)})\|_{P,2}^2}{\sigma_n^2}.$$

This enables the use of Theorem 5.1 of Chernozhukov et al. (2014) with $t = \log(n)$ such that for any fixed $\eta^{(1)} \in \tilde{\mathcal{T}}_N^{(1)}$

$$\begin{aligned}
\|\mathbf{G}_{n,k}\|_{\mathcal{F}_2(\eta^{(1)})} &\leq (1 + \alpha) \mathbb{E} \left[\|\mathbf{G}_{n,k}\|_{\mathcal{F}_2(\eta^{(1)})} \right] \\
&\quad + C(q) \left[\left(\sigma_n + \frac{\|M\|_{P,q}}{\sqrt{n}} \right) \sqrt{\log(n)} + \frac{\|M\|_{P,2} \log(n)}{\alpha \sqrt{n}} \right] \\
&\lesssim (1 + \alpha) \left(u_n \|F_2(\eta^{(1)})\|_{P,2} + n^{1/q-1/2} V_n u_n^2 \frac{\|F_2(\eta^{(1)})\|_{P,2}^2}{\sigma_n^2} \right) \\
&\quad + C(q) \left((\sigma_n + n^{1/q-1/2} V_n) \sqrt{\log(n)} + n^{1/q-1/2} V_n \frac{\log(n)}{\alpha} \right)
\end{aligned}$$

with probability $> 1 - \log(n)^{-q/2}$ for all $\alpha > 0$ and $C(q) > 0$ is a constant only depending

on q . Consequently

$$\begin{aligned} \|\mathbf{G}_{n,k}\|_{\mathcal{F}_2(\eta^{(1)})} &\lesssim u_n \|F_2(\eta^{(1)})\|_{P,2} + \sigma_n \sqrt{\log(n)} \\ &\quad + n^{1/q-1/2} V_n \left(u_n^2 \frac{\|F_2(\eta^{(1)})\|_{P,2}^2}{\sigma_n^2} \vee \log(n) \right) \\ &\leq \tilde{r}_N \end{aligned}$$

with probability $> 1 - c \log(n)^{-1}$, where \tilde{r}_N does not depend on $\eta^{(1)}$ due to growth condition 4 (iii). Hence, by Lemma 6.1 in Chernozhukov et al. (2018)

$$\mathcal{I}_{3,k}^{(1)} = O_{P_N}(\tilde{r}_N).$$

This implies that

$$|\tilde{R}_{N,2}| = O_{P_N}(N^{-1/2}(r'_N + \tilde{r}_N) + \lambda_N + \lambda'_N)$$

Next, we show $|\tilde{R}_{N,1}| = |\hat{J}_0 - J_0| = O_{P_N}(N^{-1/2} + r_N + \tilde{r}_N^a)$. As in Chernozhukov et al. (2018) it suffices to show that for any $k \in [K]$,

$$\begin{aligned} &\left| \mathbb{E}_{n,k} \left[\psi^a \left(W; (\hat{\eta}_{0,k}^{(1)}, \tilde{\eta}_{0,k}^{(2)}) \right) \right] - \mathbb{E} \left[\psi^a \left(W; (\eta_0^{(1)}, \eta_{0,k}^{(2)}) \right) \right] \right| \\ &= O_{P_N}(N^{-1/2} + r_N + \tilde{r}_N). \end{aligned}$$

It holds

$$\begin{aligned} &\left| \mathbb{E}_{n,k} \left[\psi^a \left(W; (\hat{\eta}_{0,k}^{(1)}, \tilde{\eta}_{0,k}^{(2)}) \right) \right] - \mathbb{E} \left[\psi^a \left(W; (\eta_0^{(1)}, \eta_{0,k}^{(2)}) \right) \right] \right| \\ &\leq \left| \mathbb{E}_{n,k} \left[\psi^a \left(W; (\hat{\eta}_{0,k}^{(1)}, \tilde{\eta}_{0,k}^{(2)}) \right) \right] - \mathbb{E}_{n,k} \left[\psi^a \left(W; (\hat{\eta}_{0,k}^{(1)}, \eta_0^{(2)}) \right) \right] \right| \\ &\quad + \left| \mathbb{E}_{n,k} \left[\psi^a \left(W; (\hat{\eta}_{0,k}^{(1)}, \eta_0^{(2)}) \right) \right] - \mathbb{E} \left[\psi^a \left(W; (\hat{\eta}_{0,k}^{(1)}, \eta_0^{(2)}) \right) \mid (W_i)_{i \in I_k^c} \right] \right| \\ &\quad + \left| \mathbb{E} \left[\psi^a \left(W; (\hat{\eta}_{0,k}^{(1)}, \eta_0^{(2)}) \right) \mid (W_i)_{i \in I_k^c} \right] - \mathbb{E} \left[\psi^a \left(W; (\eta_0^{(1)}, \eta_{0,k}^{(2)}) \right) \right] \right| \\ &= \mathcal{I}_{1,k}^{(1)} + \mathcal{I}_{1,k}^{(2)} + \mathcal{I}_{2,k}, \end{aligned}$$

where $\mathcal{I}_{1,k}^{(2)} = O_{P_N}(N^{-1/2})$ and $\mathcal{I}_{2,k} = O_{P_N}(r_N)$ by the same terms as in Step 2 of the proof of Theorem 3.1 in Chernozhukov et al. (2018). Next, we show $\mathcal{I}_{1,k}^{(1)} = O_{P_N}(r_N + \tilde{r}_N)$.

$$\begin{aligned} \mathcal{I}_{1,k}^{(1)} &= \left| \mathbb{E}_{n,k} \left[\psi^a \left(W; (\hat{\eta}_{0,k}^{(1)}, \tilde{\eta}_{0,k}^{(2)}) \right) \right] - \mathbb{E}_{n,k} \left[\psi^a \left(W; (\hat{\eta}_{0,k}^{(1)}, \eta_0^{(2)}) \right) \right] \right| \\ &\leq \left| \mathbf{G}_{n,k} \left[\psi^a \left(W; (\hat{\eta}_{0,k}^{(1)}, \tilde{\eta}_{0,k}^{(2)}) \right) \right] - \mathbf{G}_{n,k} \left[\psi^a \left(W; (\hat{\eta}_{0,k}^{(1)}, \eta_0^{(2)}) \right) \right] \right| \\ &\quad + \left| \mathbb{E} \left[\psi^a \left(W; (\hat{\eta}_{0,k}^{(1)}, \tilde{\eta}_{0,k}^{(2)}) \right) \right] - \mathbb{E} \left[\psi^a \left(W; (\hat{\eta}_{0,k}^{(1)}, \eta_0^{(2)}) \right) \right] \right| \end{aligned}$$

At first, remark

$$\begin{aligned}
& \left| \mathbb{E} \left[\psi^a \left(W; (\hat{\eta}_{0,k}^{(1)}, \tilde{\eta}_{0,k}^{(2)}) \right) \right] - \mathbb{E} \left[\psi^a \left(W; (\hat{\eta}_{0,k}^{(1)}, \eta_0^{(2)}) \right) \right] \right| \\
& \leq \left| \mathbb{E} \left[\psi^a \left(W; (\hat{\eta}_{0,k}^{(1)}, \tilde{\eta}_{0,k}^{(2)}) \right) \right] - \mathbb{E} \left[\psi^a \left(W; (\eta_0^{(1)}, \eta_0^{(2)}) \right) \right] \right| \\
& \quad + \left| \mathbb{E} \left[\psi^a \left(W; (\eta_0^{(1)}, \eta_0^{(2)}) \right) \right] - \mathbb{E} \left[\psi^a \left(W; (\hat{\eta}_{0,k}^{(1)}, \eta_0^{(2)}) \right) \right] \right| \\
& \lesssim r_N + \tilde{r}_N^a
\end{aligned}$$

by Assumption 4 (ii). Further, with the same argument as above

$$\begin{aligned}
& \mathbb{E} \left[\left| \mathbf{G}_{n,k} \left[\psi^a \left(W; (\hat{\eta}_{0,k}^{(1)}, \tilde{\eta}_{0,k}^{(2)}) \right) - \psi^a \left(W; (\hat{\eta}_{0,k}^{(1)}, \eta_0^{(2)}) \right) \right] \right| \middle| (W_i)_{i \in I_k^c} \right] \\
& \leq \sup_{\eta^{(1)} \in \tilde{\mathcal{T}}_N^{(1)}} \|\mathbf{G}_{n,k}\|_{\mathcal{F}_2^a(\eta^{(1)})}
\end{aligned}$$

with

$$\mathcal{F}_2^a(\eta^{(1)}) := \left\{ \psi^a \left(\cdot; (\eta^{(1)}, \eta^{(2)}) \right) - \psi^a \left(\cdot; (\eta^{(1)}, \eta_0^{(2)}) \right) \mid (\eta^{(1)}, \eta^{(2)}) \in \tilde{\mathcal{T}}_N \right\}.$$

Following the same arguments as above, combined with Assumption 4 (ii), we obtain

$$\begin{aligned}
\|\mathbf{G}_{n,k}\|_{\mathcal{F}_2^a(\eta^{(1)})} & \lesssim u_{n,a} \|F_2^a(\eta^{(1)})\|_{P,2} + \sigma_{n,a} \sqrt{\log(n)} \\
& \quad + n^{1/q-1/2} V_{n,a} \left(u_{n,a}^2 \frac{\|F_2^a(\eta^{(1)})\|_{P,2}^2}{\sigma_{n,a}^2} \vee \log(n) \right) \\
& \leq \tilde{r}_N^a.
\end{aligned}$$

Again, by Lemma 6.1 in Chernozhukov et al. (2018)

$$\mathcal{I}_{1,k}^{(1)} = O_{P_N}(r_N + \tilde{r}_N^a)$$

and therefore

$$|\tilde{R}_{N,1}| = O_{P_N} \left(N^{-1/2} + r_N + \tilde{r}_N^a \right).$$

□

Proof of Theorem 2.

The first part is an application of Theorem 5.1 Chernozhukov et al. (2018) with nuisance realization set $\tilde{\mathcal{T}}_N$.

The second part follows by verifying Assumption 4. At first remark that Assumption 4(ii) holds since

$$\psi^a(W; \eta) = -1$$

for all $\eta \in T$. Further, it holds

$$\begin{aligned} & \mathbb{E} \left[\left(\psi \left(W; \theta_0, (\eta^{(1)}, \eta^{(2)}) \right) - \psi \left(W; \theta_0, (\eta^{(1)}, \eta_0^{(2)}) \right) \right)^2 \right]^{1/2} \\ &= \left\| \psi \left(W; \theta_0, (\eta^{(1)}, \eta^{(2)}) \right) - \psi \left(W; \theta_0, (\eta^{(1)}, \eta_0^{(2)}) \right) \right\|_{P,2} \\ &\leq \mathcal{I}_1 + \mathcal{I}_2 \end{aligned}$$

with

$$\begin{aligned} \mathcal{I}_1 &:= \left\| \left(\tilde{m}(X)^{-1} - m_0(X)^{-1} \right) D(Y - g(1, X)) \right\|_{P,2} \\ \mathcal{I}_2 &:= \left\| \left((1 - \tilde{m}(X))^{-1} - (1 - m_0(X))^{-1} \right) (1 - D)(Y - g(0, X)) \right\|_{P,2}. \end{aligned}$$

Remark that $\epsilon \leq m_0(X) \leq 1 - \epsilon$ and $\epsilon \leq \tilde{m}(X) \leq 1 - \epsilon$, such that

$$\begin{aligned} \mathcal{I}_1 &\leq \epsilon^{-2} \|(m_0(X) - \tilde{m}(X))D(Y - g(1, X))\|_{P,2} \\ &\leq \epsilon^{-2} \|(m_0(X) - \tilde{m}(X))(g_0(1, X) + U - g(1, X))\|_{P,2} \\ &\leq \epsilon^{-2} \|(m_0(X) - \tilde{m}(X))(g_0(1, X) - g(1, X))\|_{P,2} + \epsilon^{-2} \|(m_0(X) - \tilde{m}(X))U\|_{P,2} \\ &\lesssim \|m_0(X) - \tilde{m}(X)\|_{P,2} \end{aligned}$$

since $\mathbb{E}[U^2|X] \leq C$ and $\|g - g_0\|_{P,\infty} \leq C$. With an analogous argument it holds

$$\mathcal{I}_2 \lesssim \|m_0(X) - \tilde{m}(X)\|_{P,2}.$$

This implies

$$\begin{aligned} & \sup_{f \in \mathcal{F}_2(\eta^{(1)})} \|f\|_{P,2}^2 \\ &\leq \sup_{(\eta^{(1)}, \eta^{(2)}) \in \tilde{\mathcal{T}}_N} \mathbb{E} \left[\left(\psi \left(W; \theta_0, (\eta^{(1)}, \eta^{(2)}) \right) - \psi \left(W; \theta_0, (\eta^{(1)}, \eta_0^{(2)}) \right) \right)^2 \right] \\ &\leq C \|m_0(X) - \tilde{m}(X)\|_{P,2}^2 \\ &\lesssim \epsilon_N^2. \end{aligned}$$

Further, remark that using the same argument as above

$$\begin{aligned} & \left| \psi \left(W; \theta_0, (\eta^{(1)}, \eta^{(2)}) \right) - \psi \left(W; \theta_0, (\eta^{(1)}, \eta_0^{(2)}) \right) \right| \\ &\lesssim |m_0(X) - \tilde{m}(X)| |D(Y - g(1, X)) + (1 - D)(Y - g(0, X))| \\ &\leq L(W) |m_0(X) - \tilde{m}(X)| \end{aligned}$$

where

$$\sup_{\eta^{(1)} \in \tilde{\mathcal{T}}_N^{(1)}} \|L(W)\|_{P,q} \lesssim \|U\|_{P,q} + \sup_{\eta^{(1)} \in \tilde{\mathcal{T}}_N^{(1)}} \|g_0(D, X) - g(D, X)\|_{P,q} \lesssim 1.$$

Applying Lemma O.1 from [Belloni et al. \(2018\)](#) implies

$$\begin{aligned} & \log \sup_Q N(\epsilon \|L(W)\|_{Q,2}, \mathcal{F}_2(\eta^{(1)}), \|\cdot\|_{Q,2}) \\ & \leq \log \sup_Q N(\epsilon, \mathcal{M}, \|\cdot\|_{Q,2}) \\ & \leq C\epsilon^{-1} \end{aligned}$$

by Assumption 6 (ii), where we can use 1 as an envelope for \mathcal{M} . According to the discussion of Assumption 4, it holds

$$u_n \lesssim \sigma_n^{1/2} \|F_2(\eta^{(1)})\|_{P,2}^{-1/2}.$$

Further,

$$\begin{aligned} \|F_2(\eta^{(1)})\|_{P,q} & \leq \left\| \sup_{\eta^{(2)} \in \tilde{\mathcal{T}}_N^{(2)}} \left(\psi(W; \theta_0, (\eta^{(1)}, \eta^{(2)})) - \psi(W; \theta_0, (\eta^{(1)}, \eta_0^{(2)})) \right) \right\|_{P,q} \\ & = \left\| L(W) \sup_{\eta^{(2)} \in \tilde{\mathcal{T}}_N^{(2)}} |\eta^{(2)}(X) - \eta_0^{(2)}(X)| \right\|_{P,q} \\ & \lesssim 1. \end{aligned}$$

Choose $\sigma_n = \epsilon_N \vee \log^{1/2}(n) n^{1/q-1/2}$, such that

$$\sup_{f \in \mathcal{F}_2(\eta^{(1)})} \|f\|_{P,2}^2 \leq \sigma_n^2 \leq \|F_2(\eta^{(1)})\|_{P,2}^2$$

for each $\eta^{(1)}$ and n large enough. Consequently,

$$\begin{aligned} & \sigma_n^{1/2} \sup_{\eta^{(1)} \in \tilde{\mathcal{T}}_N^{(1)}} \|F_2(\eta^{(1)})\|_{P,2}^{1/2} + \sigma_n \sqrt{\log(n)} \\ & \quad + n^{1/q-1/2} V_n \left(\frac{\sup_{\eta^{(1)} \in \tilde{\mathcal{T}}_N^{(1)}} \|F_2(\eta^{(1)})\|_{P,2}}{\sigma_n} \vee \log(n) \right) \\ & \leq C\sigma_n + \sigma_n \sqrt{\log(n)} + Cn^{1/q-1/2} (\sigma_n^{-1} \vee \log(n)) \\ & = o(1). \end{aligned}$$

□

B Details on the DGPs

DGP 2 Drug Effectiveness, Detailed Description

In our second DGP, data units were generated as follows:

- Gender indicator X_1 and age X_2 are simulated as:

$$X_1 \sim \text{Bin}(0, 0.5), \quad X_2 \sim \Gamma(\kappa_{\text{age}}, \psi_{\text{age}}).$$

The distribution of age is gender dependent:

$$\kappa_{\text{age}} = \left(\frac{\mu_{\text{age}}}{\sigma_{\text{age}}} \right)^2, \quad \psi_{\text{age}} = \frac{\sigma_{\text{age}}^2}{\mu_{\text{age}}}, \text{ and}$$

$$\mu_{\text{age}} = \begin{cases} 49 & \text{if } X_1 = 1, \\ 51 & \text{if } X_1 = 0, \end{cases} \quad \sigma_{\text{age}} = \begin{cases} 7 & \text{if } X_1 = 1, \\ 8 & \text{if } X_1 = 0. \end{cases}$$

- Disease severity X_3 is simulated based on age:

$$\mu_{\text{disease}} = \text{clip} \left(\frac{X_2 - 20}{20}, 0.1, 5 \right), \quad X_3 \sim \text{Beta}(\mu_{\text{disease}}, 2).$$

- Propensity scores are generated using linear predictors, incorporating adjustable levels of overlap through the parameter β :

$$\text{coefficients} = \begin{bmatrix} (-0.4, 0.2, 0.8), \\ (-0.4 + 2(1 - \beta), 0.2, 0.8), \\ (-0.4 + 2(1 - \beta), 0.3, 1), \\ (-0.4 + 2(1 - \beta), 0.1, 1.2), \\ (-0.4 + 2(1 - \beta), 0.1, 1.2) \end{bmatrix},$$

$$\begin{aligned} \text{linear_predictors} &= \left(b_0 + b_1 \cdot \text{normalize}(X_2) + b_2 \cdot \text{normalize}(X_3) \right. \\ &\quad \left. + \epsilon \mid (b_0, b_1, b_2) \in \text{coefficients} \right), \\ \epsilon &\sim \mathcal{N}(0, 0.5). \end{aligned}$$

Propensity scores are computed via logistic transformation:

$$\text{prop_scores} = \left[\frac{1}{1 + \exp(-\text{lp})} \mid \text{lp} \in \text{linear_predictors} \right].$$

- Treatment assignment m_0 is initialized with $\text{prop_scores}[0]$ and updated based on con-

ditions:

$$\text{conditions} = \begin{cases} ((X_1 = 0) \text{ and } (X_2 > 55) \text{ and } (X_3 \leq 0.55), \text{prop_scores}[1]), \\ ((X_1 = 1) \text{ and } (X_2 > 55) \text{ and } (X_3 \leq 0.55), \text{prop_scores}[2]), \\ ((X_1 = 0) \text{ and } (X_3 > 0.55), \text{prop_scores}[3]), \\ ((X_1 = 1) \text{ and } (X_3 > 0.55), \text{prop_scores}[4]) \end{cases}$$

for $(\text{condition}, \text{score}) \in \text{conditions} : m_0[\text{condition}] = \text{score}[\text{condition}]$.

Final treatment assignment D_i is:

$$D_i \sim \text{Bin}(1, m_0).$$

- The outcome Y_i is simulated as:

$$Y_{di} = \text{Pois}(2 + 0.5X_1 + 0.03X_2 + 2X_3 - d), \quad Y_i = D_i \cdot Y_{1i} + (1 - D_i) \cdot Y_{0i}.$$

This DGP captures complex relationships between gender, age, disease severity, and treatment assignment, providing a realistic framework for evaluating causal inference methods. The treatment assignments are highly nonlinear and resemble decision trees with underlying local linearities.

DGP 3 Nonlinear, Detailed Description

For the nonlinear outcome regression, the detailed data generation process is as follows:

$$X \sim \text{Unif}[-1, 1]^4, \quad D|X \sim \text{Bin}(1, p(X)), \quad Y \sim \text{Bin}(1, \mu(X, D))$$

with the treatment assignment probability given by:

$$p(X) = \text{expit}\{-0.25 - X_1 + 0.5X_2 - X_3 + 0.5X_4\}.$$

The outcome function is based on nonlinear transformations of the covariates, with added treatment effect interactions.

$$\begin{aligned} \mu(X, D) &= 1.5 + 1.5D + 2D|X_1||X_2| - 2.5(1 - D)|X_2|X_3 + 2.5X_3 \\ &+ 2.5(1 - D)\sqrt{|X_4|} - 1.5D \cdot I(X_2 < 0.5) + 1.5(1 - D)I(X_4 < 0). \end{aligned}$$

The outcome is then generated by:

$$Y_d \sim \text{N}(\mu(X, D), 1), \quad Y = DY_1 + (1 - D)Y_0.$$

DGP 4 Unbalanced, Detailed Description

The unbalanced treatment assignment setting follows [Ballinari \(2024\)](#) and is adapted

from Nie and Wager (2020).

$$X_i \sim \text{Unif}[0, 1]^{20}, \quad D|X \sim \text{Bin}(1, p(X)), \quad \epsilon_i \stackrel{\text{iid}}{\sim} \mathcal{N}(0, 1),$$

$$Y = b(X) + (D - 0.5)(X_1 + X_2) + \epsilon_i.$$

The baseline main effect is the scaled Friedman (1991) function:

$$b(X_i) = \sin(\pi X_1 X_2) + 2(X_3 - 0.5)^2 + X_4 + 0.5X_5.$$

For the propensity score, we follow Künzel et al. (2019) and set:

$$m_0(X) = \alpha (1 + \beta_{2,4}(\min(X_1, X_2))),$$

where $\beta_{2,4}(\cdot)$ is the beta cumulative distribution function with shape parameters 2 and 4. This unbalanced setting entails difficult nuisance components and an easy treatment effect function, favoring doubly robust causal models compared to IPW.

The share of treated is $\mathbb{E}[D] = (31/21)\alpha$. Three settings of the share of treated $\mathbb{E}[D]$ are tested: $\mathbb{E}[D] \in \{0.05, 0.1, 0.2\}$. For unbalanced applications, several adjustments for ATE estimators exist to address positivity violations. The most commonly used method is clipping the propensity scores to preset levels. Throughout our simulations, we tested three different levels of clipping thresholds.

As Imbens (2004) points out, for the IPTW with $n = 4000$ observations, choosing a clipping cut-off at 0.01 ⁸ limits the contribution of a single observation to 0.025. We also tested more severe clipping as employed in Nie and Wager (2020), with a clipping level at 0.1, and alternatively, without clipping⁹. Particularly, for the setting with only 5% treated, we expect that a clipping threshold of 0.1 introduces a strong bias.

⁸Given the majority non-treatment class, a lower threshold is sufficient.

⁹To ensure computational stability we set the threshold at $1e - 12$.

C Detailed Simulation Results

Table 5: IPW Results 2

DGP	Method	m = Logit			m = Random Forest			m = LGBM		
		MAE	RMSE	Std. dev.	MAE	RMSE	Std. dev.	MAE	RMSE	Std. dev.
1	Alg-1-Clipped	0.08	0.11	0.11	0.18	0.19	0.06	0.94	0.98	0.31
	Alg-1-Uncalib	0.10	0.16	0.16	1.09e+06	1.09e+07	1.09e+07	1.57	1.77	0.83
	Alg-2-nested-cf-IVAP	0.10	0.12	0.09	0.14	0.15	0.07	0.17	0.19	0.08
	Alg-2-nested-cf-Iso	0.20	0.25	0.19	0.13	0.17	0.16	0.13	0.16	0.16
	Alg-2-nested-cf-Platt	0.10	0.17	0.17	0.14	0.15	0.06	0.22	0.23	0.06
	Alg-3-cf-IVAP	0.11	0.13	0.07	0.14	0.16	0.07	0.17	0.18	0.07
	Alg-3-cf-Iso	0.09	0.11	0.07	0.13	0.15	0.06	0.15	0.17	0.06
	Alg-3-cf-Platt	0.13	0.14	0.06	0.35	0.36	0.05	0.31	0.31	0.05
	Alg-4-single-split-IVAP	0.11	0.12	0.07	0.31	0.31	0.03	0.33	0.33	0.04
	Alg-4-single-split-Iso	0.13	0.18	0.16	0.30	0.30	0.03	0.32	0.32	0.04
	Alg-4-single-split-Platt	0.10	0.12	0.09	0.16	0.17	0.06	0.23	0.24	0.06
	Alg-5-full-sample-IVAP	0.08	0.10	0.08	0.12	0.14	0.07	0.14	0.16	0.07
	Alg-5-full-sample-Iso	0.07	0.09	0.08	0.12	0.14	0.06	0.14	0.16	0.07
Alg-5-full-sample-Platt	0.09	0.11	0.10	0.14	0.16	0.06	0.22	0.22	0.05	
2	Alg-1-Clipped	0.09	0.12	0.11	4.45	4.59	1.11	2.67	2.74	0.61
	Alg-1-Uncalib	0.09	0.12	0.11	1.17e+10	1.37e+10	7.23e+09	2.86	2.98	0.81
	Alg-2-nested-cf-IVAP	0.21	0.26	0.26	0.28	0.33	0.26	0.29	0.33	0.25
	Alg-2-nested-cf-Iso	0.60	0.81	0.66	0.47	0.61	0.61	0.48	0.64	0.62
	Alg-2-nested-cf-Platt	0.20	0.25	0.25	0.29	0.34	0.24	0.29	0.34	0.23
	Alg-3-cf-IVAP	0.10	0.12	0.12	0.21	0.24	0.12	0.20	0.23	0.11
	Alg-3-cf-Iso	0.09	0.11	0.11	0.21	0.24	0.11	0.20	0.23	0.11
	Alg-3-cf-Platt	0.13	0.16	0.11	0.44	0.45	0.11	0.50	0.51	0.10
	Alg-4-single-split-IVAP	0.11	0.14	0.14	0.96	0.97	0.14	0.90	0.91	0.11
	Alg-4-single-split-Iso	0.61	0.77	0.53	0.95	0.96	0.14	0.87	0.88	0.11
	Alg-4-single-split-Platt	0.10	0.12	0.11	0.26	0.28	0.12	0.27	0.29	0.11
	Alg-5-full-sample-IVAP	0.09	0.11	0.11	0.20	0.22	0.11	0.18	0.20	0.11
	Alg-5-full-sample-Iso	0.09	0.11	0.11	0.20	0.23	0.10	0.18	0.20	0.10
Alg-5-full-sample-Platt	0.10	0.12	0.11	0.27	0.29	0.10	0.27	0.29	0.10	
3	Alg-1-Clipped	0.06	0.08	0.08	0.54	0.58	0.21	2.00	2.02	0.31
	Alg-1-Uncalib	0.06	0.08	0.08	3.07e+08	8.49e+08	7.91e+08	2.05	2.07	0.34
	Alg-2-nested-cf-IVAP	0.12	0.15	0.14	0.36	0.38	0.11	0.46	0.48	0.11
	Alg-2-nested-cf-Iso	0.94	1.03	0.41	0.26	0.32	0.31	0.27	0.34	0.34
	Alg-2-nested-cf-Platt	0.11	0.14	0.14	0.40	0.42	0.10	0.53	0.54	0.10
	Alg-3-cf-IVAP	0.07	0.08	0.08	0.32	0.33	0.08	0.38	0.38	0.07
	Alg-3-cf-Iso	0.07	0.09	0.08	0.36	0.37	0.07	0.42	0.42	0.07
	Alg-3-cf-Platt	0.12	0.14	0.07	0.87	0.87	0.08	0.82	0.82	0.08
	Alg-4-single-split-IVAP	0.07	0.09	0.09	1.13	1.13	0.07	1.03	1.03	0.08
	Alg-4-single-split-Iso	0.73	0.80	0.34	1.13	1.13	0.07	1.03	1.03	0.08
	Alg-4-single-split-Platt	0.08	0.09	0.08	0.44	0.45	0.08	0.57	0.57	0.08
	Alg-5-full-sample-IVAP	0.06	0.08	0.08	0.35	0.36	0.07	0.40	0.41	0.07
	Alg-5-full-sample-Iso	0.06	0.08	0.08	0.37	0.37	0.07	0.42	0.43	0.07
Alg-5-full-sample-Platt	0.07	0.09	0.08	0.42	0.43	0.07	0.52	0.53	0.07	
4	Alg-1-Clipped	0.13	0.15	0.06	0.54	0.55	0.13	6.14	6.17	0.52
	Alg-1-Uncalib	0.13	0.15	0.06	4.64e+08	6.89e+08	5.11e+08	8.37	8.45	1.21
	Alg-2-nested-cf-IVAP	0.10	0.13	0.11	0.12	0.15	0.11	0.11	0.14	0.11
	Alg-2-nested-cf-Iso	0.21	0.24	0.13	0.19	0.23	0.13	0.25	0.29	0.15
	Alg-2-nested-cf-Platt	0.13	0.16	0.11	0.15	0.18	0.11	0.15	0.18	0.12
	Alg-3-cf-IVAP	0.05	0.05	0.05	0.06	0.08	0.05	0.06	0.07	0.06
	Alg-3-cf-Iso	0.05	0.06	0.05	0.09	0.10	0.05	0.07	0.09	0.06
	Alg-3-cf-Platt	0.07	0.09	0.06	0.13	0.16	0.10	0.18	0.23	0.16
	Alg-4-single-split-IVAP	0.05	0.06	0.06	1.40	1.41	0.09	1.43	1.43	0.07
	Alg-4-single-split-Iso	0.07	0.09	0.07	0.88	0.98	0.43	0.96	1.02	0.37
	Alg-4-single-split-Platt	0.10	0.12	0.06	0.12	0.13	0.06	0.12	0.13	0.05
	Alg-5-full-sample-IVAP	0.06	0.08	0.06	0.10	0.11	0.05	0.09	0.10	0.06
	Alg-5-full-sample-Iso	0.07	0.08	0.05	0.11	0.12	0.05	0.10	0.11	0.06
Alg-5-full-sample-Platt	0.09	0.11	0.06	0.12	0.13	0.06	0.12	0.13	0.06	

DGP 1: $n = 2000$, $p = 20$, $R2.d = 0.5$; DGP 2: $n = 2000$, $p = 3$, $\text{overlap} = 0.5$;
DGP 3: $n = 2000$, $p = 4$; DGP 4: $n = 4000$, $p = 20$, $\text{share treated} = 0.1$; $g = \text{LGBM}$,
lowest RMSEs per DGP and propensity learner are highlighted

Table 6: IRM Results

DGP	Method	m = Logit			m = Random Forest			m = LGBM		
		MAE	RMSE	Std. dev.	MAE	RMSE	Std. dev.	MAE	RMSE	Std. dev.
1	Alg-1-Clipped	0.07	0.10	0.10	0.06	0.08	0.07	0.22	0.27	0.24
	Alg-1-Uncalib	0.08	0.13	0.13	1.85e+06	1.85e+07	1.84e+07	0.48	0.60	0.54
	Alg-2-nested-cf-IVAP	0.07	0.09	0.08	0.06	0.08	0.07	0.07	0.08	0.08
	Alg-2-nested-cf-Iso	0.12	0.15	0.14	0.10	0.12	0.12	0.10	0.12	0.12
	Alg-2-nested-cf-Platt	0.08	0.14	0.14	0.06	0.08	0.07	0.07	0.08	0.07
	Alg-3-cf-IVAP	0.06	0.08	0.07	0.06	0.08	0.08	0.07	0.08	0.07
	Alg-3-cf-Iso	0.06	0.08	0.07	0.06	0.08	0.08	0.06	0.08	0.07
	Alg-3-cf-Platt	0.06	0.07	0.07	0.07	0.08	0.06	0.07	0.08	0.07
	Alg-4-single-split-IVAP	0.06	0.08	0.07	0.07	0.08	0.06	0.07	0.09	0.06
	Alg-4-single-split-Iso	0.10	0.13	0.12	0.07	0.08	0.06	0.07	0.09	0.06
	Alg-4-single-split-Platt	0.07	0.08	0.08	0.06	0.08	0.07	0.07	0.08	0.07
	Alg-5-full-sample-IVAP	0.07	0.08	0.08	0.07	0.09	0.08	0.07	0.08	0.08
	Alg-5-full-sample-Iso	0.06	0.08	0.08	0.06	0.08	0.07	0.07	0.08	0.08
	Alg-5-full-sample-Platt	0.07	0.09	0.09	0.06	0.08	0.07	0.07	0.08	0.07
2	Alg-1-Clipped	0.09	0.11	0.11	0.31	0.39	0.39	0.20	0.26	0.26
	Alg-1-Uncalib	0.09	0.11	0.11	2.22e+09	2.89e+09	2.86e+09	0.24	0.32	0.32
	Alg-2-nested-cf-IVAP	0.09	0.11	0.11	0.09	0.11	0.11	0.09	0.12	0.12
	Alg-2-nested-cf-Iso	0.18	0.23	0.22	0.16	0.22	0.22	0.19	0.24	0.24
	Alg-2-nested-cf-Platt	0.09	0.11	0.11	0.09	0.11	0.11	0.09	0.11	0.11
	Alg-3-cf-IVAP	0.09	0.11	0.11	0.10	0.12	0.12	0.10	0.12	0.12
	Alg-3-cf-Iso	0.09	0.11	0.11	0.09	0.12	0.12	0.10	0.12	0.12
	Alg-3-cf-Platt	0.09	0.11	0.11	0.09	0.11	0.11	0.09	0.11	0.11
	Alg-4-single-split-IVAP	0.09	0.11	0.11	0.09	0.11	0.11	0.09	0.11	0.11
	Alg-4-single-split-Iso	0.15	0.20	0.20	0.09	0.11	0.11	0.09	0.11	0.11
	Alg-4-single-split-Platt	0.09	0.11	0.11	0.09	0.11	0.11	0.09	0.11	0.11
	Alg-5-full-sample-IVAP	0.09	0.11	0.11	0.09	0.11	0.11	0.09	0.12	0.12
	Alg-5-full-sample-Iso	0.09	0.11	0.11	0.09	0.11	0.11	0.09	0.12	0.12
	Alg-5-full-sample-Platt	0.09	0.11	0.11	0.09	0.11	0.11	0.09	0.11	0.11
3	Alg-1-Clipped	0.05	0.07	0.07	0.08	0.10	0.10	0.11	0.13	0.13
	Alg-1-Uncalib	0.05	0.07	0.07	9.97e+07	2.74e+08	2.73e+08	0.11	0.14	0.14
	Alg-2-nested-cf-IVAP	0.05	0.07	0.07	0.05	0.07	0.06	0.05	0.07	0.07
	Alg-2-nested-cf-Iso	0.10	0.13	0.12	0.08	0.10	0.10	0.10	0.13	0.13
	Alg-2-nested-cf-Platt	0.05	0.07	0.07	0.05	0.07	0.06	0.05	0.07	0.06
	Alg-3-cf-IVAP	0.05	0.07	0.06	0.06	0.07	0.07	0.05	0.07	0.07
	Alg-3-cf-Iso	0.05	0.07	0.07	0.06	0.07	0.07	0.05	0.07	0.06
	Alg-3-cf-Platt	0.05	0.06	0.06	0.05	0.07	0.06	0.05	0.07	0.06
	Alg-4-single-split-IVAP	0.05	0.07	0.07	0.05	0.07	0.06	0.05	0.07	0.06
	Alg-4-single-split-Iso	0.10	0.12	0.11	0.05	0.07	0.06	0.05	0.07	0.06
	Alg-4-single-split-Platt	0.05	0.07	0.06	0.06	0.07	0.07	0.05	0.07	0.06
	Alg-5-full-sample-IVAP	0.05	0.07	0.07	0.06	0.07	0.07	0.05	0.07	0.07
	Alg-5-full-sample-Iso	0.05	0.07	0.07	0.06	0.07	0.07	0.05	0.07	0.07
	Alg-5-full-sample-Platt	0.05	0.07	0.07	0.06	0.07	0.07	0.05	0.07	0.06
4	Alg-1-Clipped	0.04	0.06	0.06	0.07	0.09	0.09	0.17	0.21	0.20
	Alg-1-Uncalib	0.04	0.06	0.06	1.74e+08	2.70e+08	2.68e+08	0.36	0.46	0.43
	Alg-2-nested-cf-IVAP	0.04	0.05	0.05	0.05	0.06	0.06	0.04	0.06	0.06
	Alg-2-nested-cf-Iso	0.05	0.07	0.07	0.05	0.07	0.07	0.06	0.07	0.07
	Alg-2-nested-cf-Platt	0.04	0.06	0.05	0.05	0.06	0.06	0.04	0.06	0.06
	Alg-3-cf-IVAP	0.04	0.06	0.06	0.05	0.06	0.06	0.05	0.06	0.06
	Alg-3-cf-Iso	0.04	0.06	0.06	0.05	0.06	0.06	0.05	0.06	0.06
	Alg-3-cf-Platt	0.04	0.06	0.06	0.05	0.06	0.06	0.05	0.06	0.06
	Alg-4-single-split-IVAP	0.04	0.06	0.06	0.04	0.06	0.06	0.04	0.06	0.06
	Alg-4-single-split-Iso	0.05	0.06	0.06	0.05	0.06	0.06	0.04	0.06	0.06
	Alg-4-single-split-Platt	0.04	0.06	0.06	0.05	0.06	0.06	0.04	0.06	0.06
	Alg-5-full-sample-IVAP	0.04	0.06	0.06	0.05	0.06	0.06	0.04	0.06	0.06
	Alg-5-full-sample-Iso	0.04	0.06	0.06	0.05	0.06	0.06	0.04	0.06	0.06
	Alg-5-full-sample-Platt	0.04	0.06	0.06	0.05	0.06	0.06	0.04	0.06	0.05

DGP 1: n = 2000, p = 20, R2_d = 0.5; DGP 2: n = 2000, p = 3, overlap = 0.5;
DGP 3: n = 2000, p = 4; DGP 4: n = 4000, p = 20, share treated = 0.1; g = LGBM,
lowest RMSEs per DGP and propensity learner are highlighted

Table 7: PLR Results

DGP	Method	m = Logit			m = Random Forest			m = LGBM		
		MAE	RMSE	Std. dev.	MAE	RMSE	Std. dev.	MAE	RMSE	Std. dev.
1	Alg-1-Clipped	0.05	0.06	0.06	0.05	0.06	0.06	0.05	0.06	0.06
	Alg-1-Uncalib	0.05	0.06	0.06	0.05	0.06	0.06	0.05	0.06	0.06
	Alg-2-nested-cf-IVAP	0.05	0.06	0.06	0.05	0.06	0.06	0.05	0.06	0.06
	Alg-2-nested-cf-Iso	0.05	0.06	0.06	0.05	0.06	0.06	0.05	0.06	0.06
	Alg-2-nested-cf-Platt	0.05	0.06	0.06	0.05	0.06	0.06	0.05	0.06	0.06
	Alg-3-cf-IVAP	0.05	0.06	0.06	0.05	0.06	0.06	0.05	0.06	0.06
	Alg-3-cf-Iso	0.05	0.06	0.06	0.05	0.06	0.06	0.05	0.07	0.07
	Alg-3-cf-Platt	0.05	0.06	0.06	0.05	0.06	0.06	0.05	0.07	0.07
	Alg-4-single-split-IVAP	0.05	0.06	0.06	0.14	0.18	0.18	0.12	0.15	0.15
	Alg-4-single-split-Iso	0.05	0.06	0.06	0.15	0.20	0.20	0.13	0.16	0.16
	Alg-4-single-split-Platt	0.05	0.06	0.06	0.05	0.06	0.06	0.05	0.06	0.06
	Alg-5-full-sample-IVAP	0.05	0.06	0.06	0.05	0.06	0.06	0.05	0.06	0.06
	Alg-5-full-sample-Iso	0.05	0.06	0.06	0.05	0.06	0.06	0.05	0.07	0.07
Alg-5-full-sample-Platt	0.05	0.06	0.06	0.05	0.06	0.06	0.05	0.06	0.06	
2	Alg-1-Clipped	0.09	0.11	0.10	0.12	0.14	0.10	0.10	0.11	0.10
	Alg-1-Uncalib	0.09	0.11	0.10	0.12	0.14	0.10	0.10	0.11	0.10
	Alg-2-nested-cf-IVAP	0.09	0.11	0.10	0.10	0.12	0.10	0.09	0.11	0.10
	Alg-2-nested-cf-Iso	0.09	0.11	0.10	0.10	0.12	0.10	0.09	0.11	0.10
	Alg-2-nested-cf-Platt	0.09	0.11	0.10	0.10	0.12	0.10	0.09	0.11	0.10
	Alg-3-cf-IVAP	0.09	0.11	0.10	0.10	0.12	0.10	0.09	0.11	0.10
	Alg-3-cf-Iso	0.09	0.11	0.11	0.09	0.11	0.10	0.09	0.10	0.10
	Alg-3-cf-Platt	0.09	0.11	0.10	0.11	0.13	0.10	0.09	0.11	0.10
	Alg-4-single-split-IVAP	0.09	0.11	0.10	0.23	0.26	0.14	0.13	0.16	0.12
	Alg-4-single-split-Iso	0.09	0.11	0.10	0.24	0.27	0.15	0.13	0.16	0.12
	Alg-4-single-split-Platt	0.09	0.11	0.10	0.09	0.11	0.10	0.09	0.11	0.10
	Alg-5-full-sample-IVAP	0.09	0.11	0.10	0.09	0.11	0.10	0.09	0.10	0.10
	Alg-5-full-sample-Iso	0.09	0.11	0.10	0.09	0.11	0.10	0.09	0.10	0.10
Alg-5-full-sample-Platt	0.09	0.11	0.10	0.09	0.11	0.10	0.09	0.11	0.10	
3	Alg-1-Clipped	0.06	0.08	0.08	0.06	0.07	0.07	0.08	0.10	0.07
	Alg-1-Uncalib	0.06	0.08	0.08	0.06	0.07	0.07	0.08	0.10	0.07
	Alg-2-nested-cf-IVAP	0.06	0.08	0.08	0.07	0.09	0.07	0.09	0.11	0.07
	Alg-2-nested-cf-Iso	0.06	0.08	0.08	0.07	0.09	0.07	0.09	0.11	0.07
	Alg-2-nested-cf-Platt	0.06	0.08	0.08	0.07	0.08	0.07	0.09	0.11	0.07
	Alg-3-cf-IVAP	0.06	0.08	0.08	0.06	0.08	0.07	0.06	0.08	0.07
	Alg-3-cf-Iso	0.07	0.09	0.08	0.06	0.08	0.08	0.06	0.08	0.08
	Alg-3-cf-Platt	0.07	0.08	0.08	0.10	0.12	0.08	0.07	0.09	0.08
	Alg-4-single-split-IVAP	0.06	0.08	0.08	1.01	1.02	0.16	0.43	0.44	0.11
	Alg-4-single-split-Iso	0.06	0.08	0.08	1.10	1.11	0.18	0.46	0.47	0.12
	Alg-4-single-split-Platt	0.06	0.08	0.08	0.06	0.08	0.08	0.08	0.09	0.07
	Alg-5-full-sample-IVAP	0.06	0.08	0.08	0.06	0.08	0.07	0.06	0.08	0.07
	Alg-5-full-sample-Iso	0.07	0.09	0.08	0.06	0.07	0.07	0.06	0.07	0.07
Alg-5-full-sample-Platt	0.06	0.08	0.08	0.06	0.08	0.08	0.06	0.07	0.07	
4	Alg-1-Clipped	0.08	0.09	0.06	0.05	0.06	0.05	0.05	0.06	0.05
	Alg-1-Uncalib	0.08	0.09	0.06	0.05	0.06	0.05	0.05	0.06	0.05
	Alg-2-nested-cf-IVAP	0.08	0.09	0.05	0.07	0.09	0.05	0.07	0.09	0.05
	Alg-2-nested-cf-Iso	0.08	0.09	0.06	0.07	0.09	0.05	0.07	0.09	0.05
	Alg-2-nested-cf-Platt	0.08	0.09	0.06	0.07	0.09	0.05	0.07	0.09	0.05
	Alg-3-cf-IVAP	0.07	0.09	0.06	0.07	0.08	0.05	0.07	0.09	0.05
	Alg-3-cf-Iso	0.08	0.10	0.06	0.08	0.09	0.05	0.08	0.10	0.05
	Alg-3-cf-Platt	0.08	0.09	0.05	0.07	0.09	0.05	0.08	0.09	0.06
	Alg-4-single-split-IVAP	0.08	0.10	0.06	0.56	0.59	0.19	0.56	0.58	0.14
	Alg-4-single-split-Iso	0.08	0.09	0.06	0.26	0.31	0.17	0.26	0.30	0.16
	Alg-4-single-split-Platt	0.08	0.09	0.06	0.07	0.09	0.05	0.08	0.09	0.05
	Alg-5-full-sample-IVAP	0.08	0.09	0.06	0.07	0.09	0.05	0.08	0.09	0.05
	Alg-5-full-sample-Iso	0.08	0.09	0.06	0.07	0.09	0.05	0.08	0.09	0.05
Alg-5-full-sample-Platt	0.08	0.09	0.06	0.07	0.09	0.05	0.08	0.09	0.05	

DGP 1: $n = 2000$, $p = 20$, $R2_d = 0.5$; DGP 2: $n = 2000$, $p = 3$, $\text{overlap} = 0.5$;
DGP 3: $n = 2000$, $p = 4$; DGP 4: $n = 4000$, $p = 20$, $\text{share treated} = 0.1$; $g = \text{LGBM}$,
lowest RMSEs per DGP and propensity learner are highlighted

The following figures display the results over 100 repetitions for the ATE estimators. Four different methods were applied: no calibration of the propensity scores (*Plain*), clipping, isotonic regression, and inductive VAP (*IVAP*). Additionally, *Oracle* estimates are provided, utilizing true propensity scores from the DGPs. Furthermore, the figures with respect to the sample size and number of covariates include the estimators with clipped propensity scores. The combination of clipping and calibration is also displayed in histogram plots. If no clipping is employed, the clipping threshold is set to 1^{-12} to ensure stability.

Propensity Scores by DGP

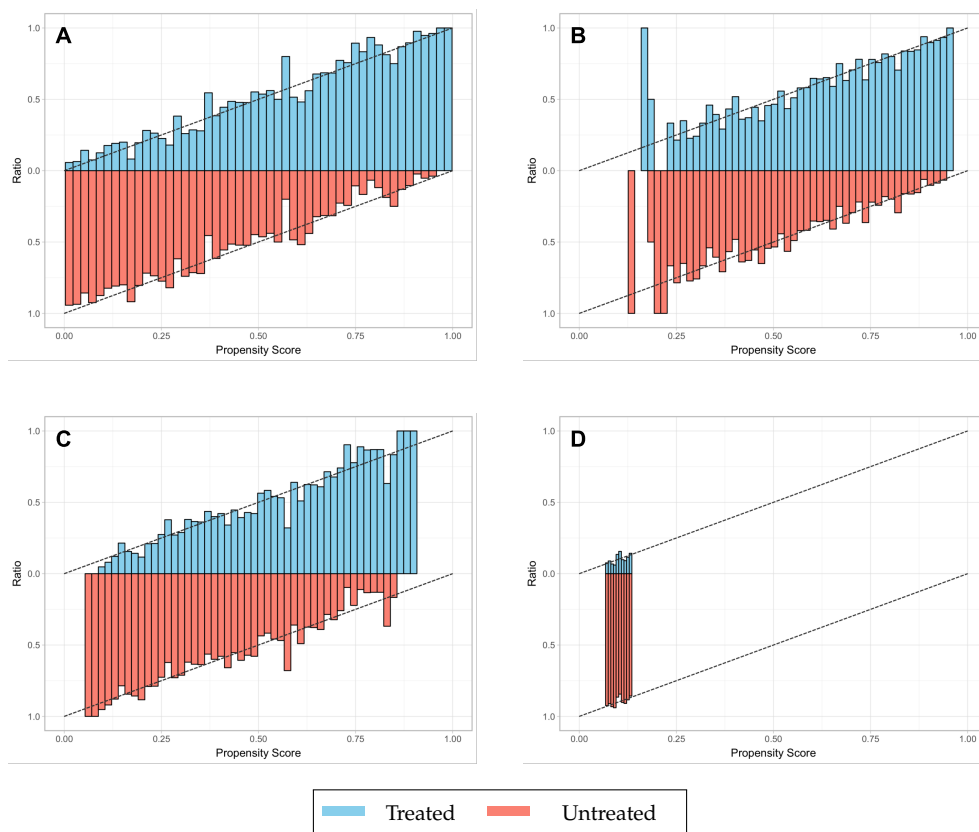


Figure 7: Underlying true propensity scores, divided by treatment allocation. The DGPs presented are: Panel A - DGP 1 (IRM), Panel B - DGP 2 (Drug), Panel C - DGP 3 (Nonlinear), and Panel D - DGP 4 (Unbalanced).

Propensity Learner

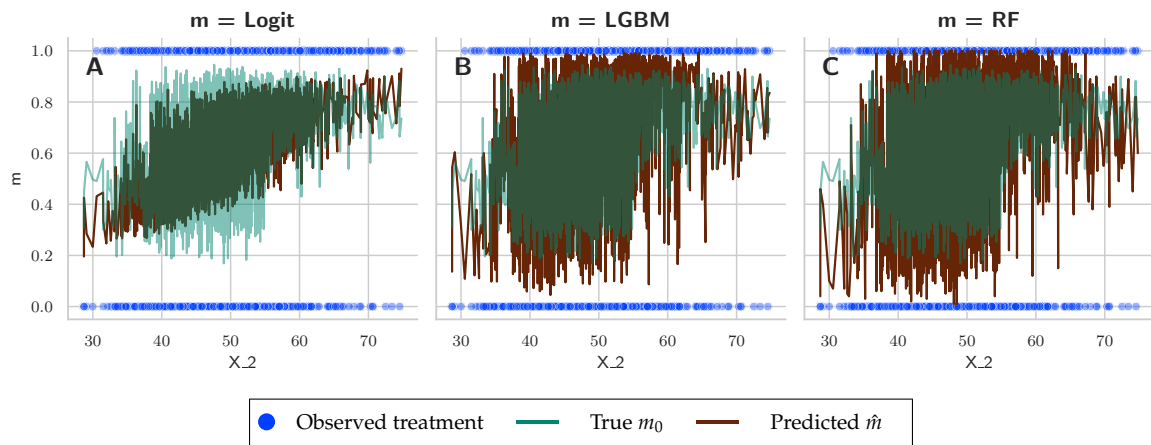


Figure 8: DGP 2 Drug, Overlap = 0.5, $n = 2000$, $p = 3$

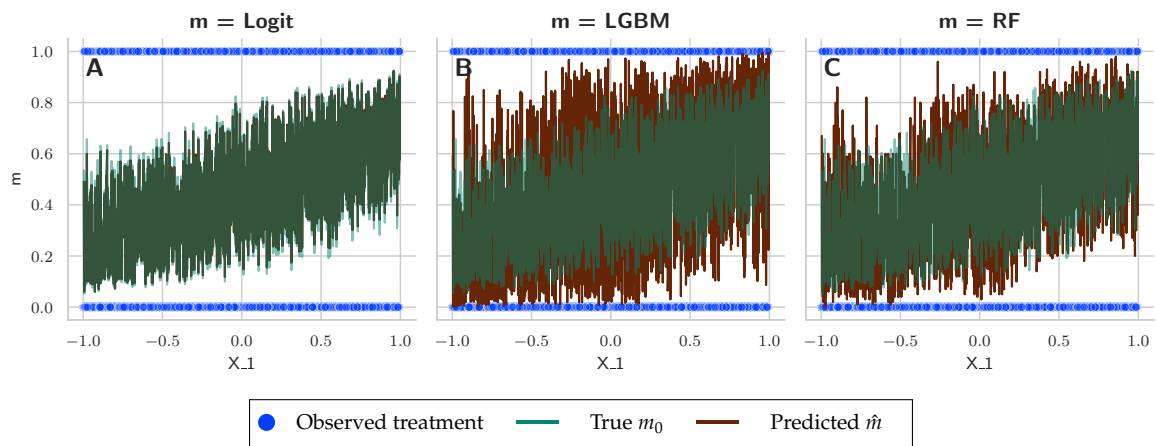


Figure 9: DGP 3 Nonlinear, $n = 2000$, $p = 4$

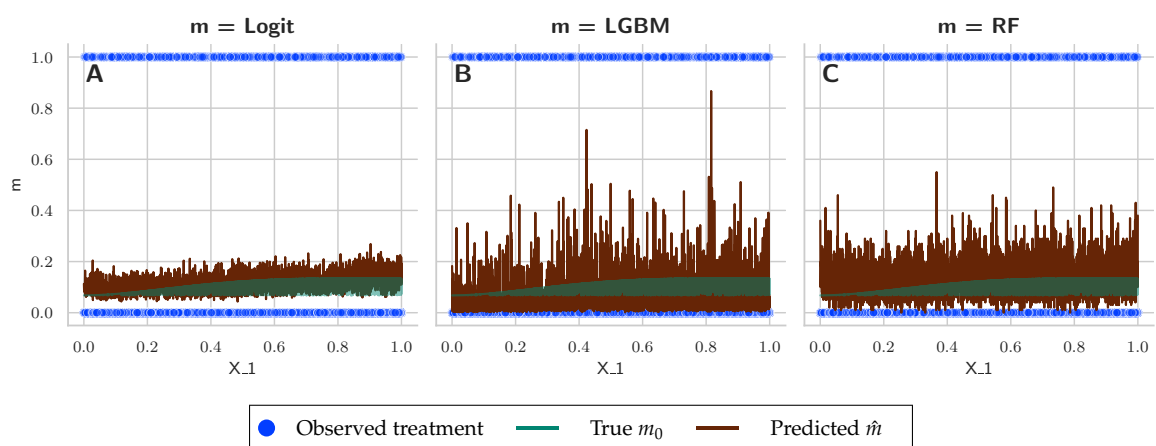


Figure 10: DGP 4 Unbalanced, $\alpha = 0.1$, $p = 20$

Calibrated Propensity Scores

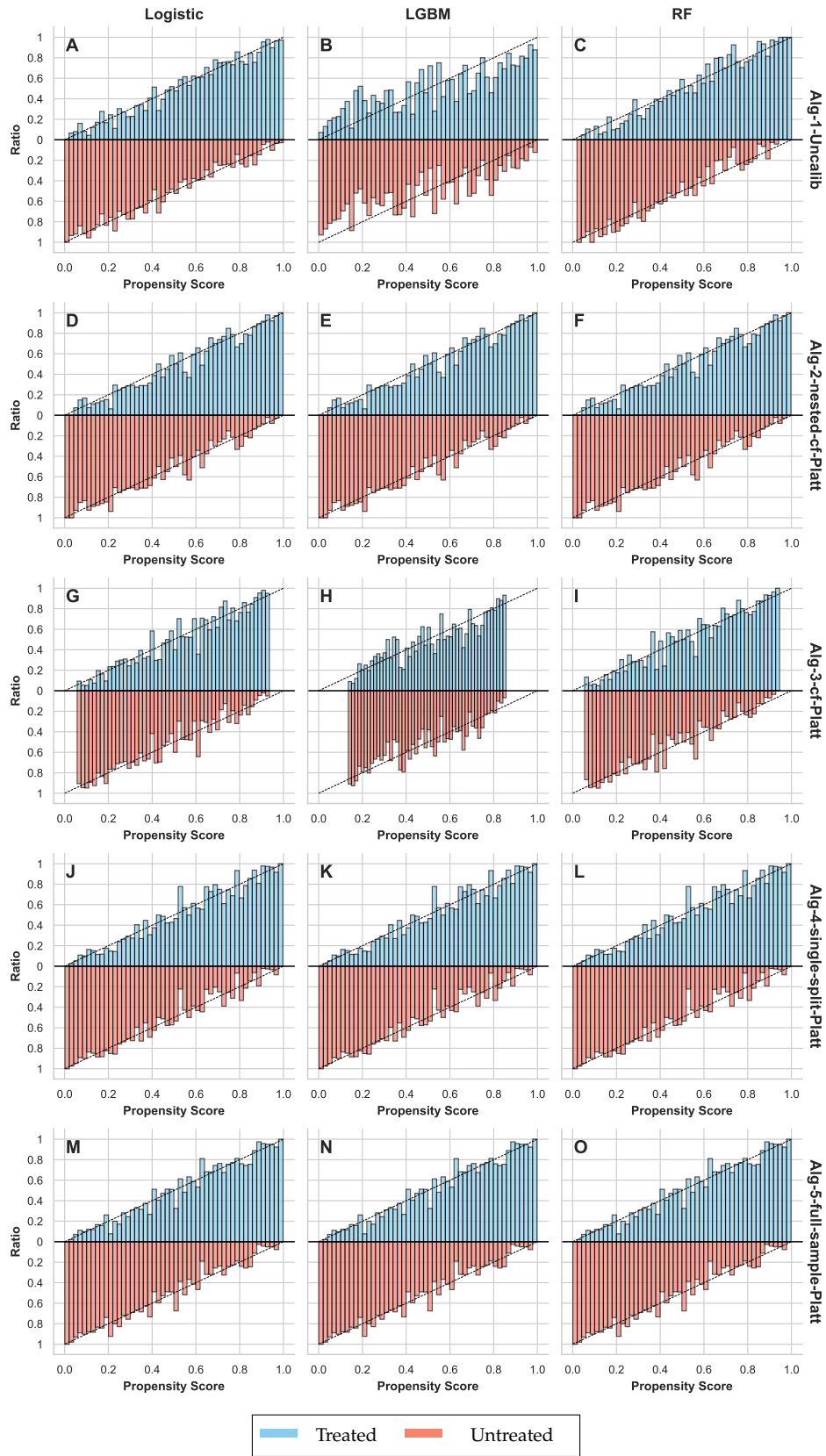


Figure 11: DGP 1 IRM, R2D = 0.5, m = LGBM, g = LGBM, n = 2000, p = 20, Calibration method for Algorithms 2-4: Platt Scaling

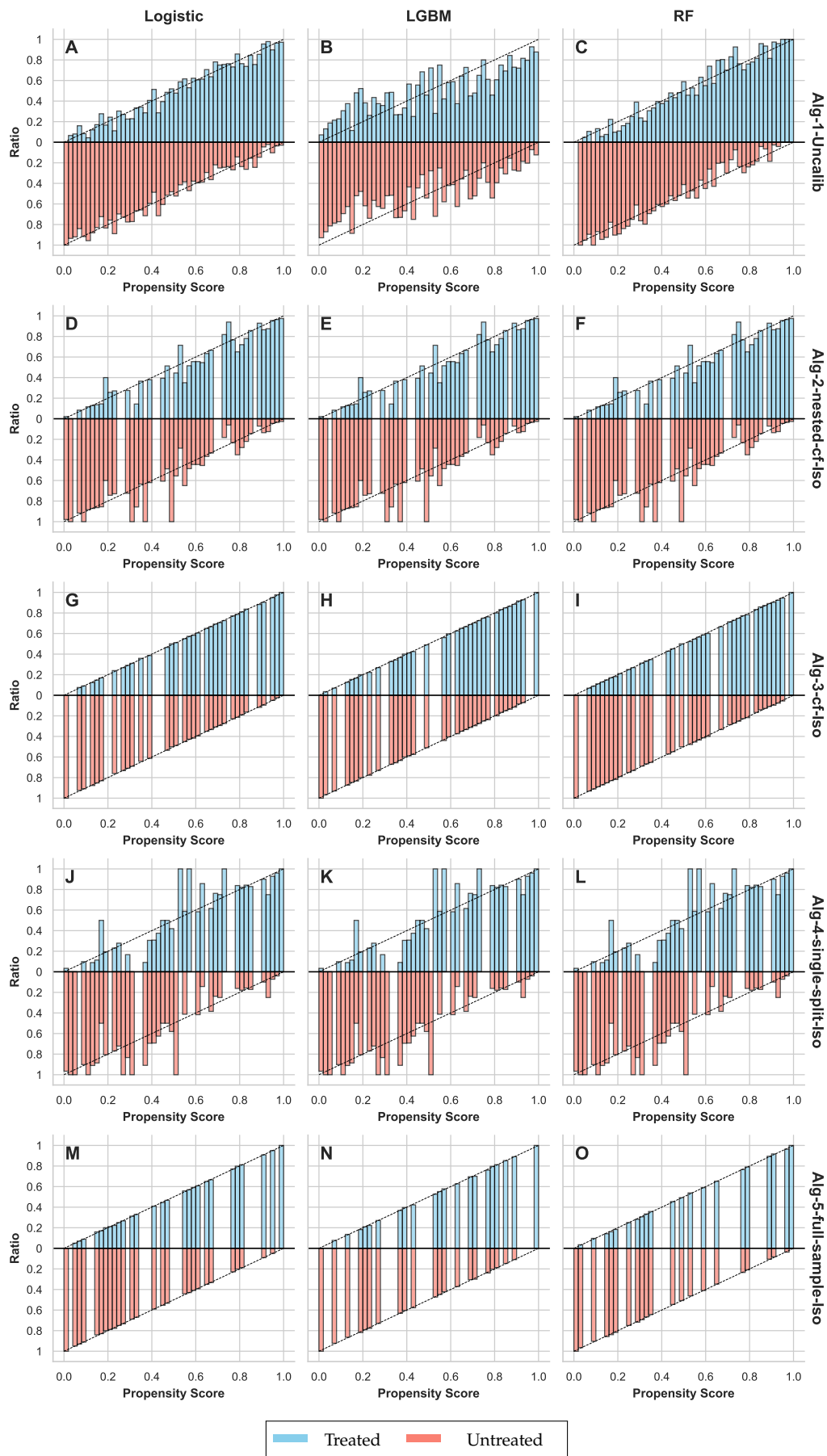


Figure 12: DGP 1 IRM, $R2D = 0.5$, $m = \text{LGBM}$, $g = \text{LGBM}$, $n = 2000$, $p = 20$, Calibration method for Algorithms 2-5: isotonic regression

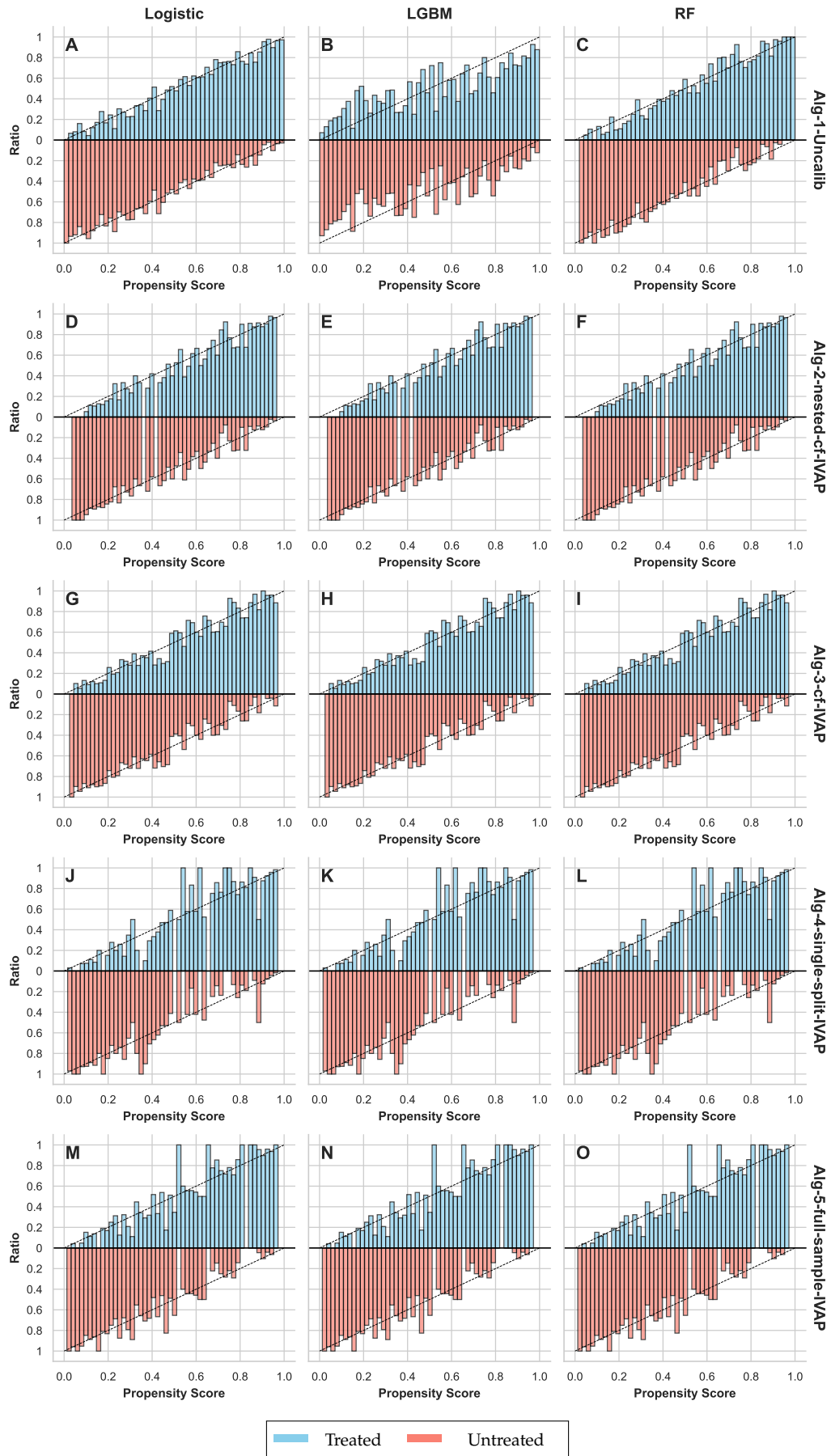


Figure 13: DGP 1 IRM, $R2D = 0.5$, $m = \text{LGBM}$, $g = \text{LGBM}$, $n = 2000$, $p = 20$, Calibration method for Algorithms 2-4: Venn-ABERS

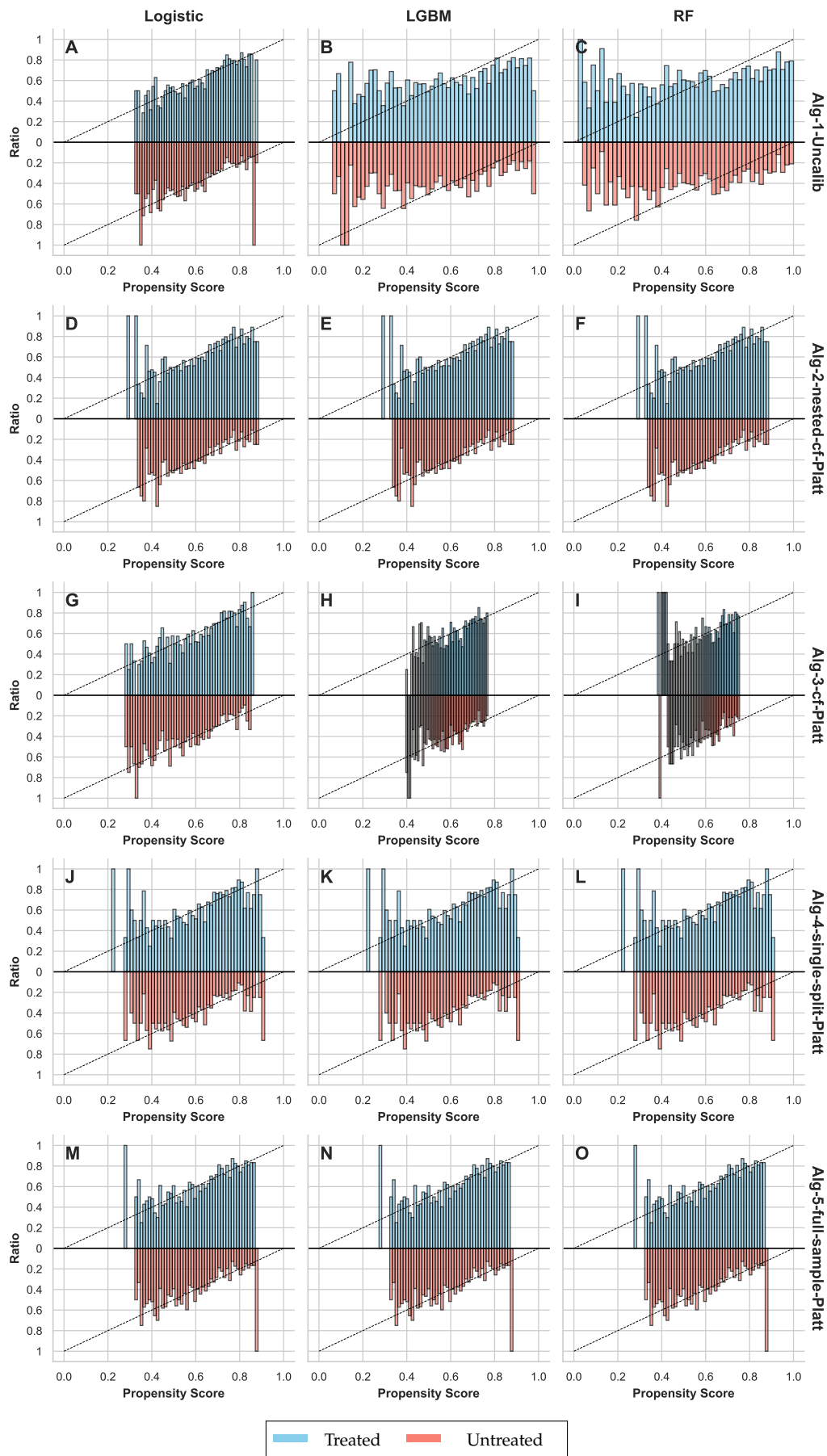


Figure 14: DGP 2 Drug, Overlap = 0.5, $m = \text{LGBM}$, $g = \text{LGBM}$, $n = 2000$, $p = 3$, Calibration method for Algorithms 2-4: Platt Scaling

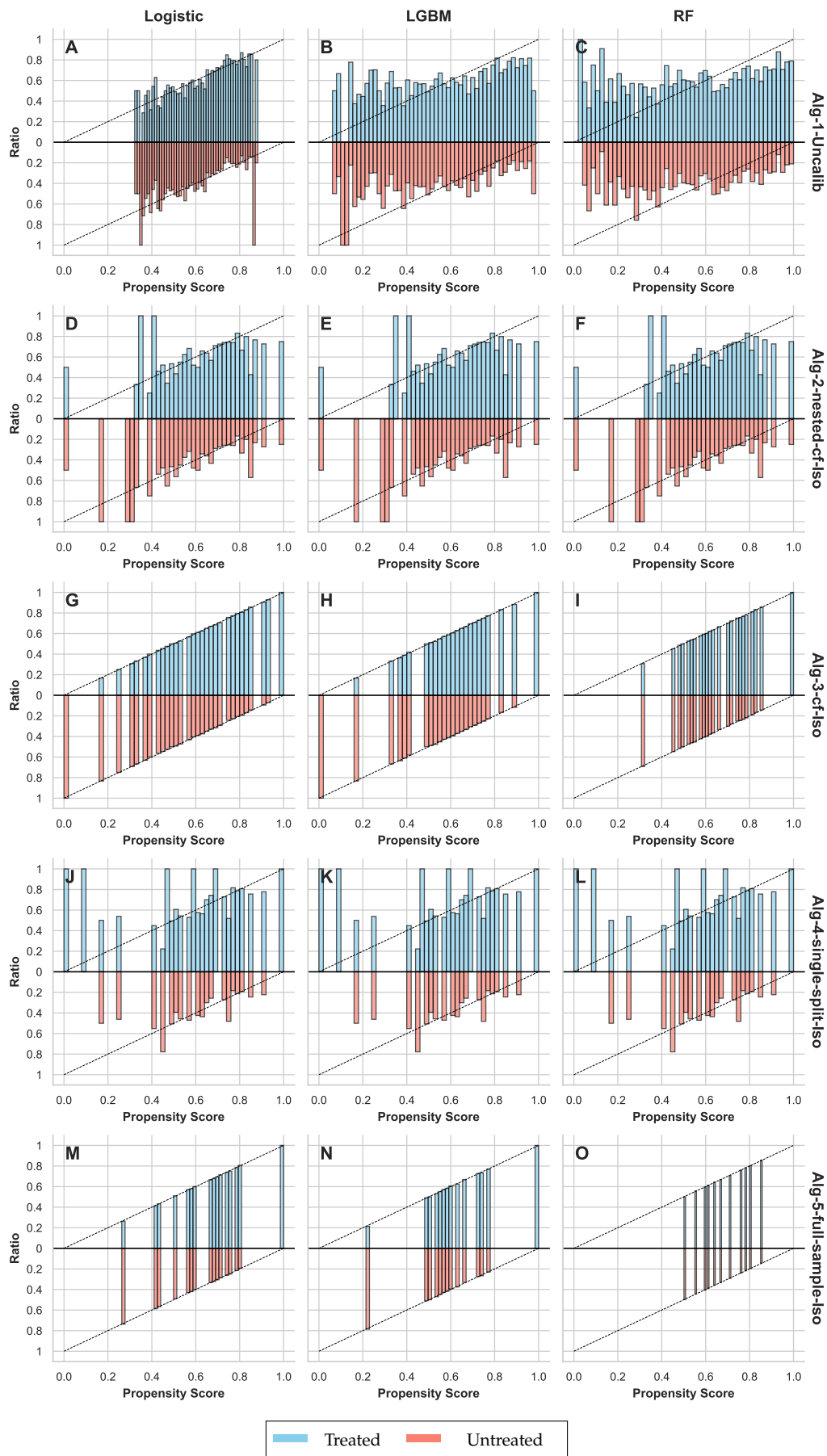


Figure 15: DGP 2 Drug, Overlap = 0.5, $m = \text{LGBM}$, $g = \text{LGBM}$, $n = 2000$, $p = 3$, Calibration method for Algorithms 2-5: isotonic regression

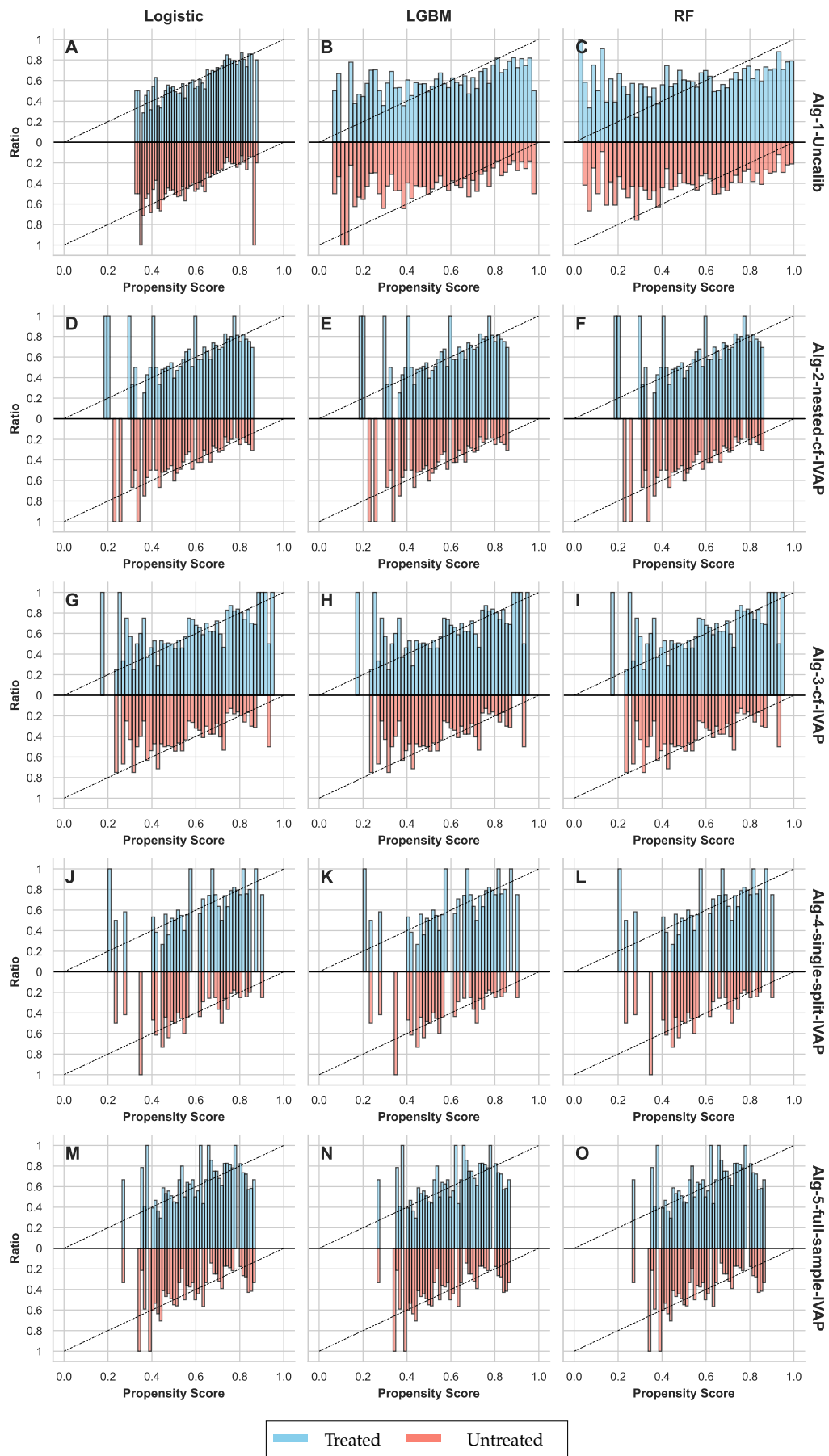


Figure 16: DGP 2 Drug, Overlap = 0.5, $m = \text{LGBM}$, $g = \text{LGBM}$, $n = 2000$, $p = 3$, Calibration method for Algorithms 2-4: Venn-ABERS

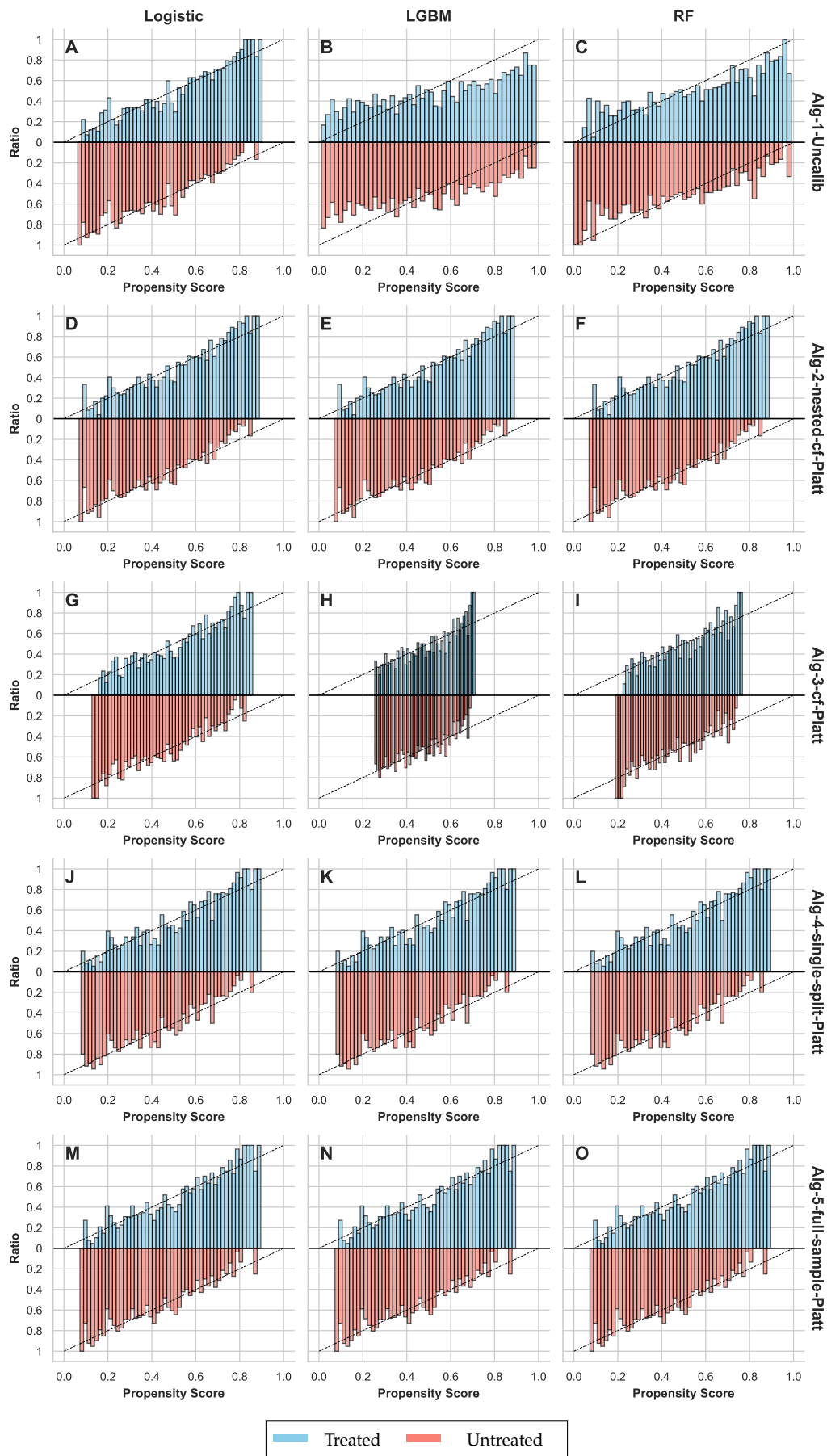


Figure 17: DGP 3 Nonlinear, $m = \text{LGBM}$, $g = \text{LGBM}$, $n = 2000$, $p = 4$, Calibration method for Algorithms 2-4: Platt Scaling

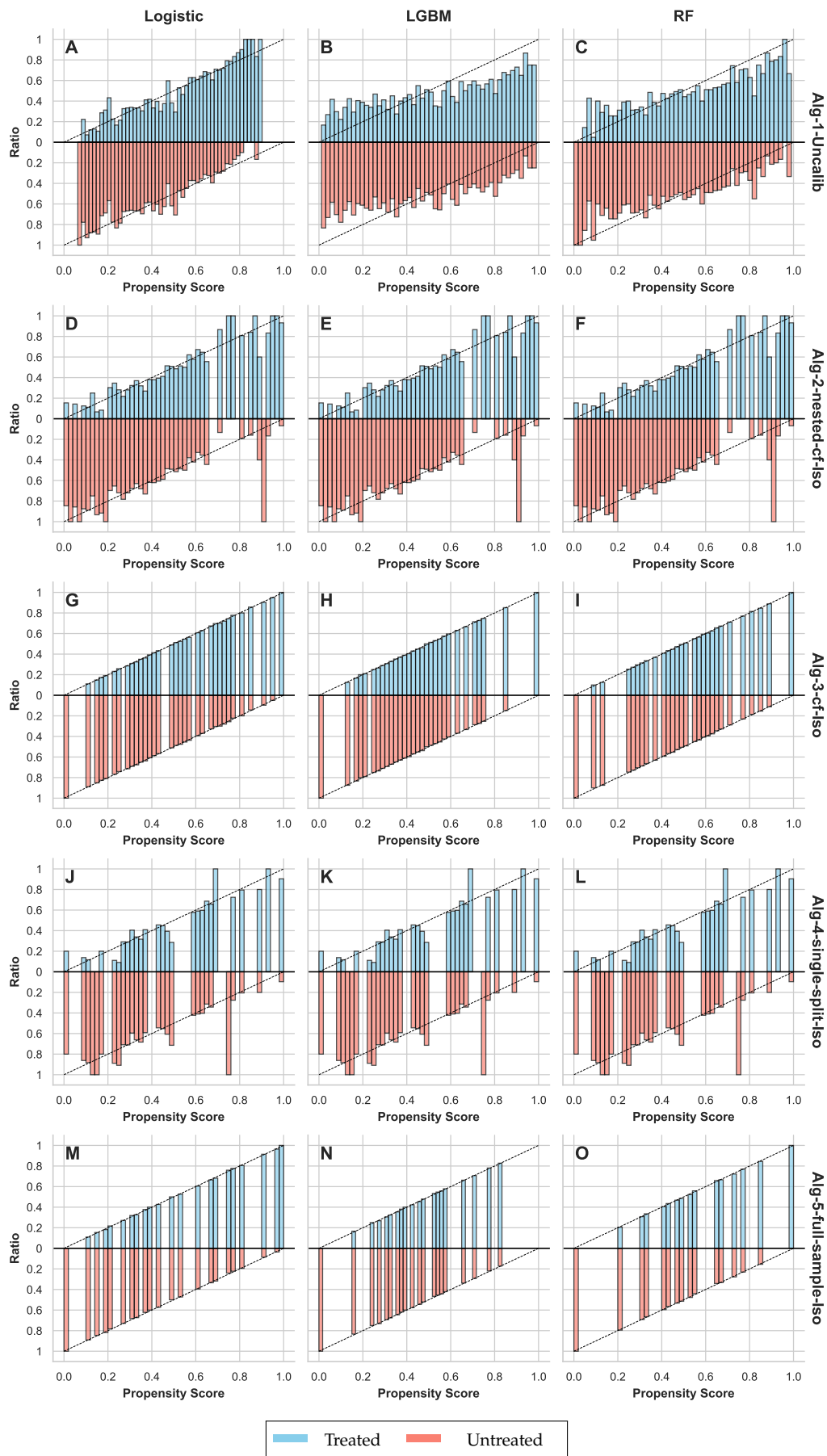


Figure 18: DGP 3 Nonlinear, $m = \text{LGBM}$, $g = \text{LGBM}$, $n = 2000$, $p = 4$, Calibration method for Algorithms 2-5: isotonic regression

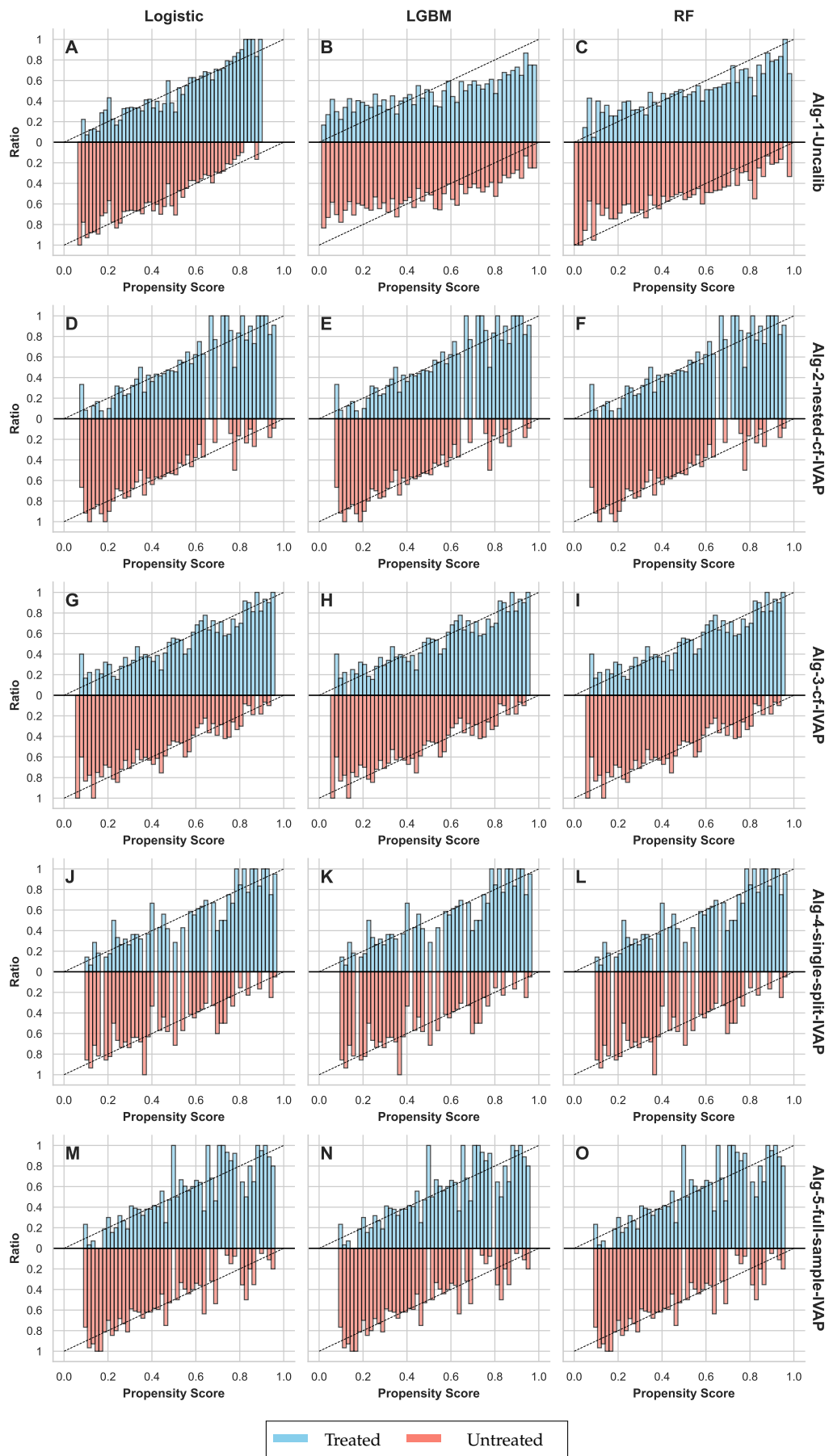


Figure 19: DGP 3 Nonlinear, $m = \text{LGBM}$, $g = \text{LGBM}$, $n = 2000$, $p = 4$, Calibration method for Algorithms 2-4: Venn-ABERS

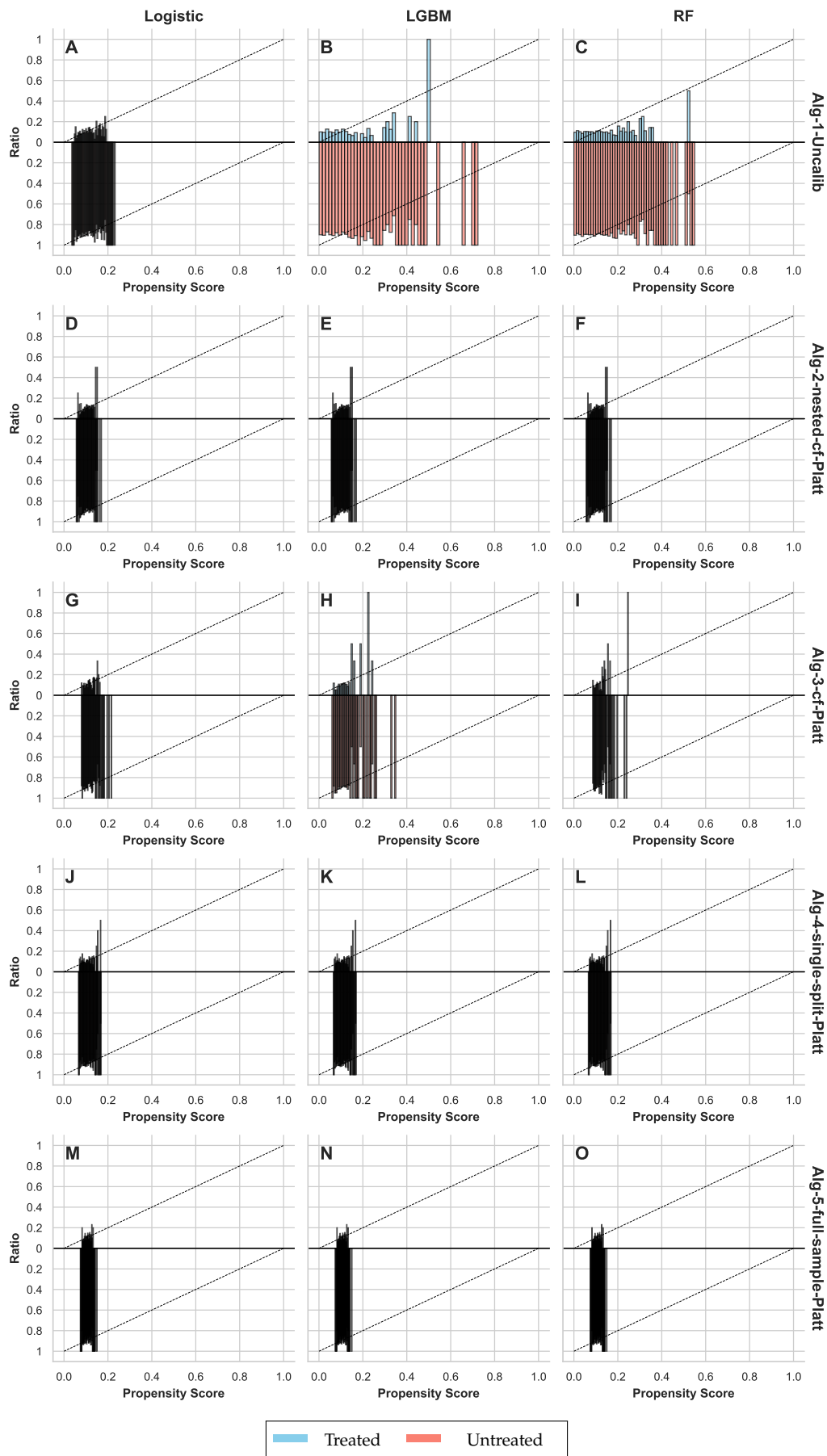


Figure 20: DGP 4 Unbalanced, $\alpha = 0.1$, $m = \text{LGBM}$, $g = \text{LGBM}$, $n = 4000$, $p = 20$, Calibration method for Algorithms 2-4: Platt Scaling

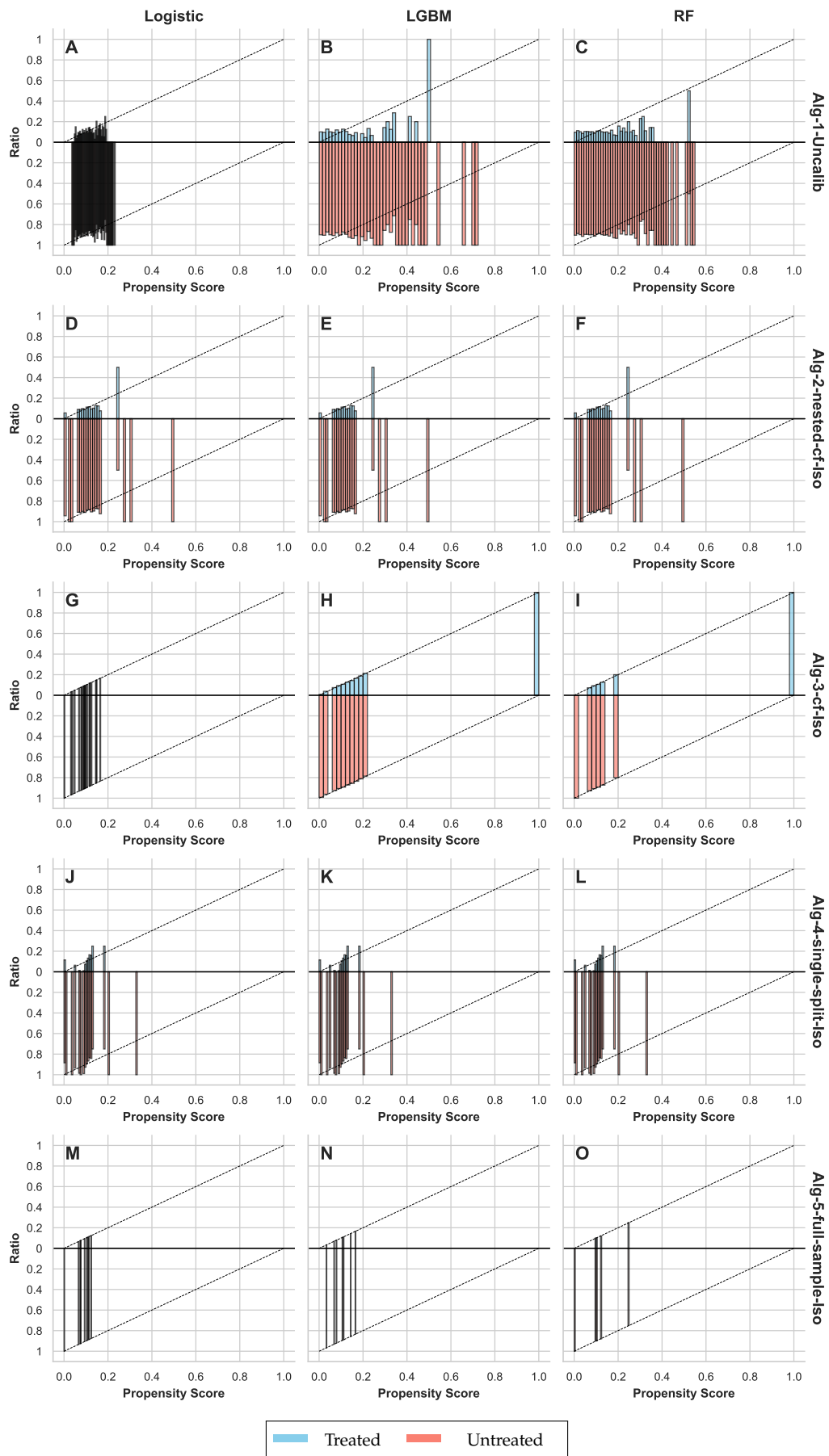


Figure 21: DGP 4 Unbalanced, $\alpha = 0.1$, $m = \text{LGBM}$, $g = \text{LGBM}$, $n = 4000$, $p = 20$, Calibration method for Algorithms 2-5: isotonic regression

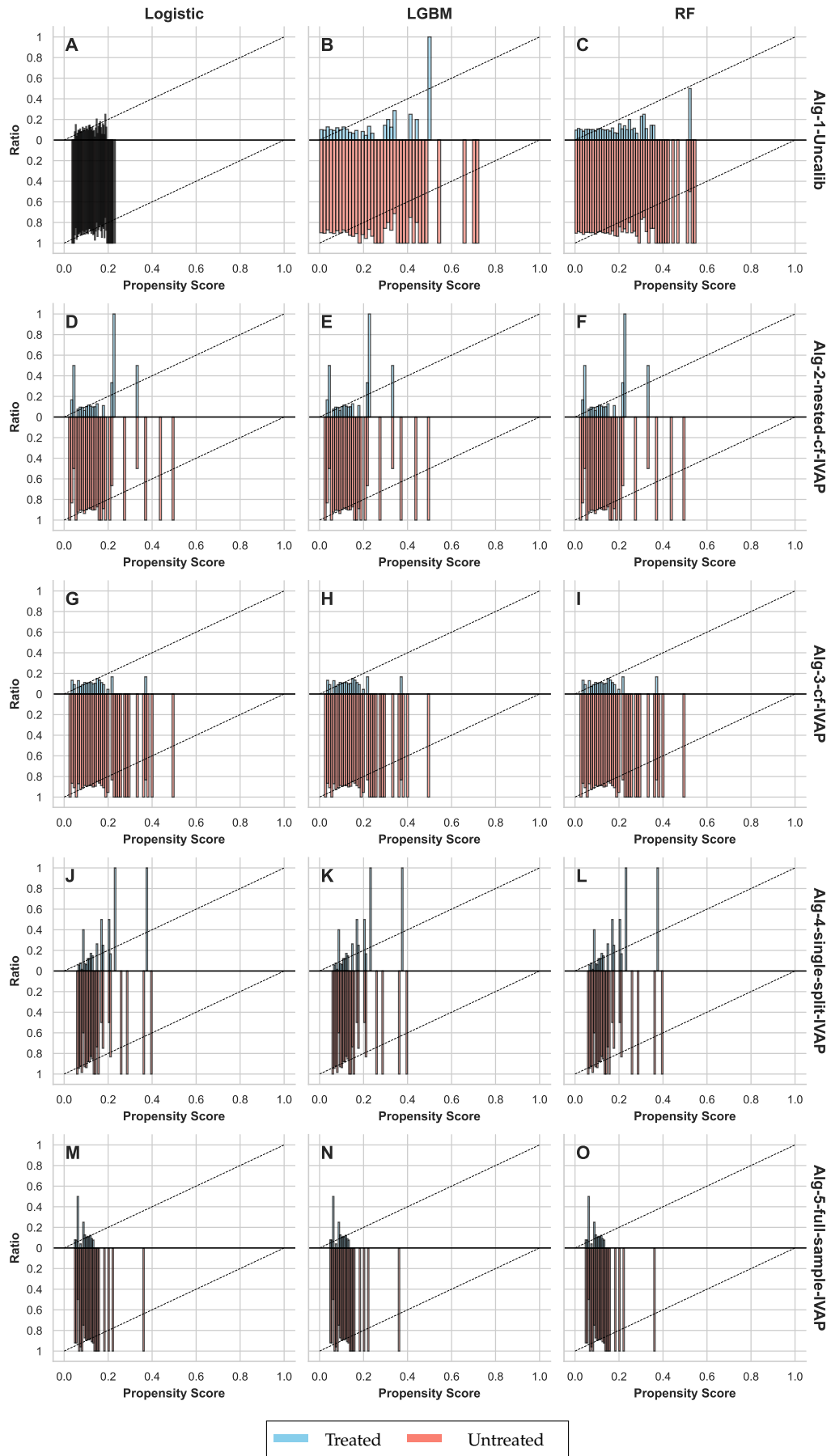


Figure 22: DGP 4 Unbalanced, $\alpha = 0.1$, $m = \text{LGBM}$, $g = \text{LGBM}$, $n = 4000$, $p = 20$, Calibration method for Algorithms 2-4: Venn-ABERS

Calibration Errors

DGP 1 IRM

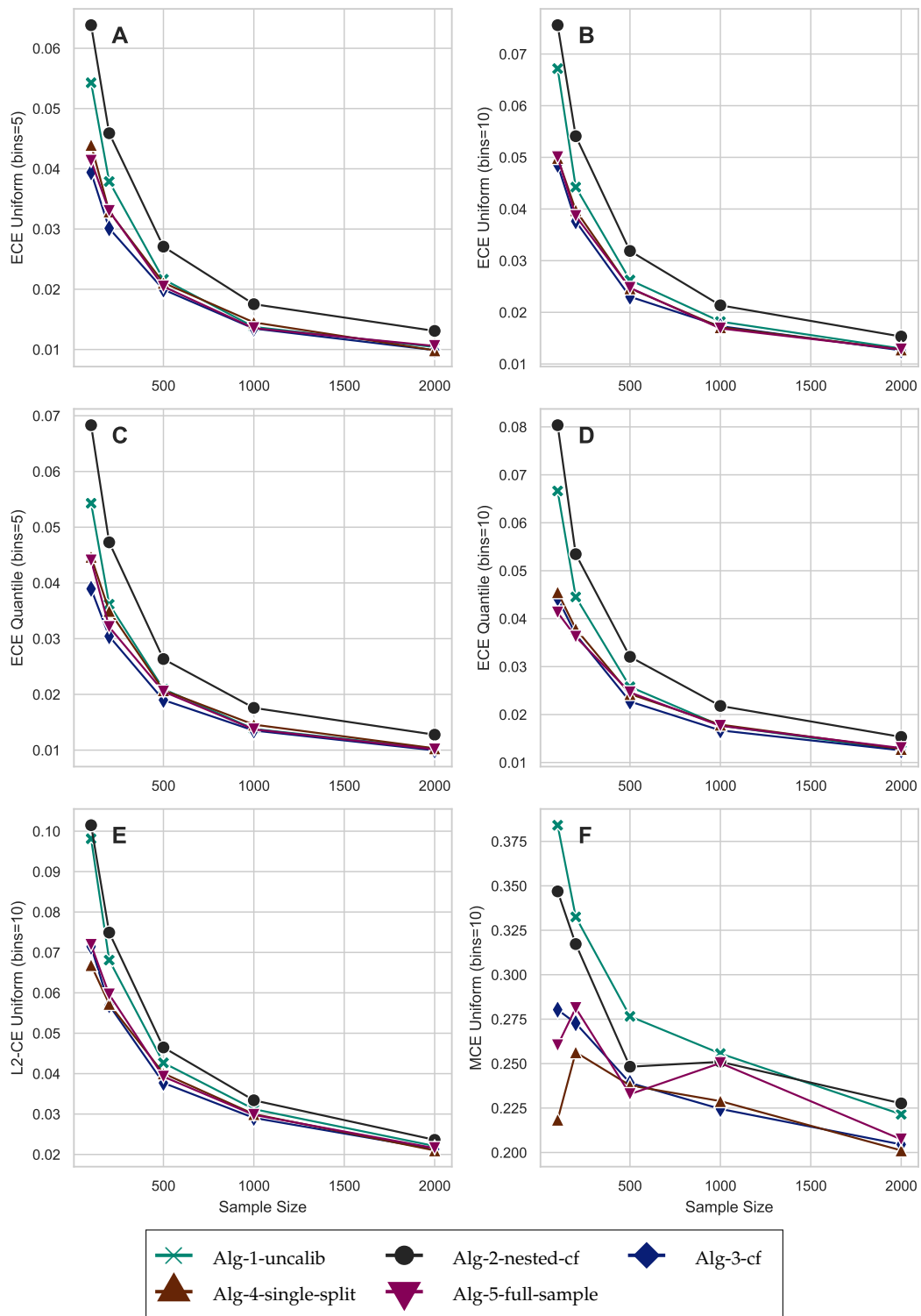


Figure 23: DGP 1 IRM, R2D = 0.5, m = Logit, p = 20, Clipping threshold for Algorithms 1,2,4 = 0.01, Calibration method for Algorithms 2-4: isotonic regression

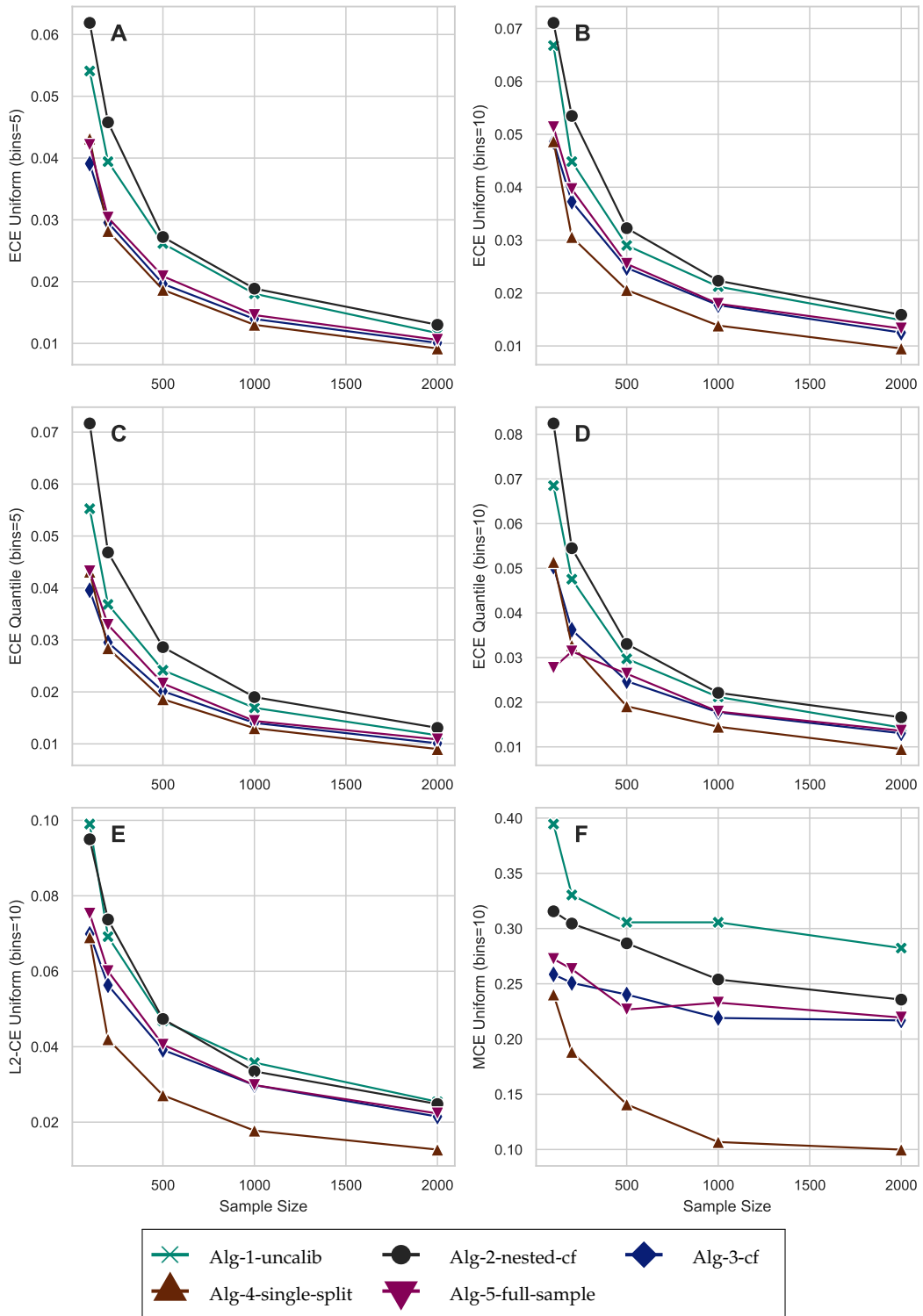


Figure 24: DGP 1 IRM, R2D = 0.5, m = LGBM, p = 20, Calibration method for Algorithms 2-5: isotonic regression

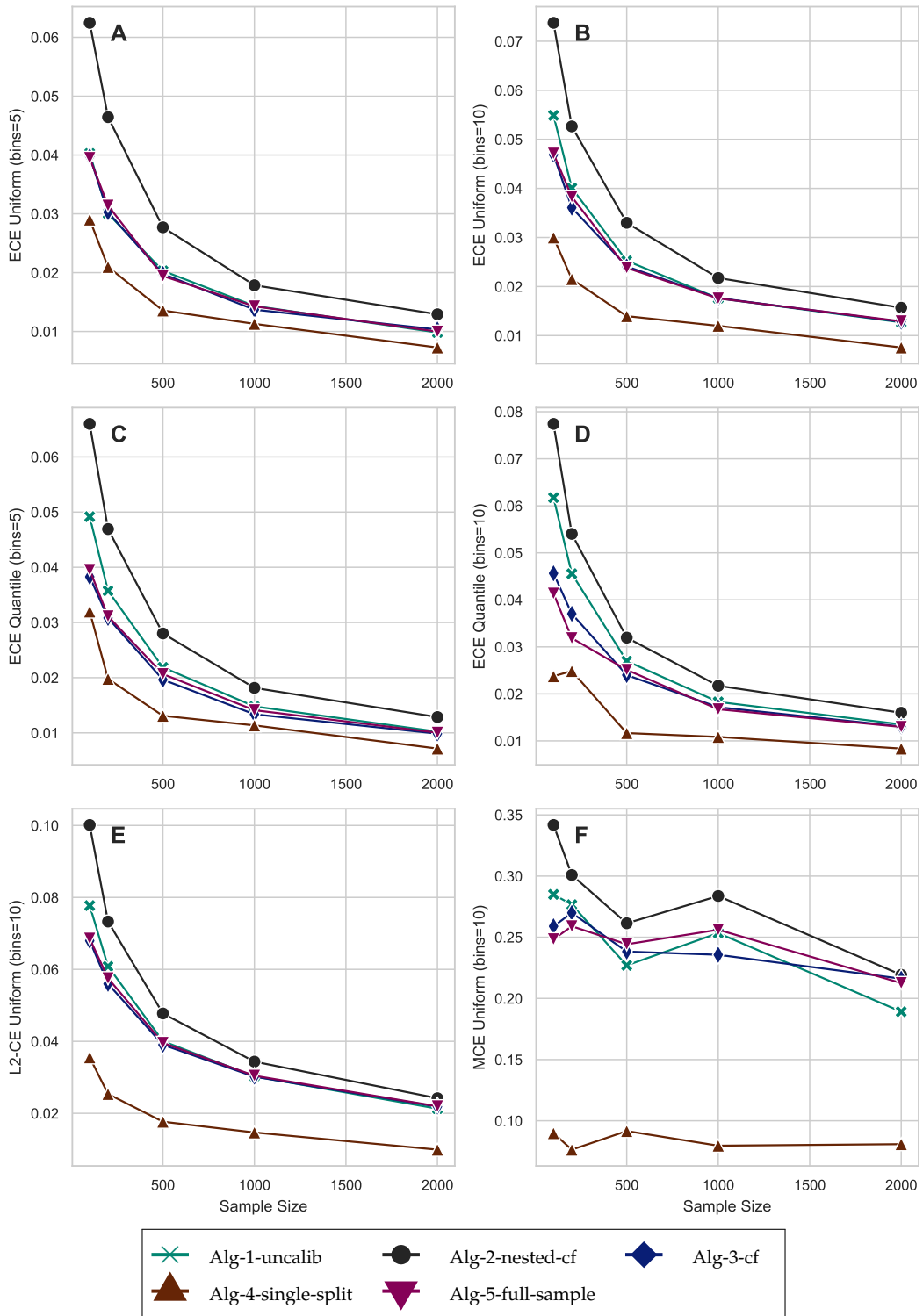


Figure 25: DGP 1 IRM, $R^2D = 0.5$, $m = \text{RF}$, $p = 20$, Calibration method for Algorithms 2-5: isotonic regression

DGP 2 Drug

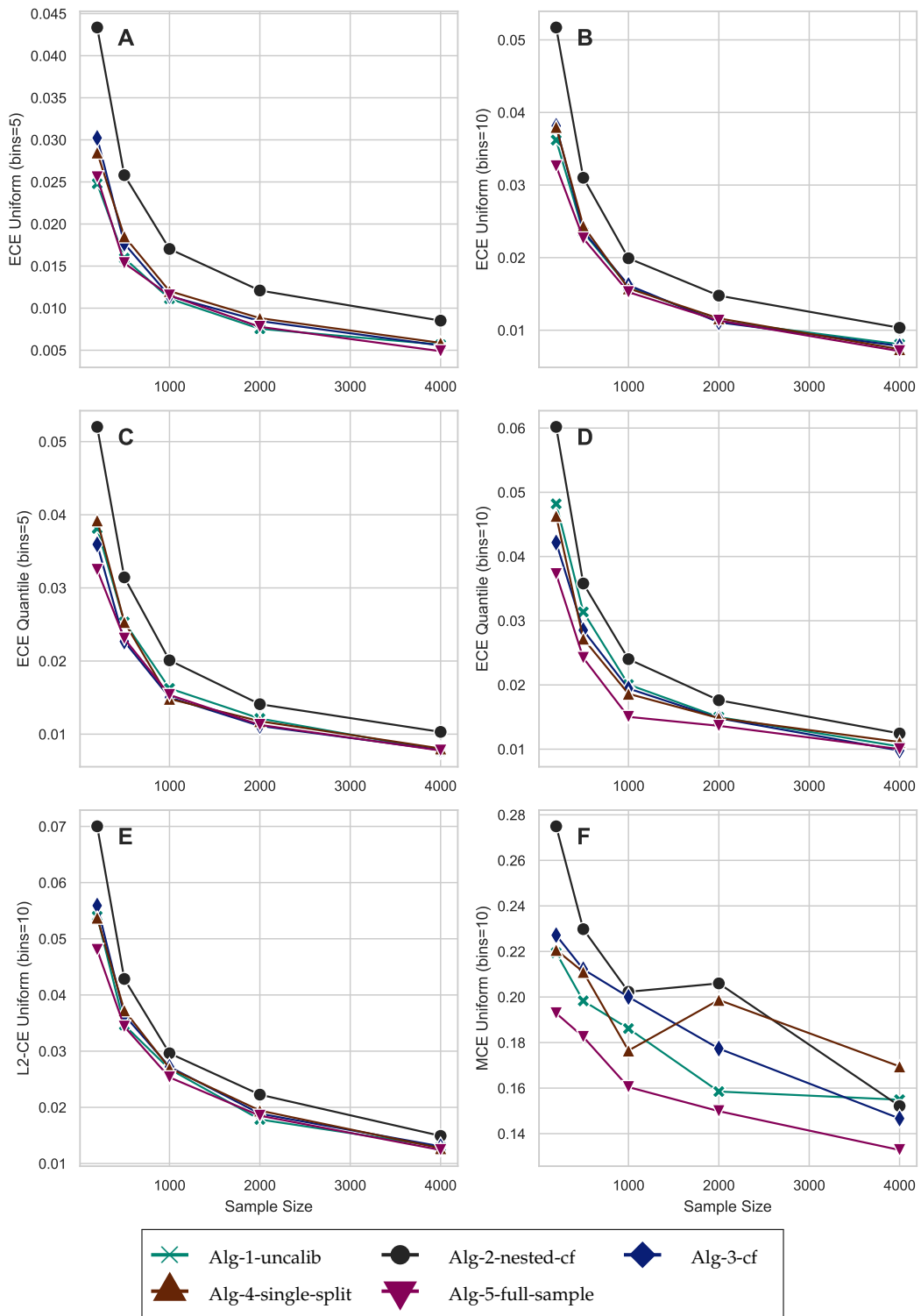


Figure 26: DGP 2 Drug, Overlap = 0.5, $m = \text{Logit}$, $n = 2000$, $p = 3$, Calibration method for Algorithms 2-4: isotonic regression

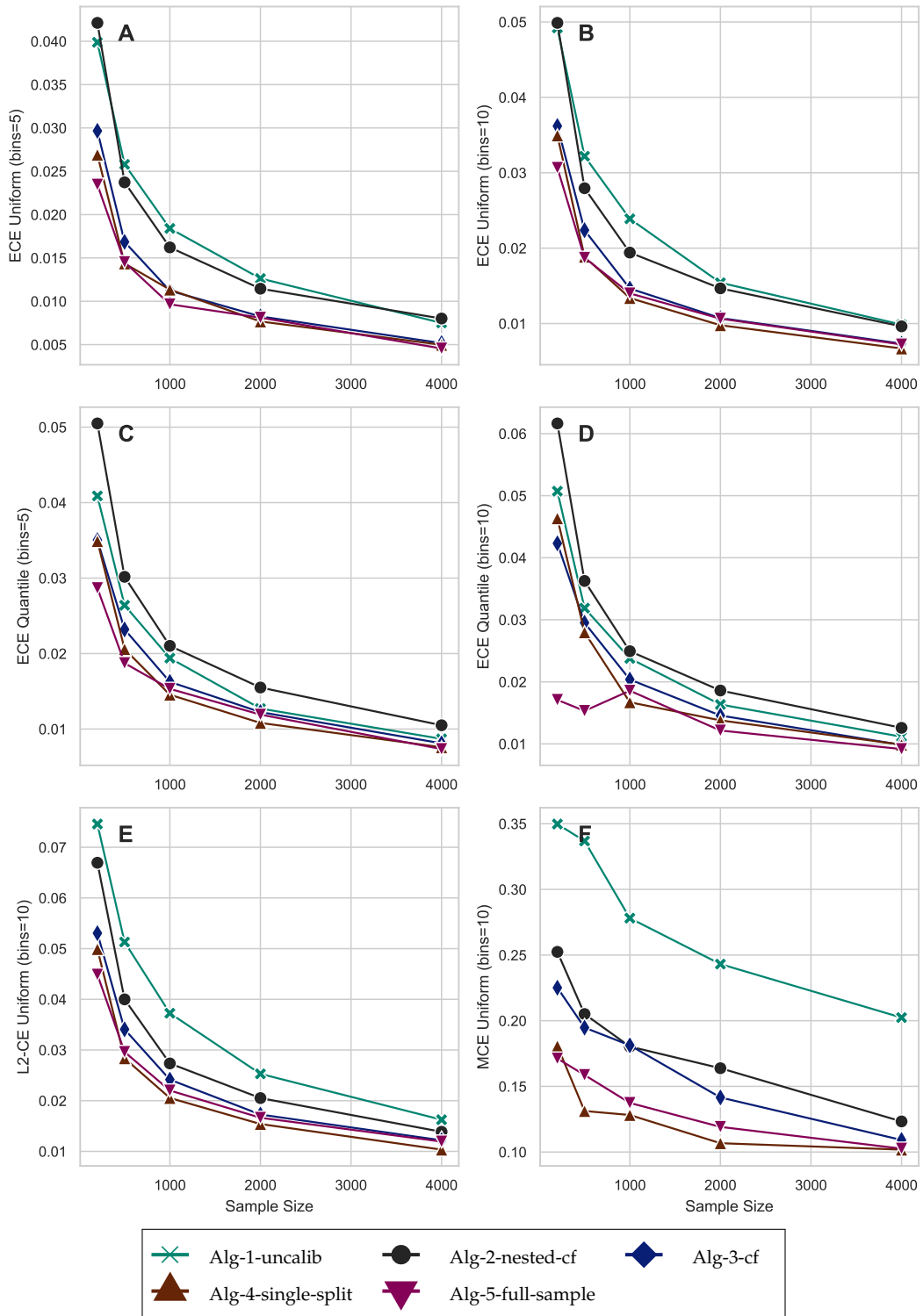


Figure 27: DGP 2 Drug, Overlap = 0.5, $m = \text{LGBM}$, $p = 3$, Calibration method for Algorithms 2-5: isotonic regression

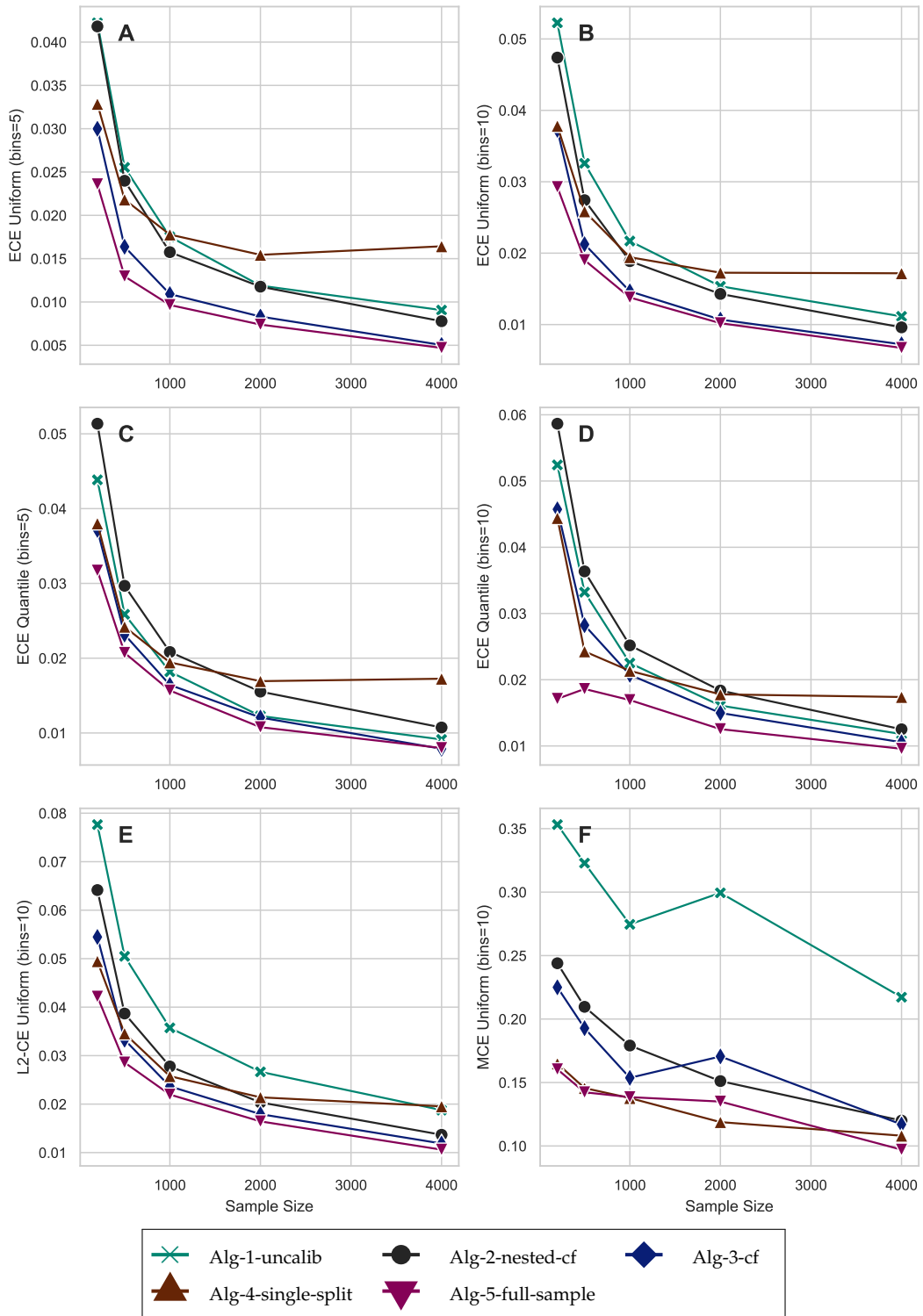


Figure 28: DGP 2 Drug, Overlap = 0.5, $m = \text{RF}$, $p = 3$, Calibration method for Algorithms 2-5: isotonic regression

Nonlinear

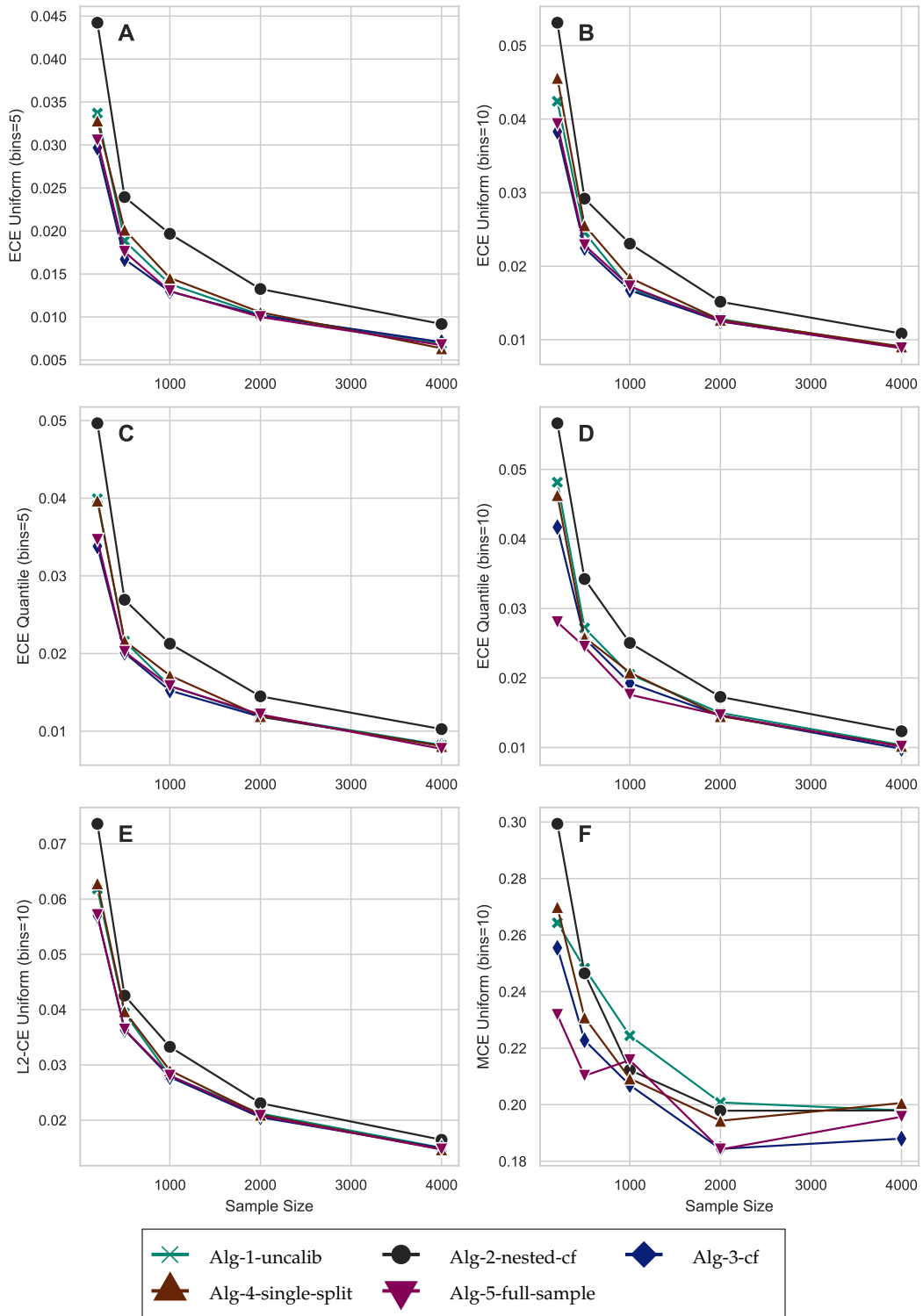


Figure 29: DGP 3 Nonlinear, $m = \text{Logit}$, $p = 4$, Calibration method for Algorithms 2-4: isotonic regression

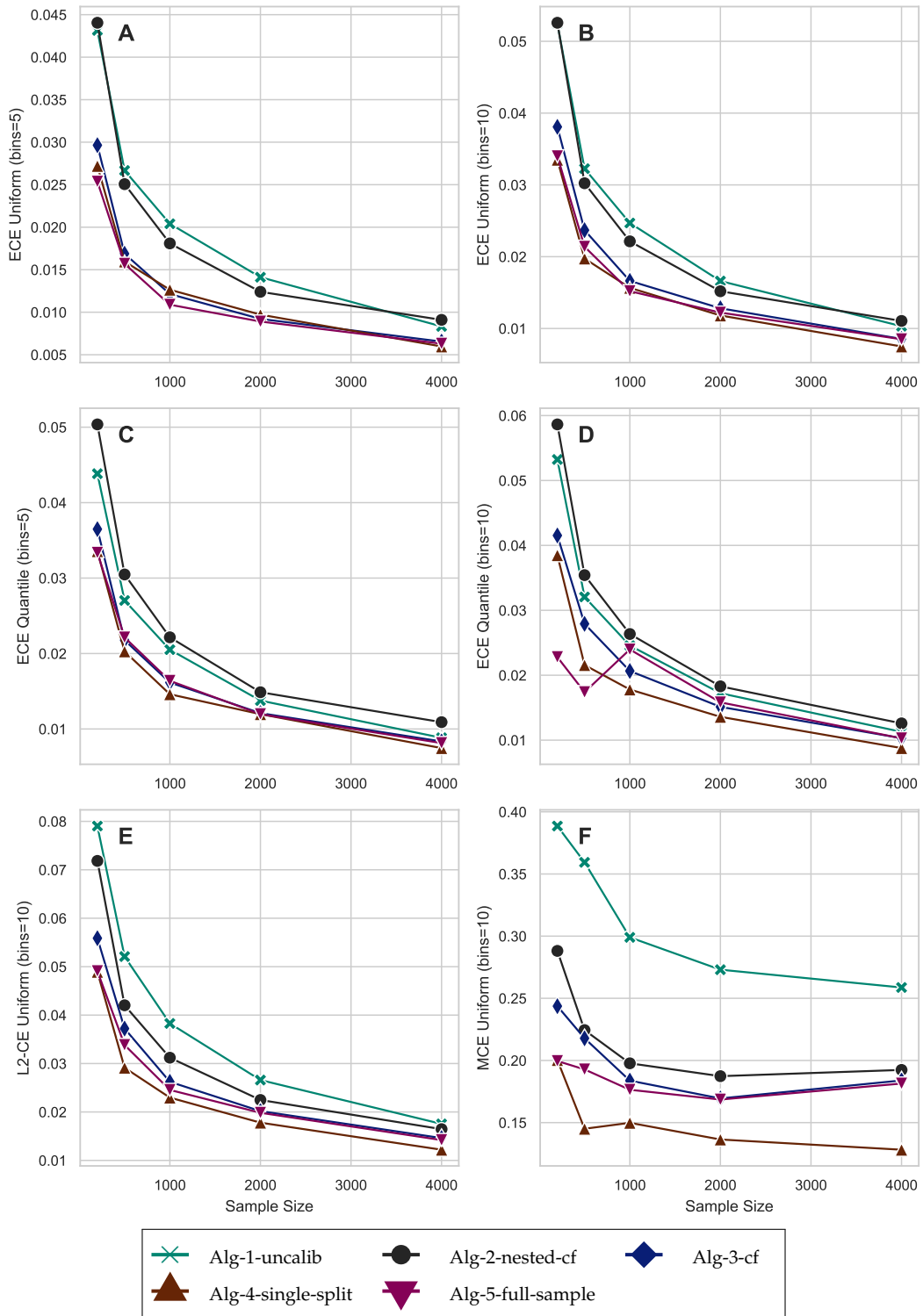


Figure 30: DGP 3 Nonlinear, $m = \text{LGBM}$, $p = 4$, Calibration method for Algorithms 2-5: isotonic regression

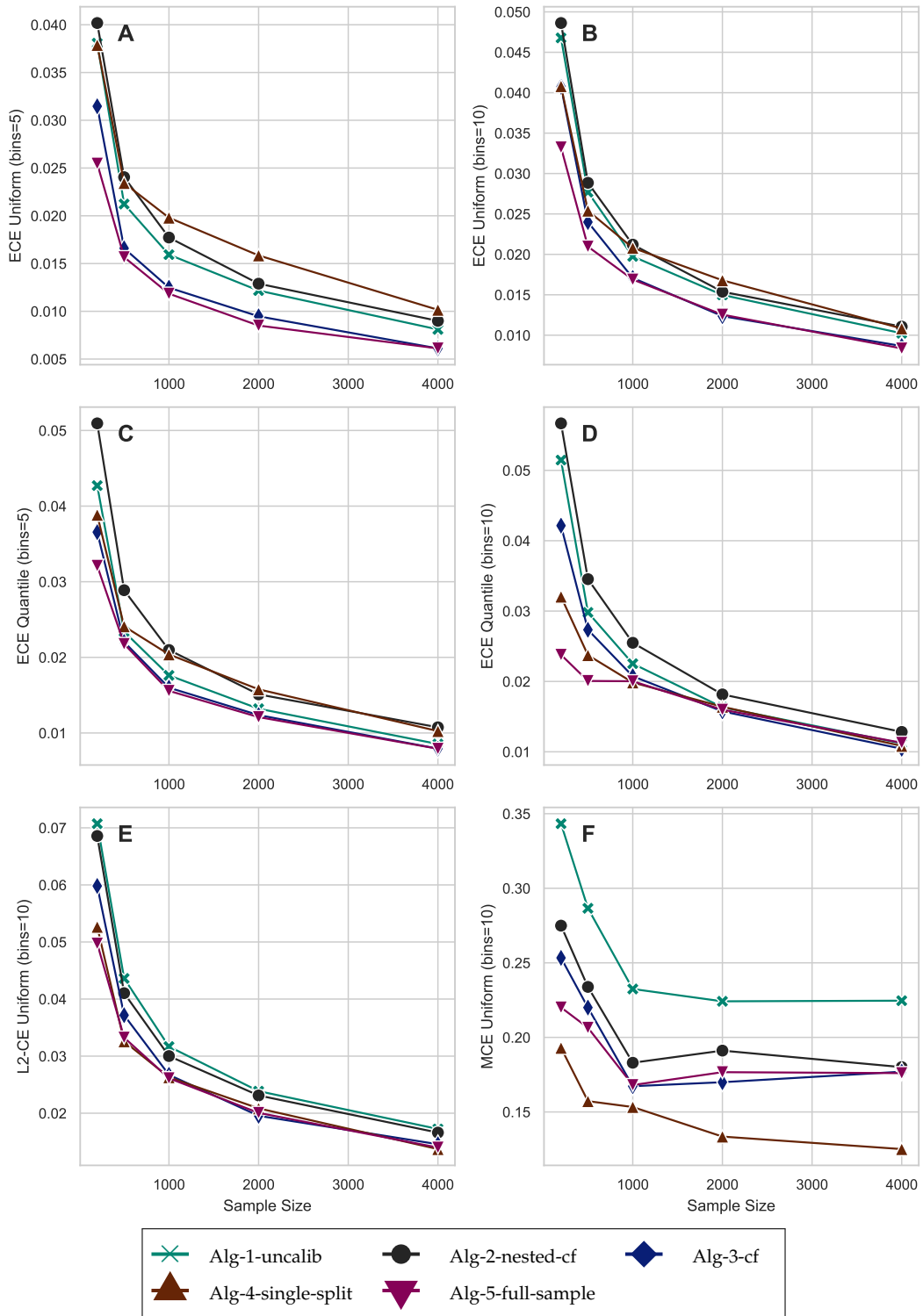


Figure 31: DGP 3 Nonlinear, $m = \text{RF}$, $p = 4$, Calibration method for Algorithms 2-5: isotonic regression

DGP 4 Unbalanced

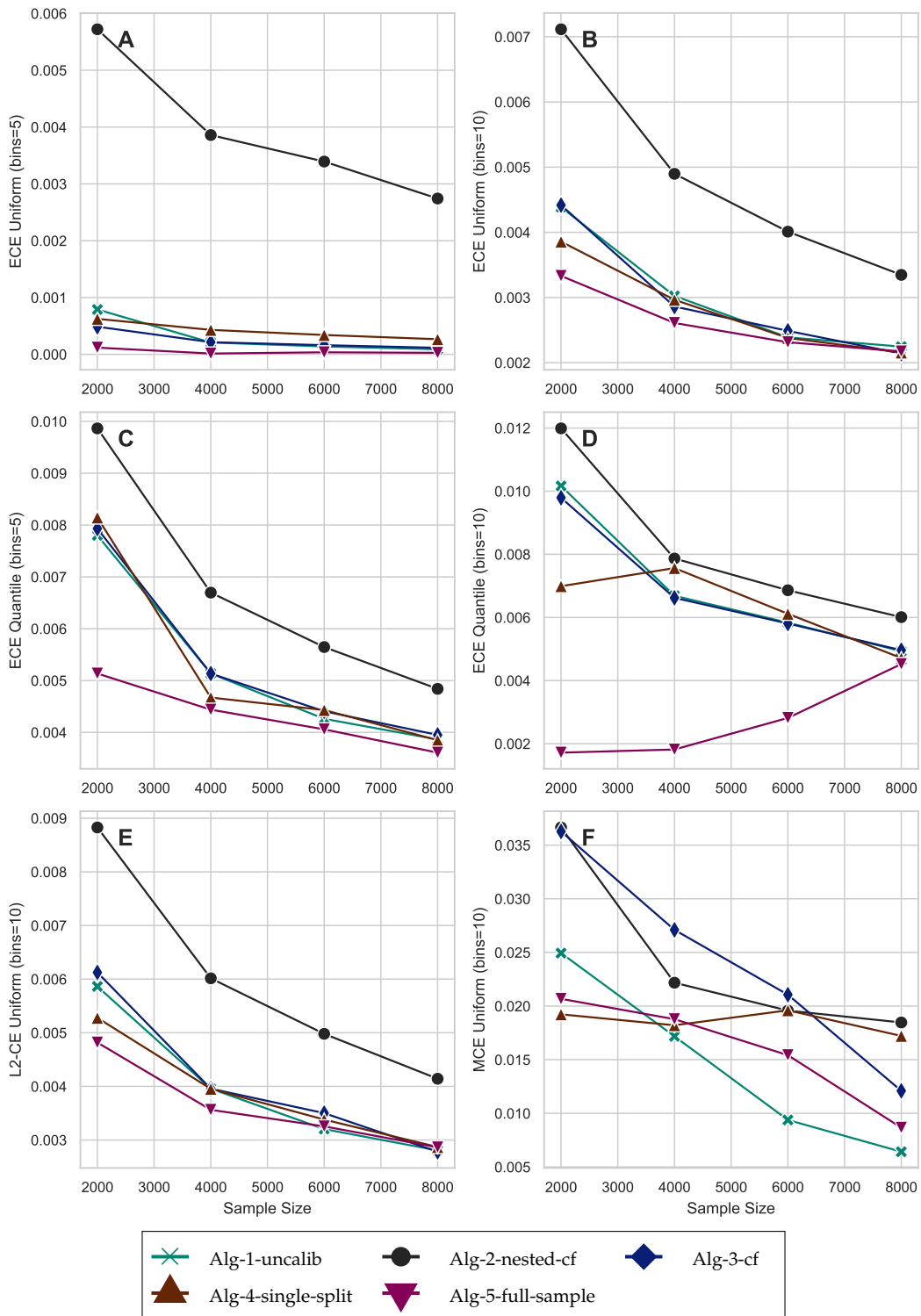


Figure 32: DGP 4 Unbalanced, Share_treated = 0.1, m = Logit, p = 20, Calibration method for Algorithms 2-4: isotonic regression

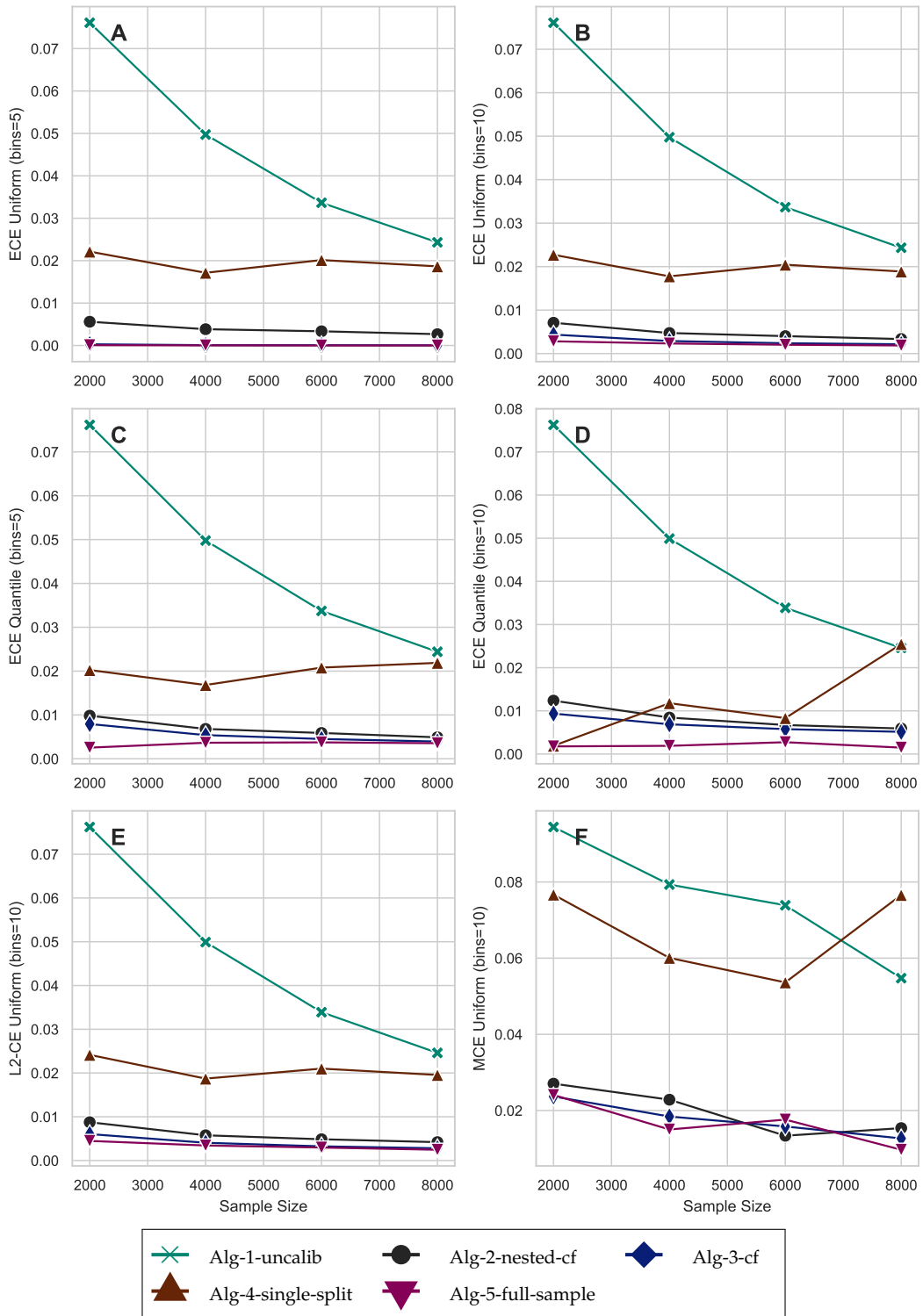


Figure 33: DGP 4 Unbalanced, Share_treated = 0.1, m = LGBM, p = 20, Calibration method for Algorithms 2-5: isotonic regression

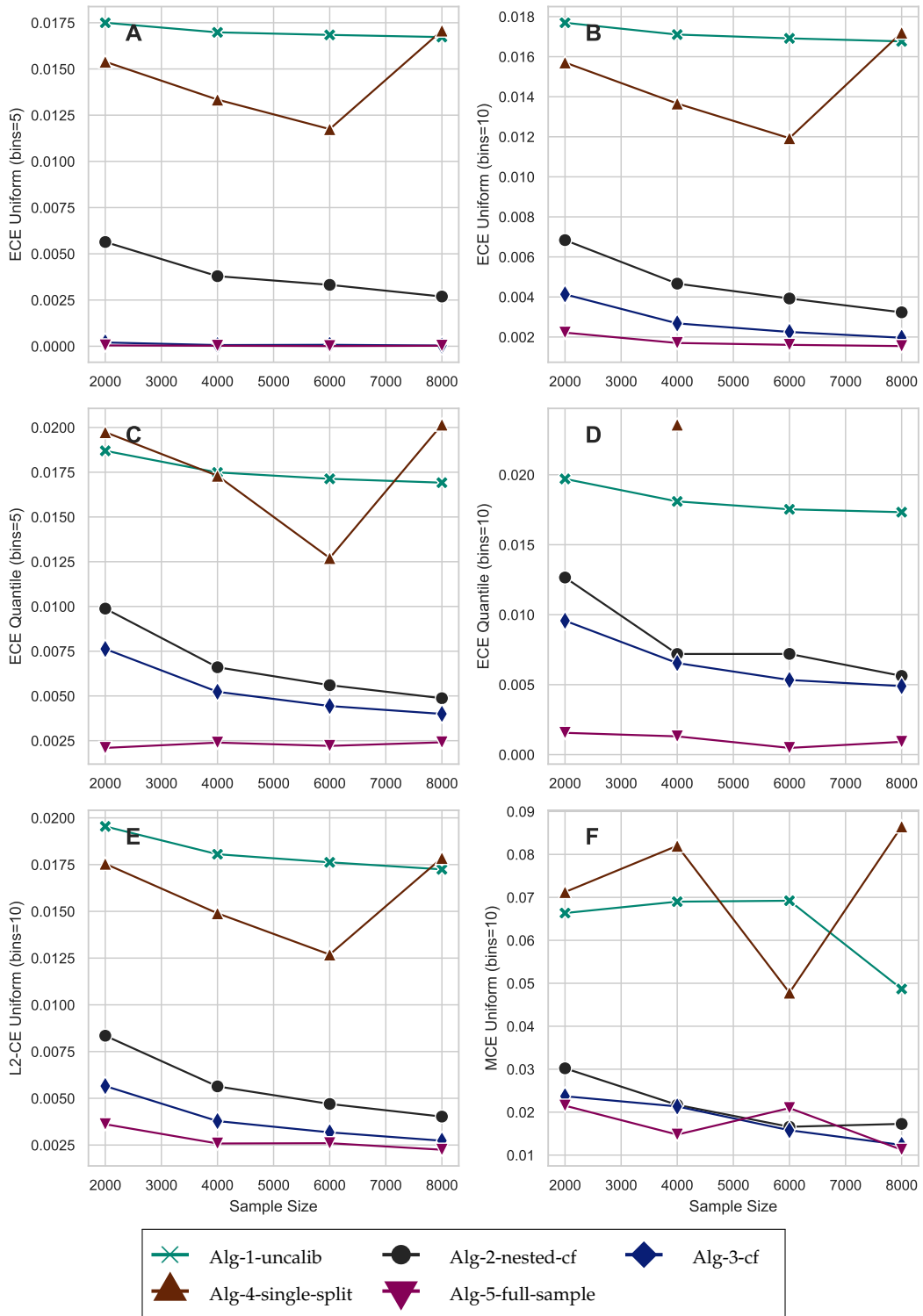


Figure 34: DGP 4 Unbalanced, Share_treated = 0.1, m = RF, p = 20, Calibration method for Algorithms 2-5: isotonic regression

ATE Errors on Sample Size

DGP 1 IRM

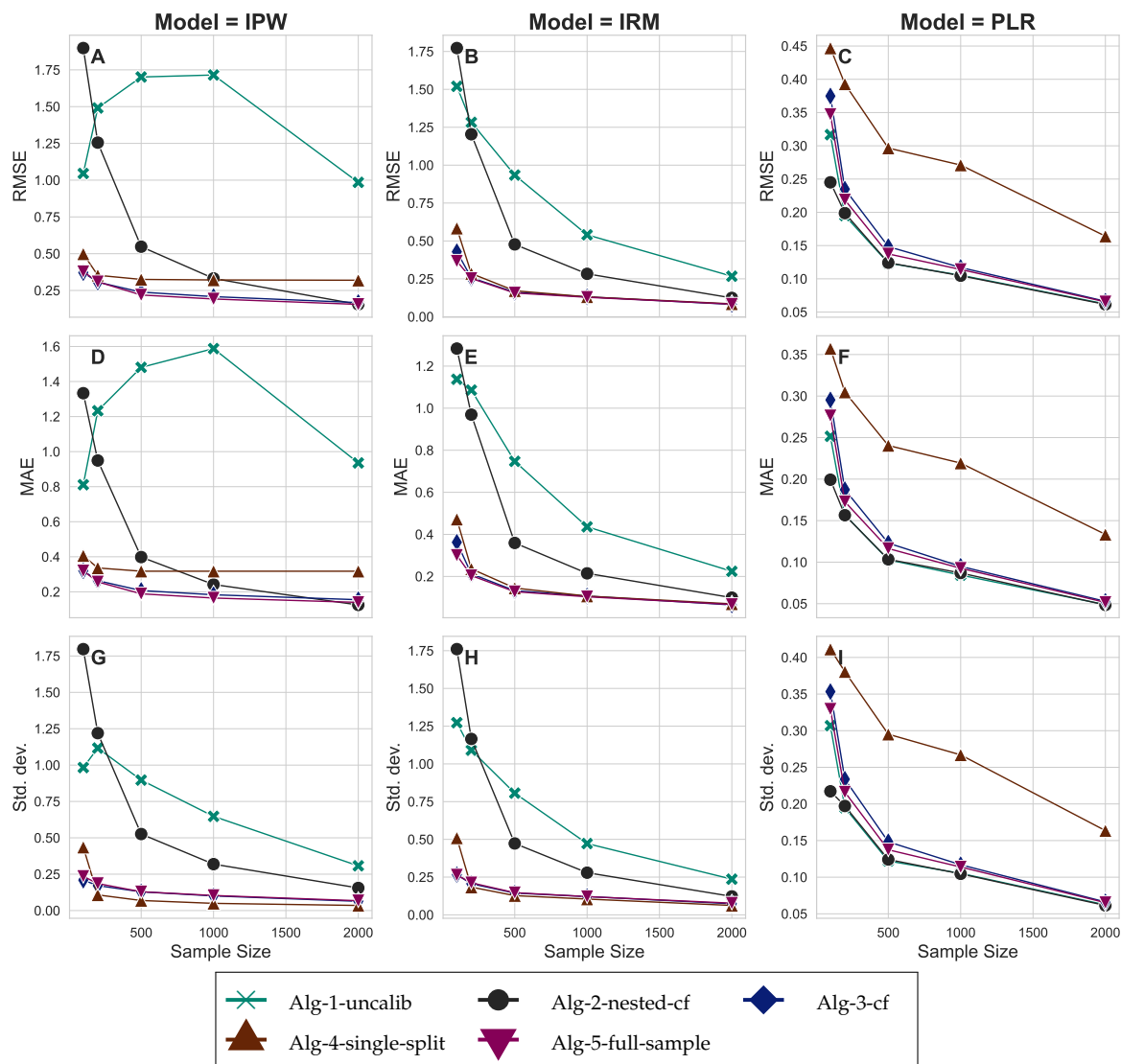


Figure 35: DGP 1 IRM, R2D = 0.5, m = LGBM, g = LGBM, p = 20, Calibration method for Algorithms 2-5: isotonic regression, Clip = 0.01

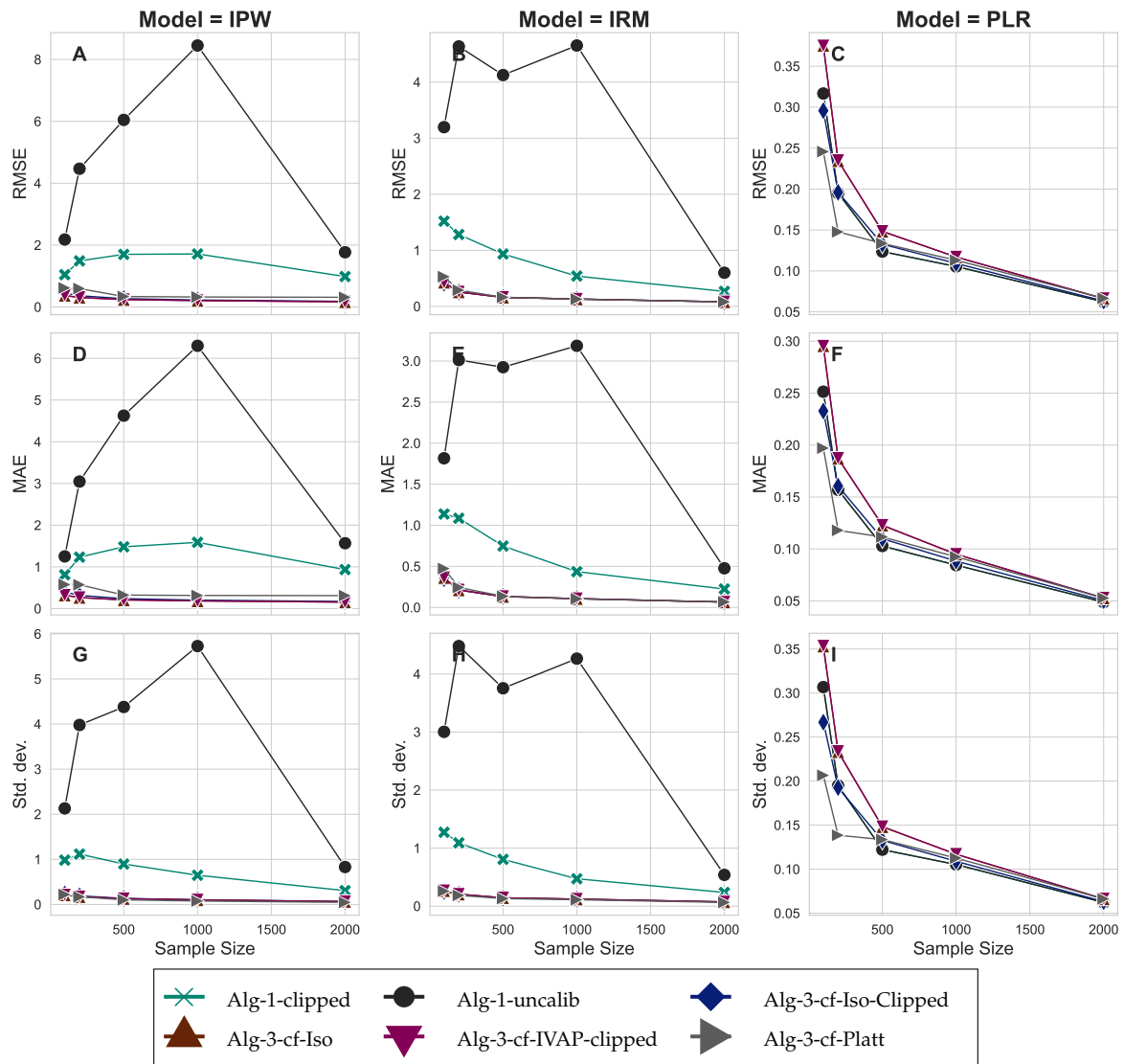


Figure 36: DGP 1 IRM, different calibration methods for Algorithm 3, $R2D = 0.5$, $m = \text{LGBM}$, $g = \text{LGBM}$, $p = 20$, $\text{Clip} = 0.01$

DGP 2 Drug

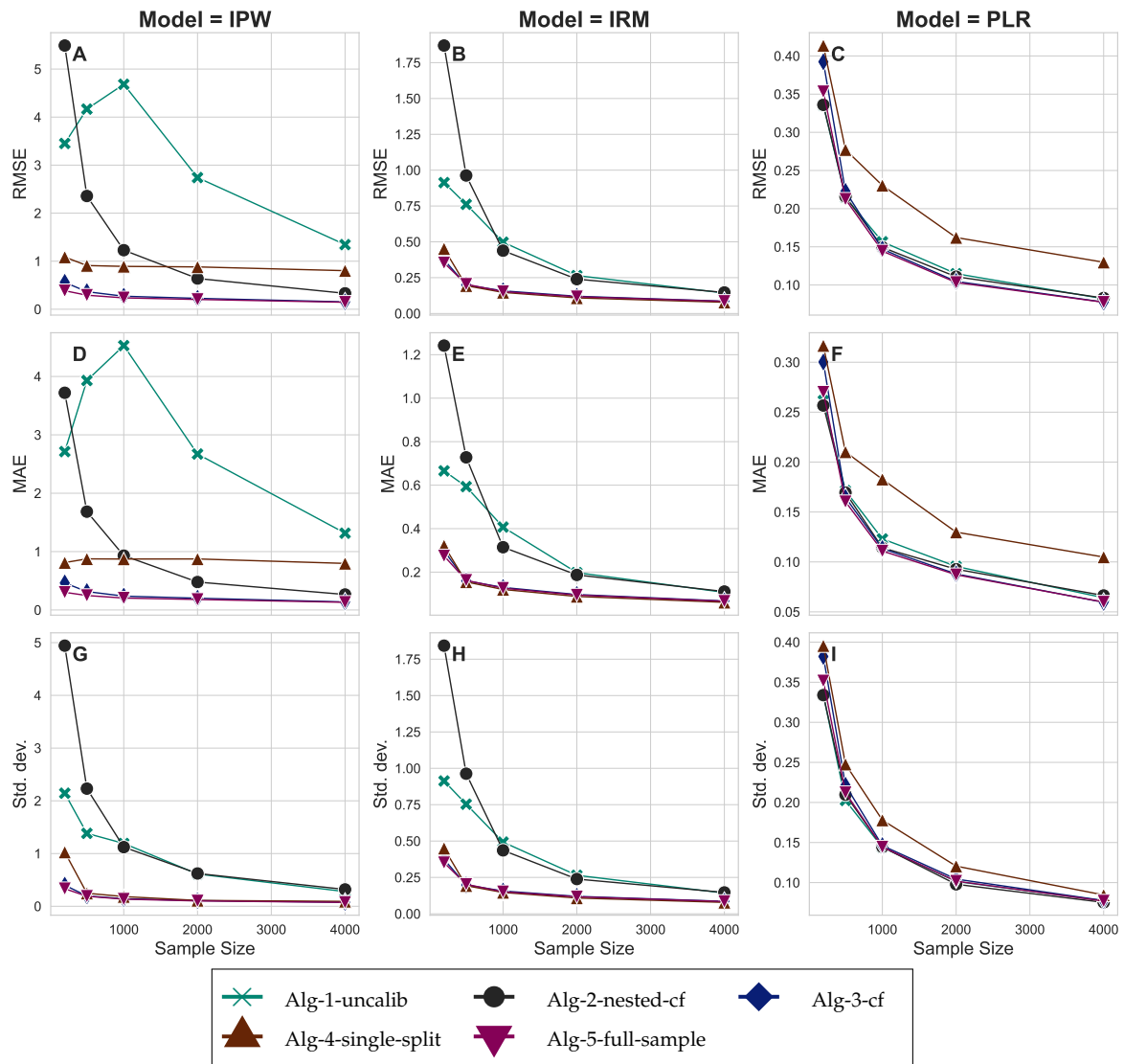


Figure 37: DGP 2 Drug, Overlap = 0.5, $m = \text{LGBM}$, $g = \text{LGBM}$, $p = 3$, Calibration method for Algorithms 2-5: isotonic regression, Clip = 0.01

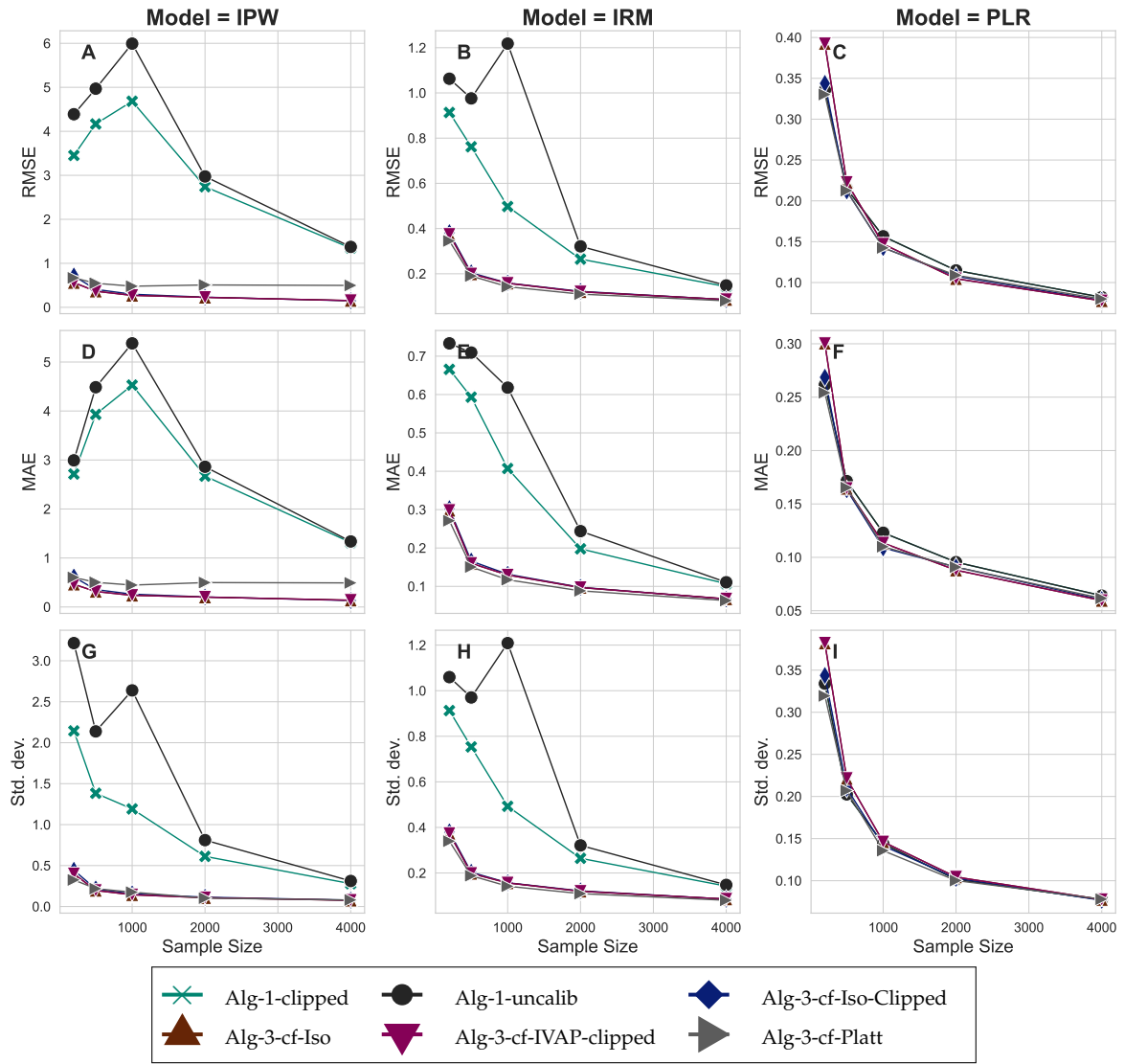


Figure 38: DGP 2 Drug, different calibration methods for Algorithm 3, Overlap = 0.5, $m =$ LGBM, $g =$ LGBM, $p = 3$, Clip = 0.01

DGP 3 Nonlinear

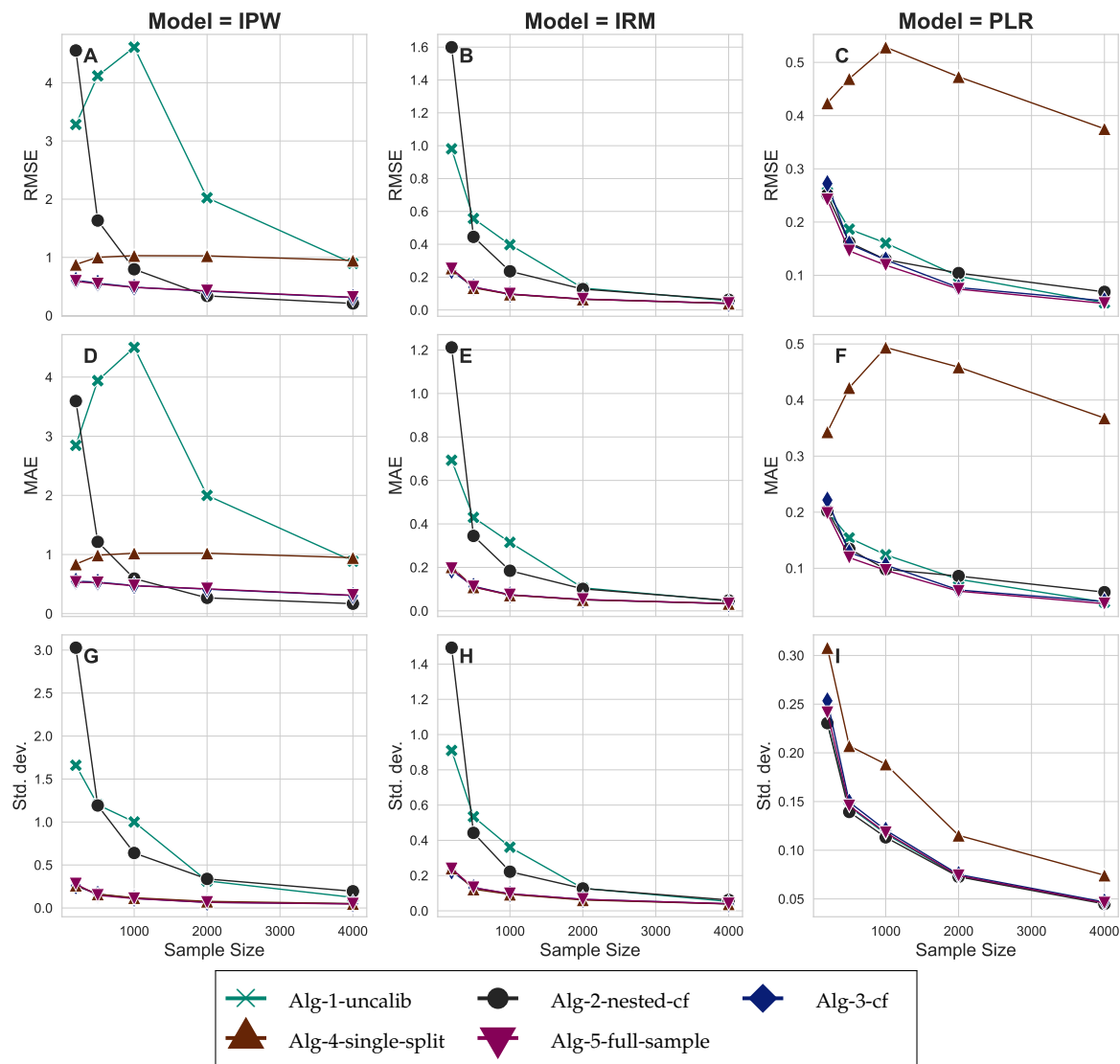


Figure 39: DGP 3 Nonlinear, $m = \text{LGBM}$, $g = \text{LGBM}$, $p = 4$, Calibration method for Algorithms 2-5: isotonic regression, $\text{Clip} = 0.01$

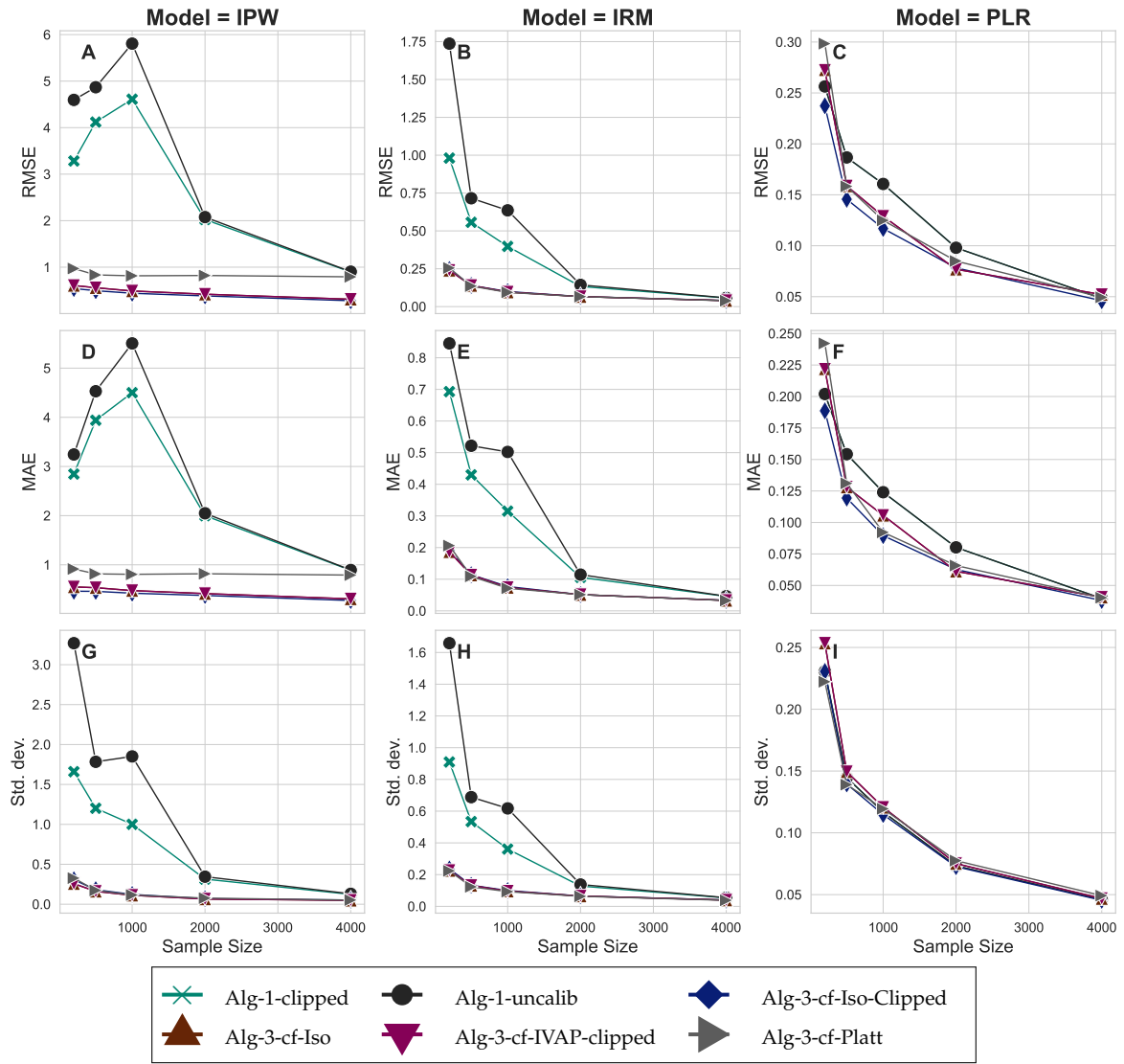


Figure 40: DGP 3 Nonlinear, different calibration methods for Algorithm 3, $m = \text{LGBM}$, $g = \text{LGBM}$, $p = 4$, $\text{Clip} = 0.01$

DGP 4 Unbalanced

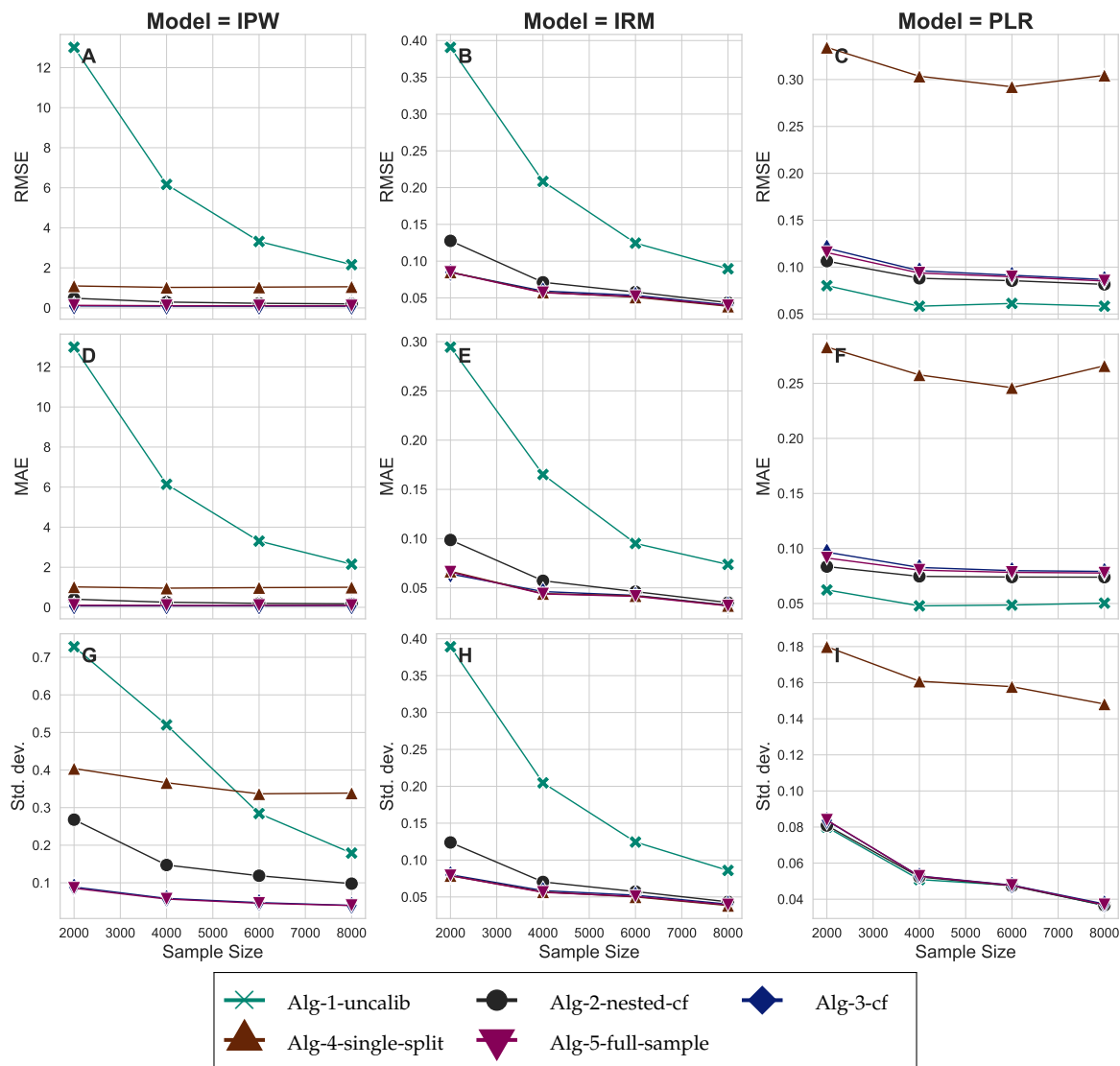


Figure 41: DGP 4 Unbalanced, Share_treated = 0.1, m = LGBM, g = LGBM, p = 20, Calibration method for Algorithms 2-5: isotonic regression, Clip = 0.01

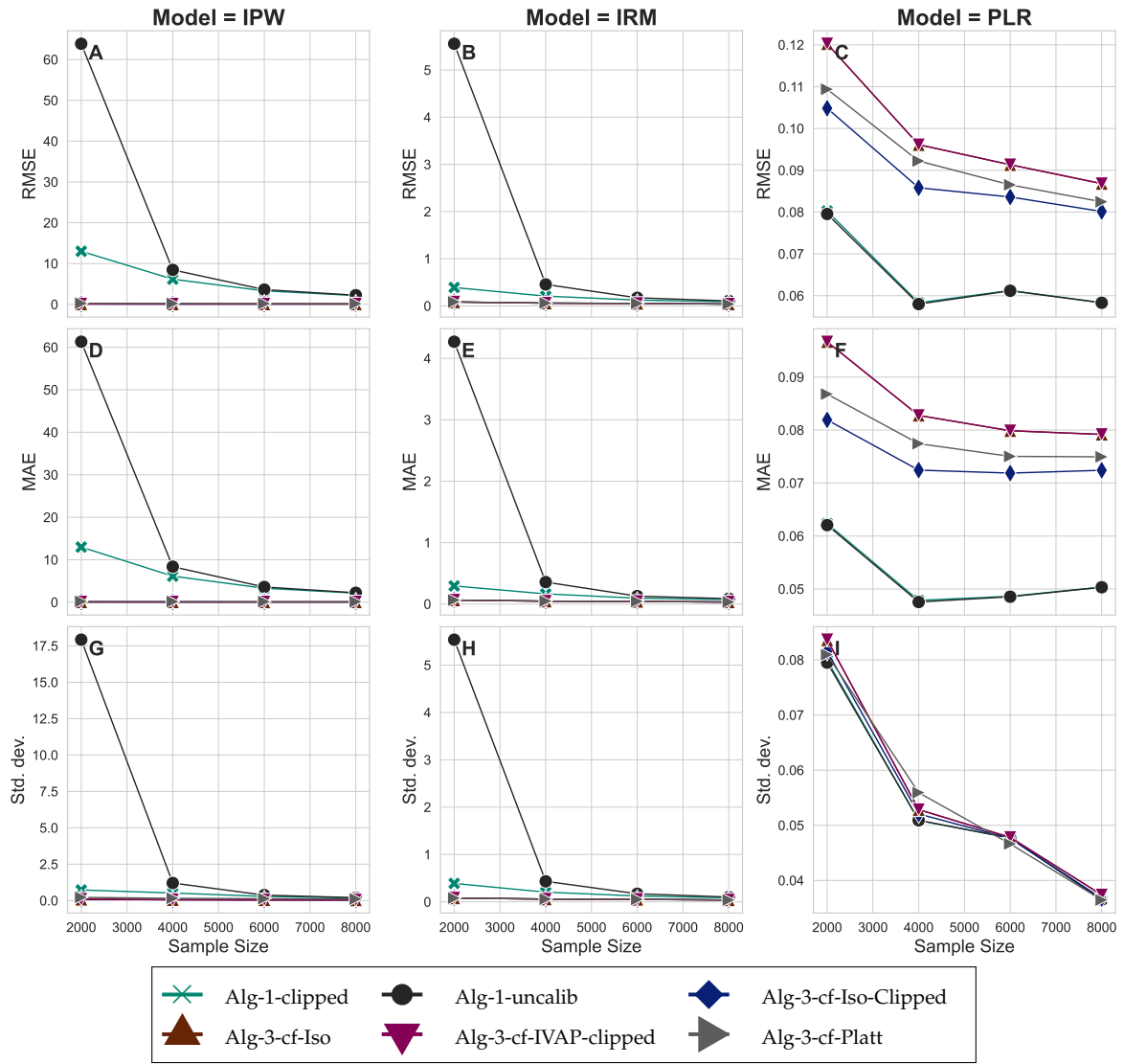


Figure 42: DGP 4 Unbalanced, different calibration methods for Algorithm 3, Share.treated = 0.1, m = LGBM, g = LGBM, p = 20, Clip = 0.01

Propensity Learner on ATE Distribution

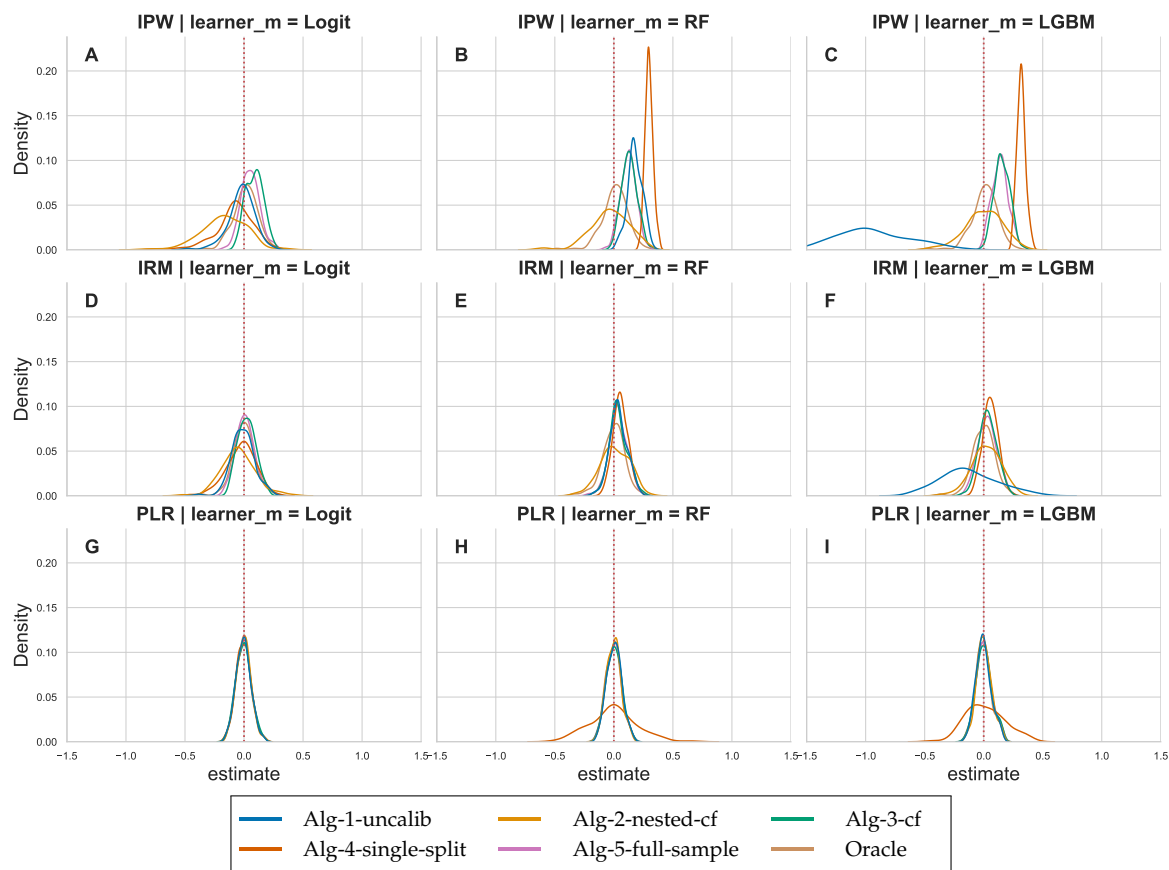


Figure 43: DGP 1 IRM, R2D = 0.5, m = LGBM, g = LGBM, n = 2000, p = 20, Calibration method for Algorithms 2-5: isotonic regression, Clip = 0.01

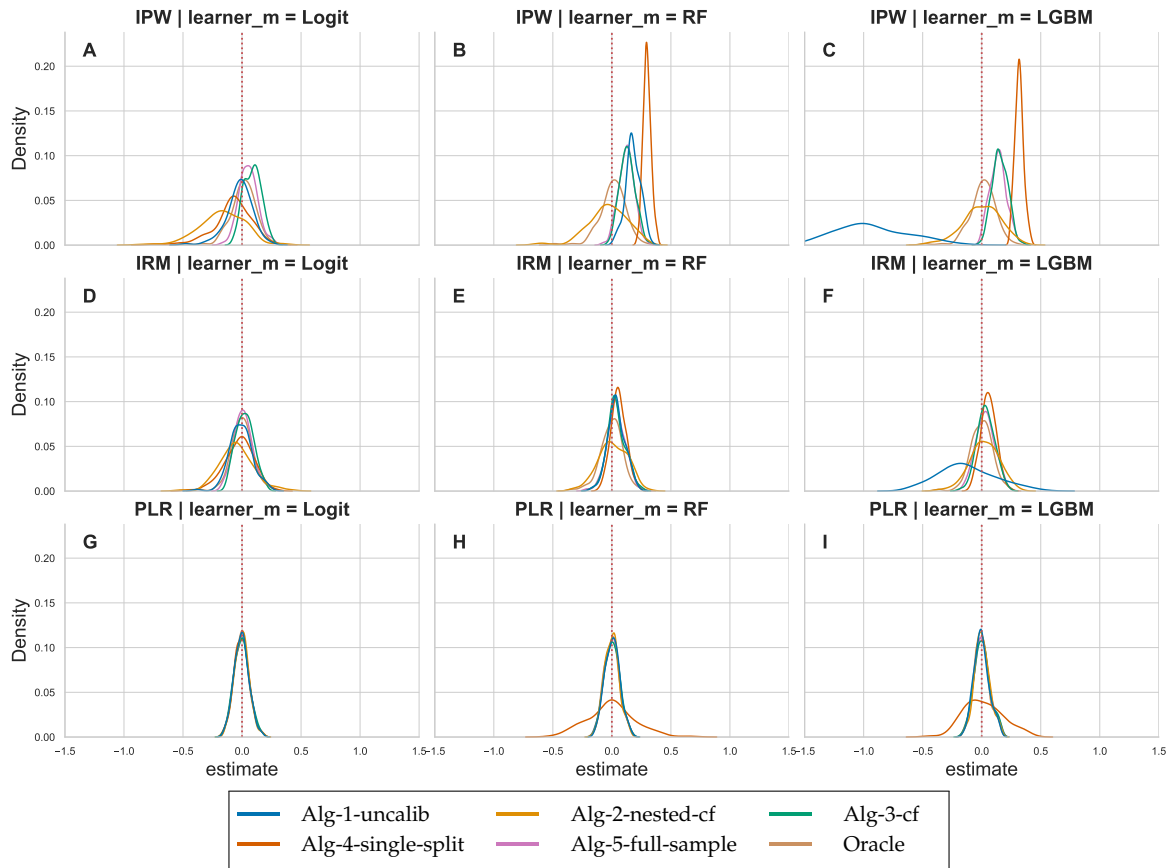


Figure 44: DGP 1 IRM, $R2D = 0.5$, $m = \text{LGBM}$, $g = \text{LGBM}$, $n = 2000$, $p = 20$, Calibration method for Algorithms 2-5: isotonic regression, $\text{Clip} = 0.01$

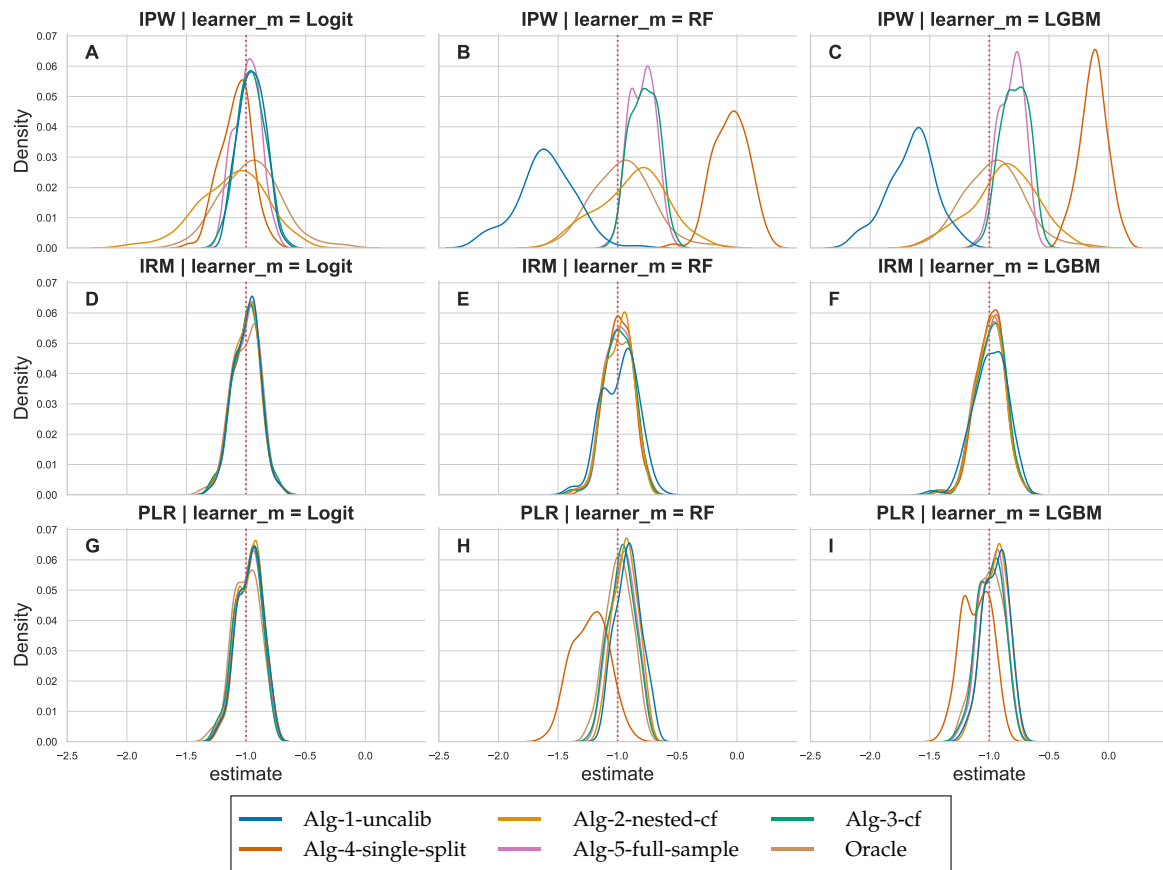


Figure 45: DGP 2 Drug, Overlap = 0.5, $m = \text{LGBM}$, $g = \text{LGBM}$, $n = 2000$, $p = 3$, Calibration method for Algorithms 2-5: isotonic regression, Clip = 0.01

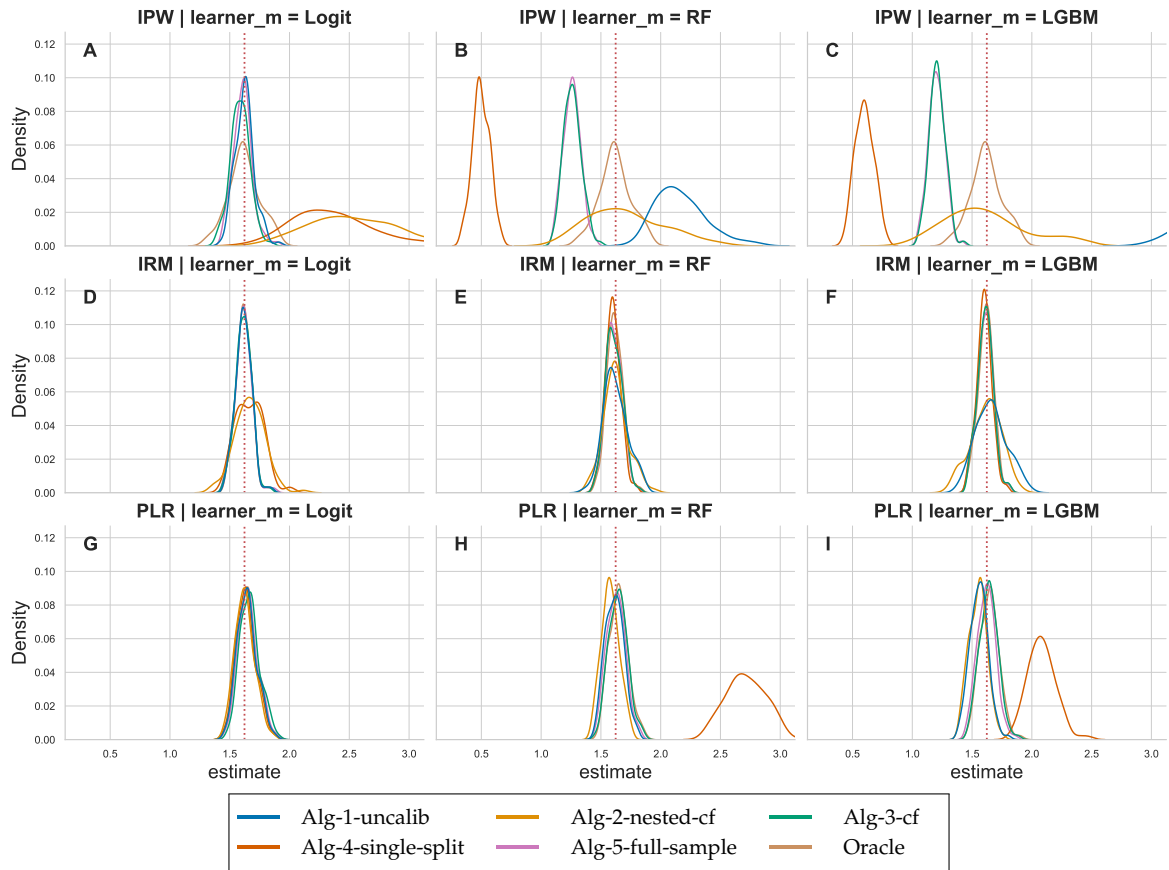


Figure 46: DGP 3 Nonlinear, $m = \text{LGBM}$, $g = \text{LGBM}$, $n = 2000$, $p = 4$, Calibration method for Algorithms 2-5: isotonic regression, $\text{Clip} = 0.01$

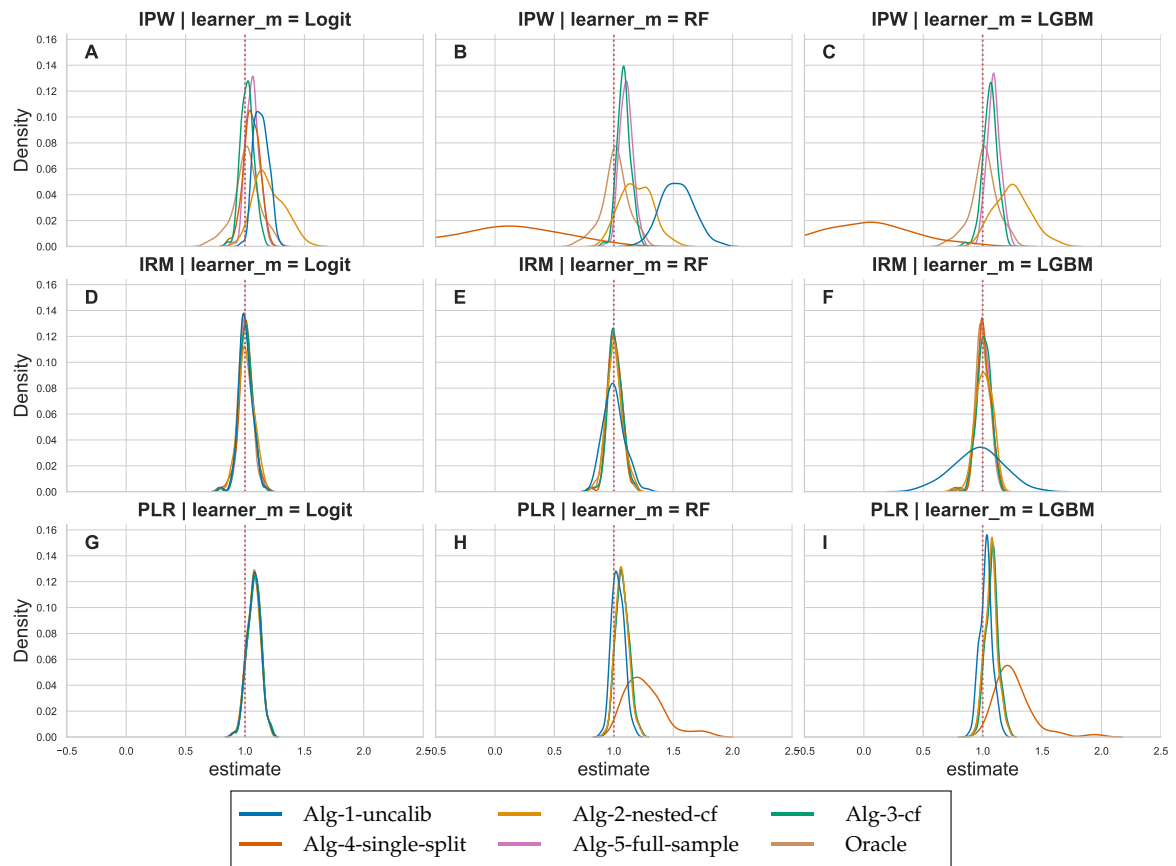


Figure 47: DGP 4 Unbalanced, Share.treated = 0.1, m = LGBM, g = LGBM, n = 4000, p = 20, Calibration method for Algorithms 2-5: isotonic regression, Clip = 0.01

Outcome Learner on ATE Distribution

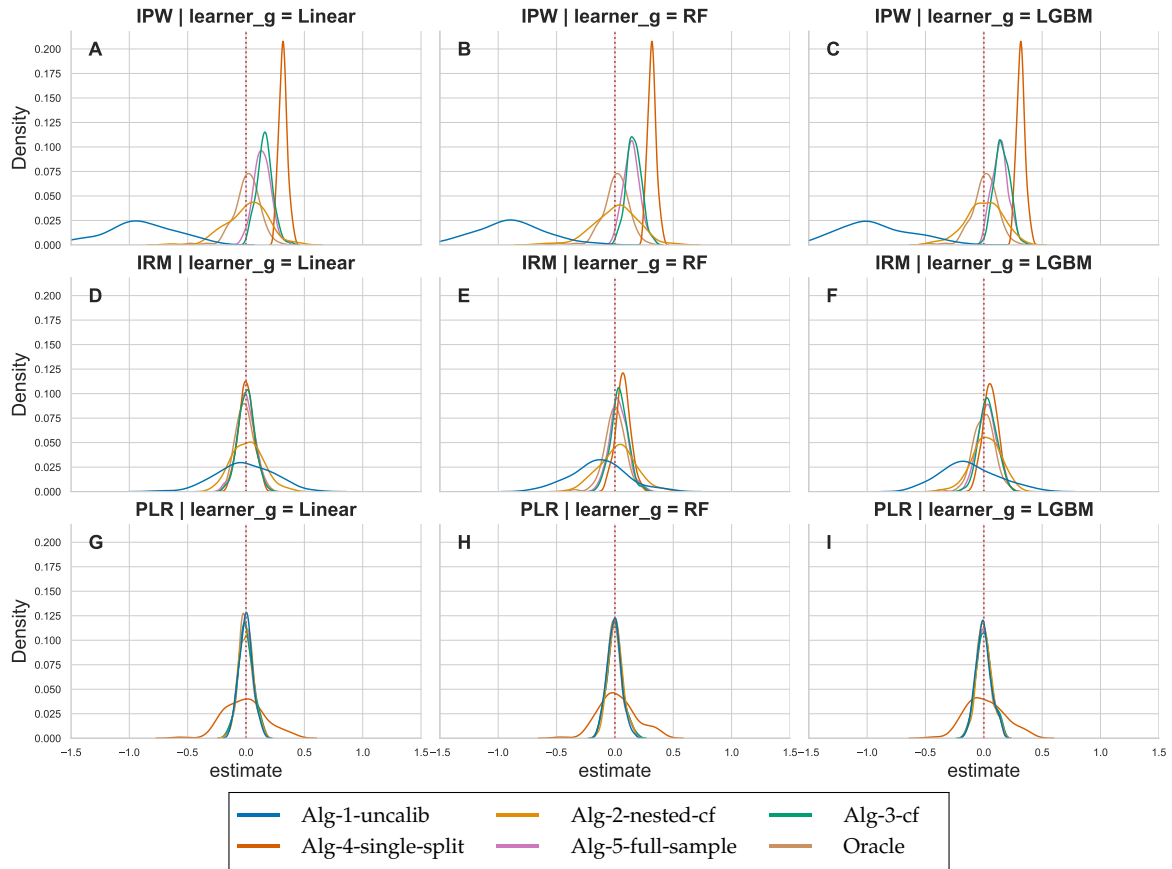


Figure 48: DGP 1 IRM, R2D = 0.5, m = LGBM, g = LGBM, n = 2000, p = 20, Calibration method for Algorithms 2-5: isotonic regression, Clip = 0.01

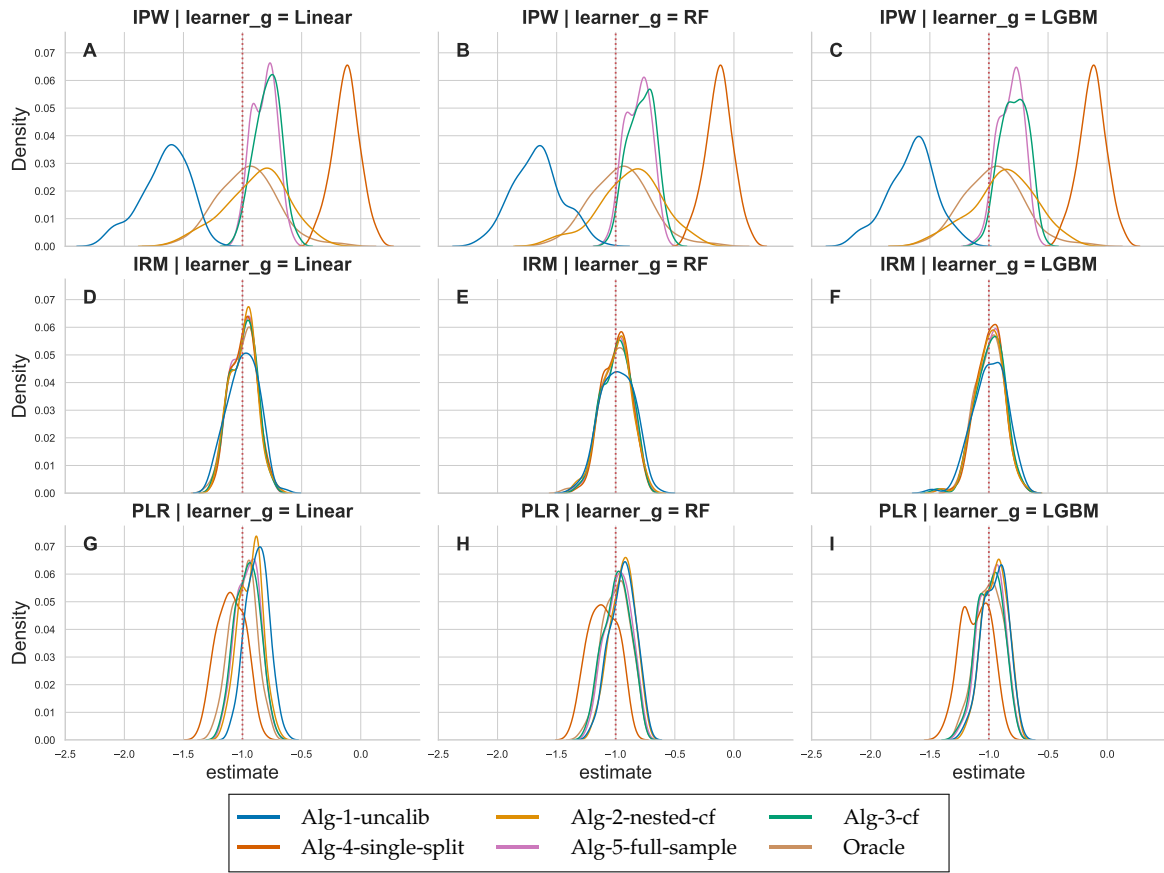


Figure 49: DGP 2 Drug, Overlap = 0.5, $m = \text{LGBM}$, $g = \text{LGBM}$, $n = 2000$, $p = 3$, Calibration method for Algorithms 2-5: isotonic regression, Clip = 0.01

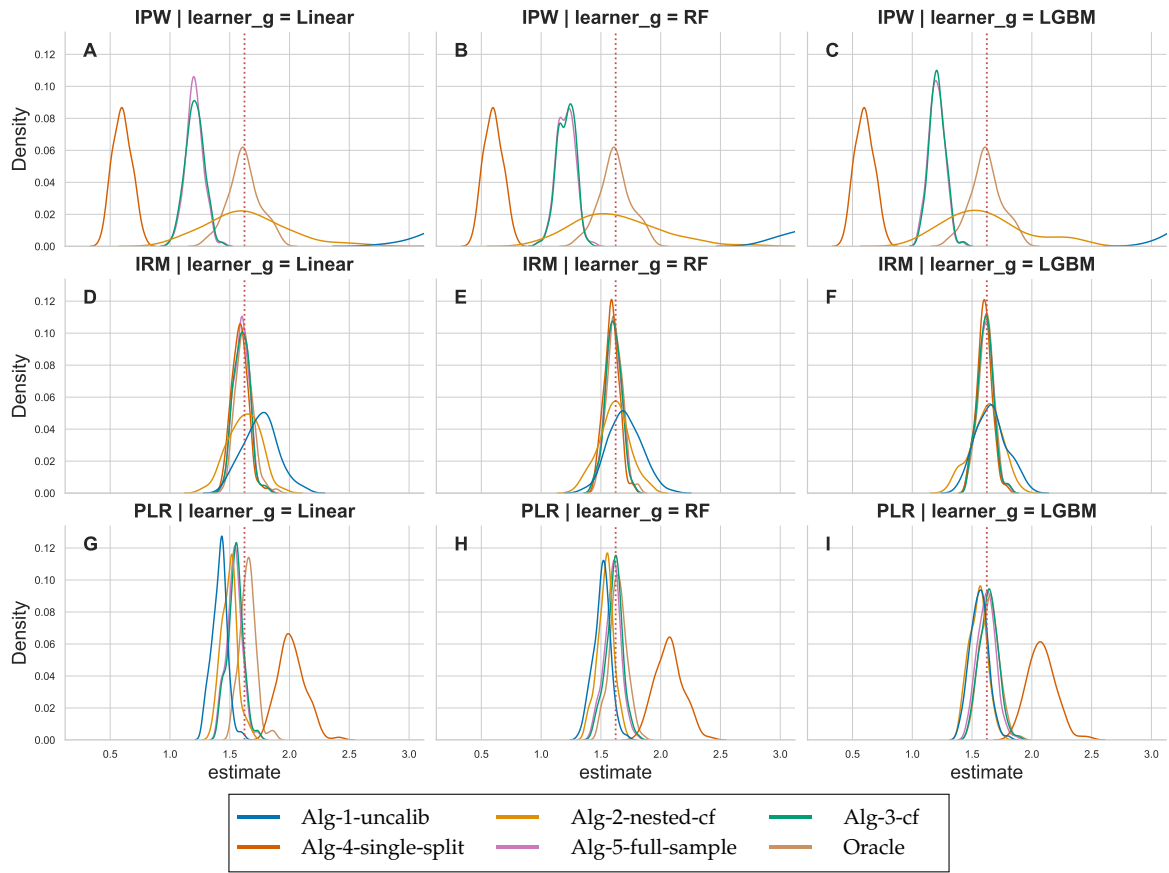


Figure 50: DGP 3 Nonlinear, $m = \text{LGBM}$, $g = \text{LGBM}$, $n = 2000$, $p = 4$, Calibration method for Algorithms 2-5: isotonic regression, $\text{Clip} = 0.01$

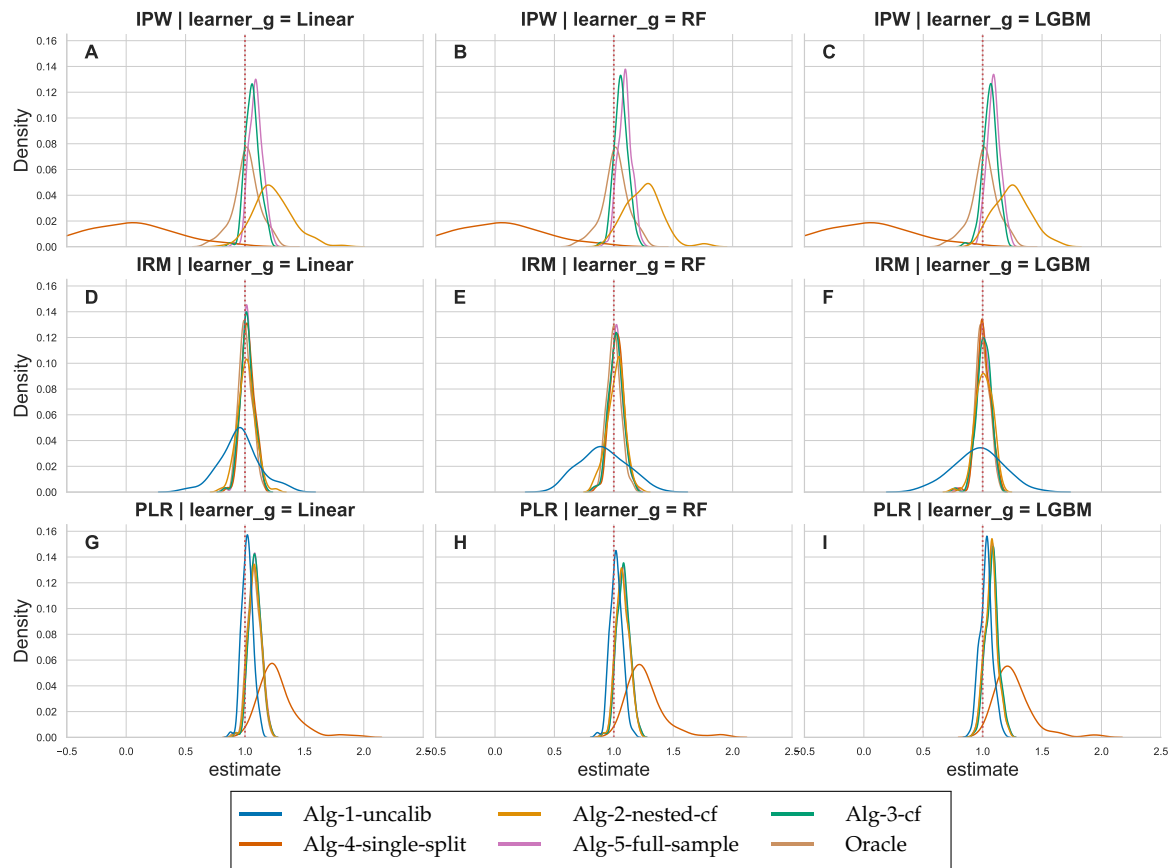


Figure 51: DGP 4 Unbalanced, Share_treated = 0.1, m = LGBM, g = LGBM, n = 4000, p = 20, Calibration method for Algorithms 2-5: isotonic regression, Clip = 0.01

Number of Covariates on ATE Distribution

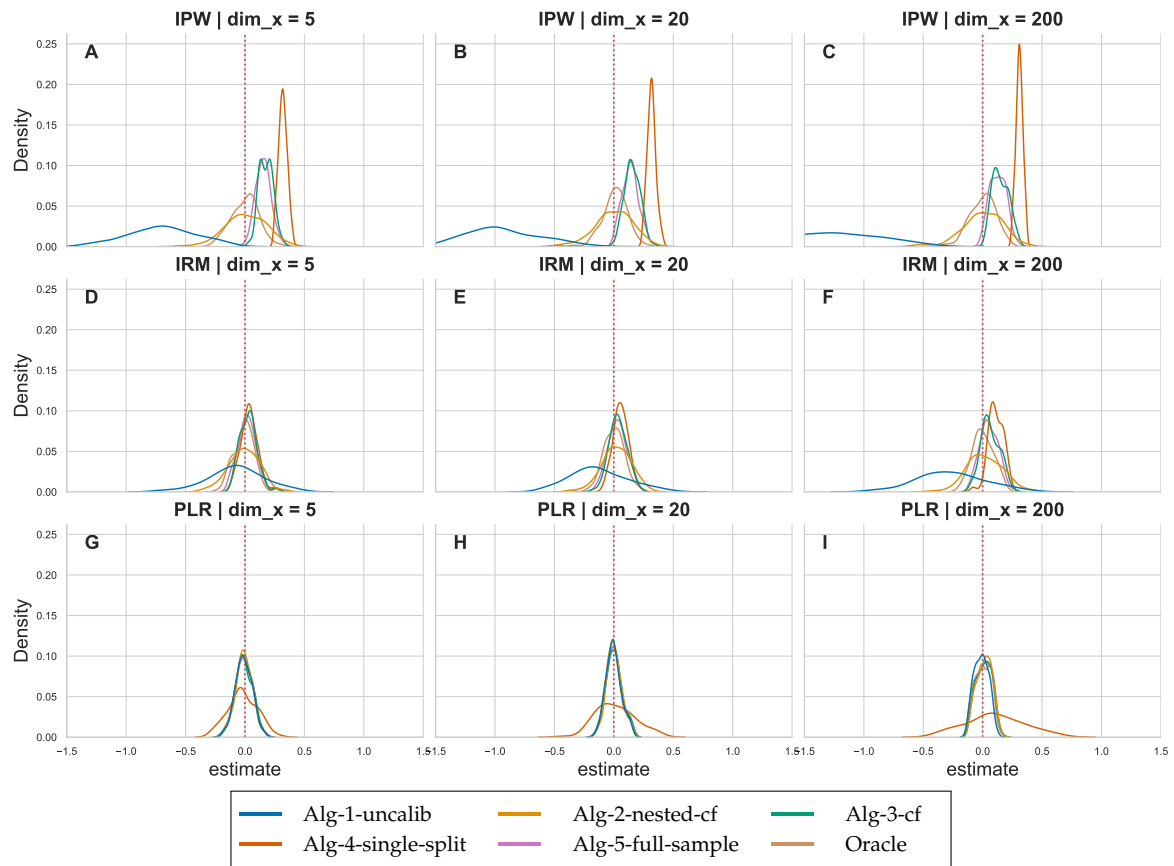


Figure 52: DGP 1 IRM, $R^2D = 0.5$, $m = \text{LGBM}$, $g = \text{LGBM}$, $n = 2000$, Calibration method for Algorithms 2-5: isotonic regression, $\text{Clip} = 0.01$

Clipping Threshold on ATE Distribution

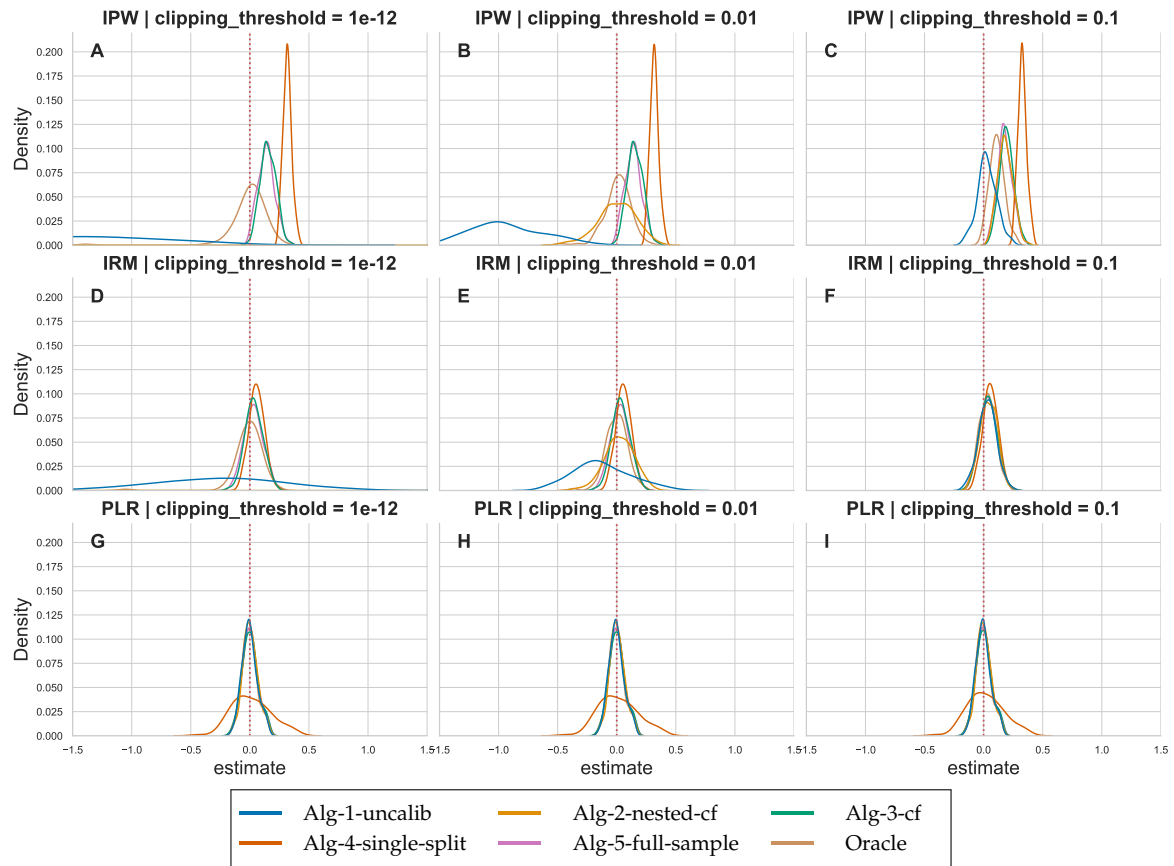


Figure 53: DGP 1 IRM, R2D = 0.5, m = LGBM, g = LGBM, n = 2000, p = 20, Calibration method for Algorithms 2-5: isotonic regression

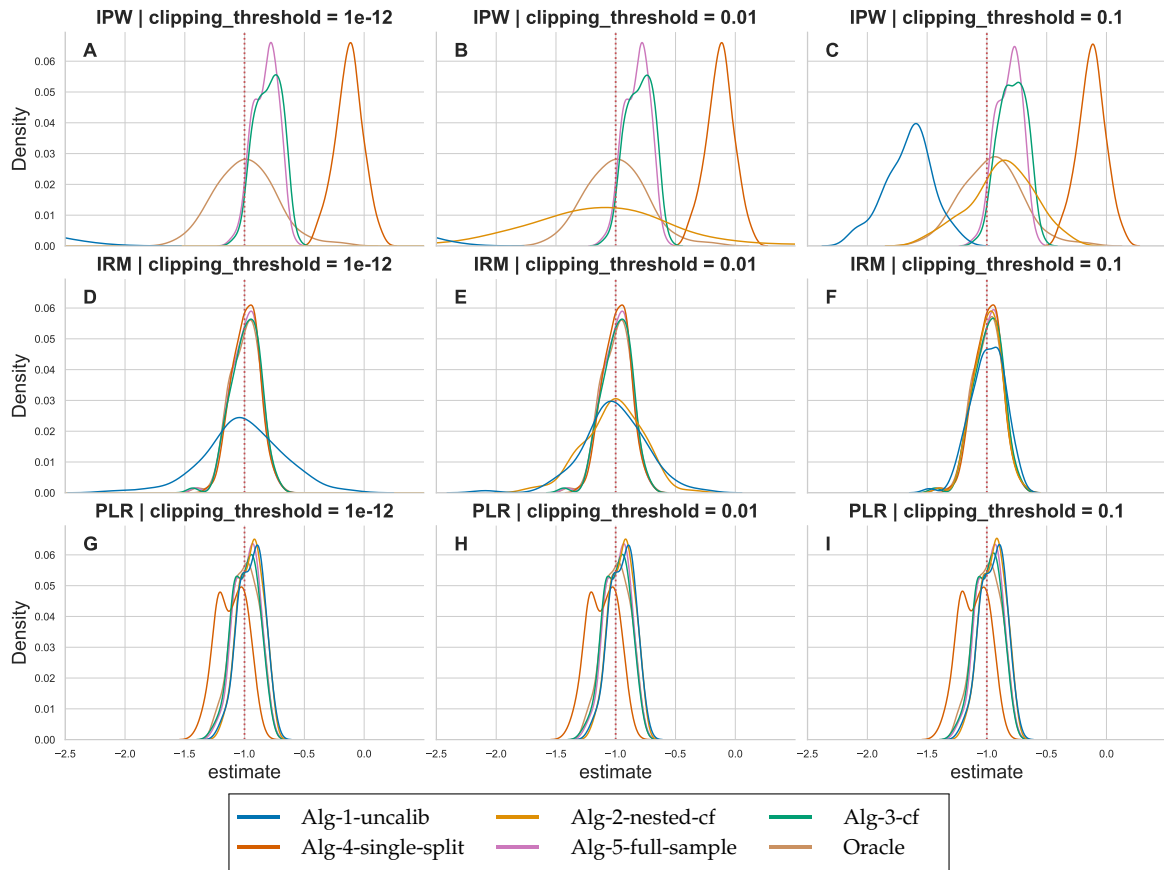


Figure 54: DGP 2 Drug, Overlap = 0.5, $m = \text{LGBM}$, $g = \text{LGBM}$, $n = 2000$, $p = 3$, Calibration method for Algorithms 2-5: isotonic regression

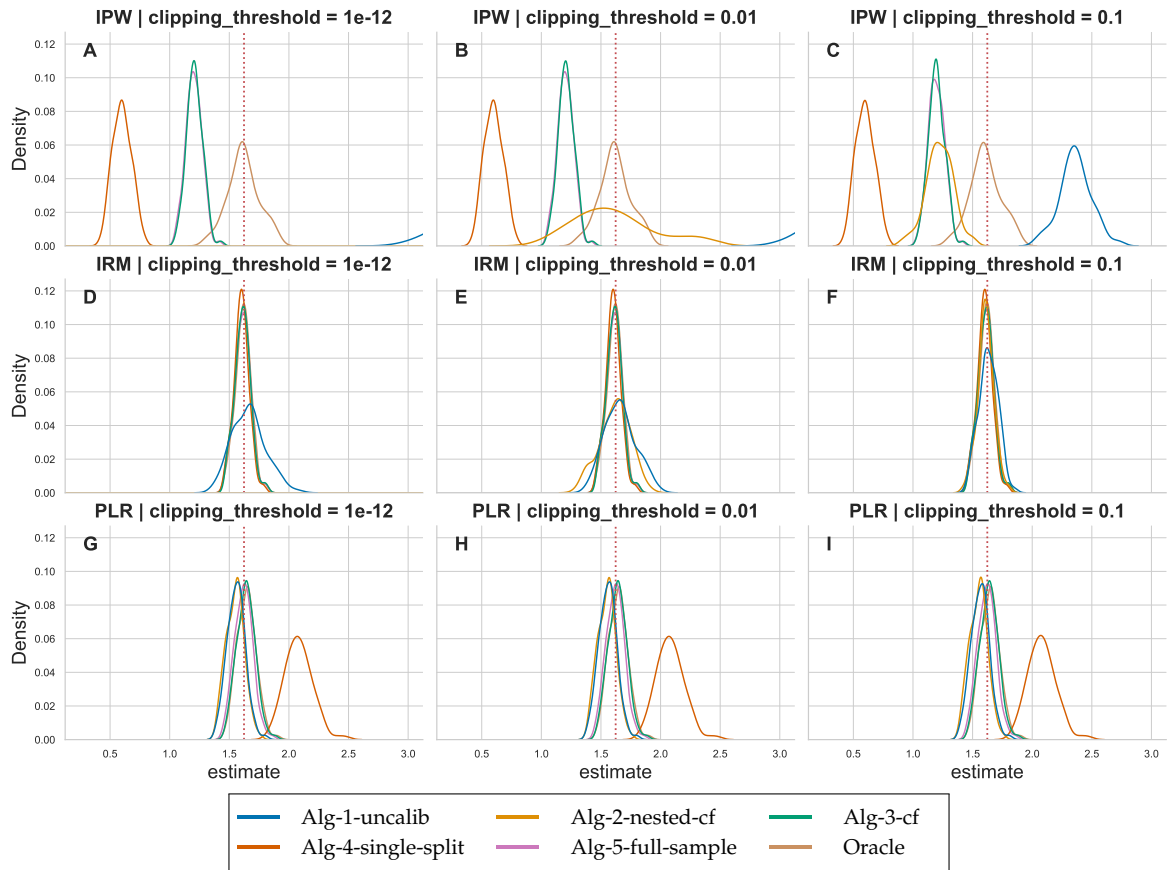


Figure 55: DGP 3 Nonlinear, $m = \text{LGBM}$, $g = \text{LGBM}$, $n = 2000$, $p = 4$, Calibration method for Algorithms 2-5: isotonic regression, $\text{Clip} = 0.01$

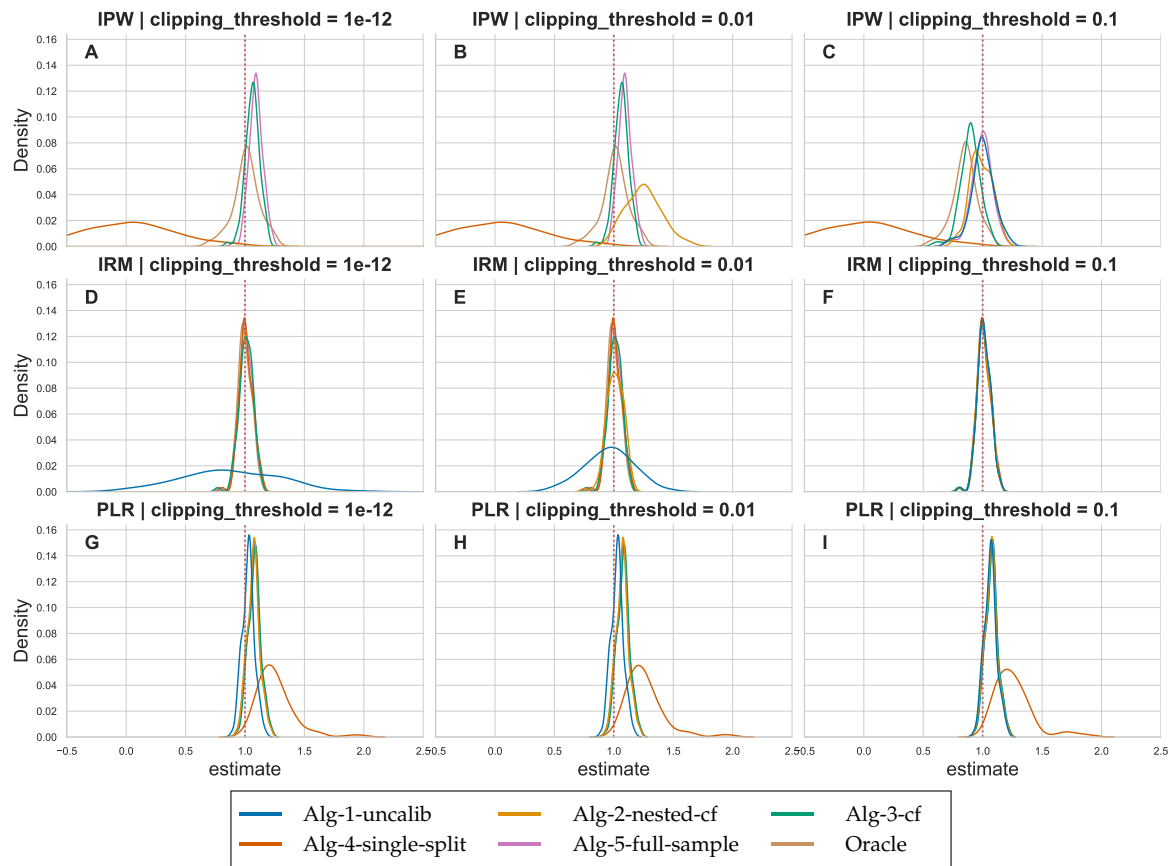


Figure 56: DGP 4 Unbalanced, Share_treated = 0.1, m = LGBM, g = LGBM, n = 4000, p = 20, Calibration method for Algorithms 2-5: isotonic regression

DGP Setting on ATE Distribution

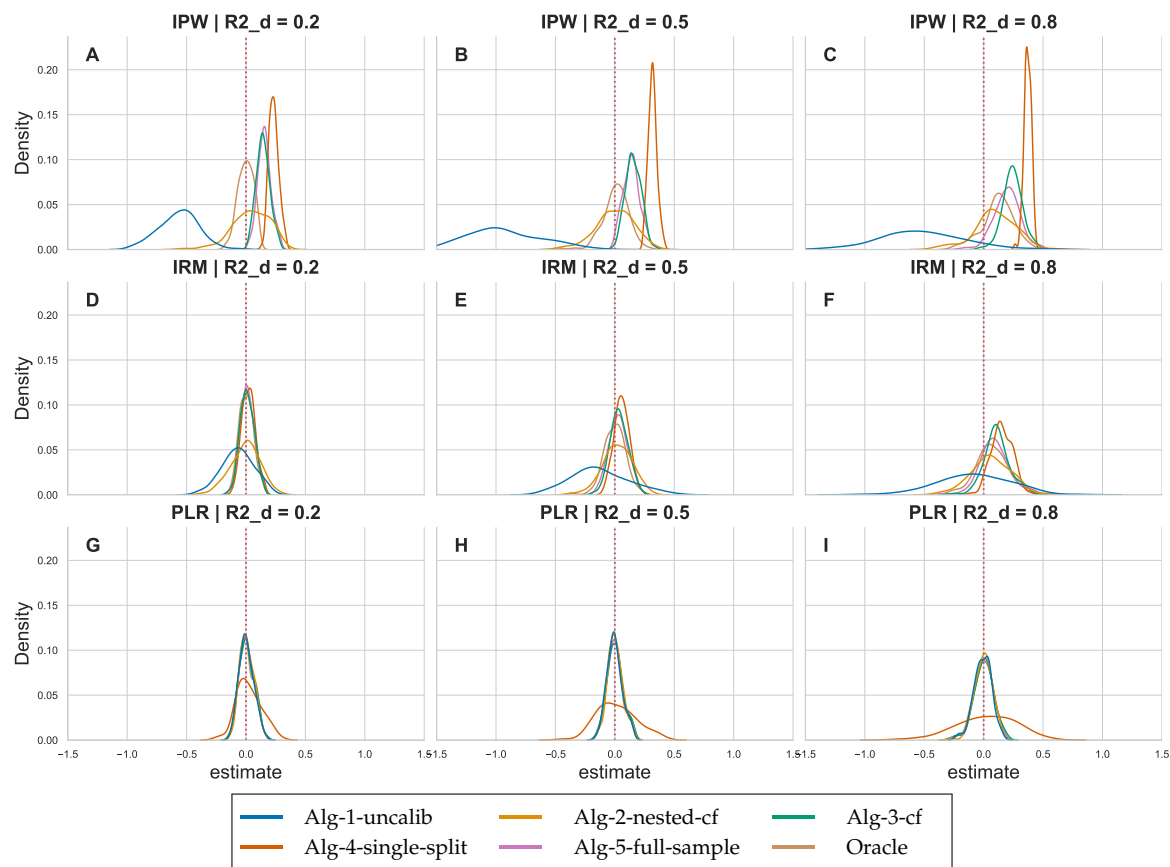


Figure 57: DGP 1 IRM, R2D on ATE, $m = \text{LGBM}$, $g = \text{LGBM}$, $n = 2000$, $p = 20$, Calibration method for Algorithms 2-5: isotonic regression, $\text{Clip} = 0.01$

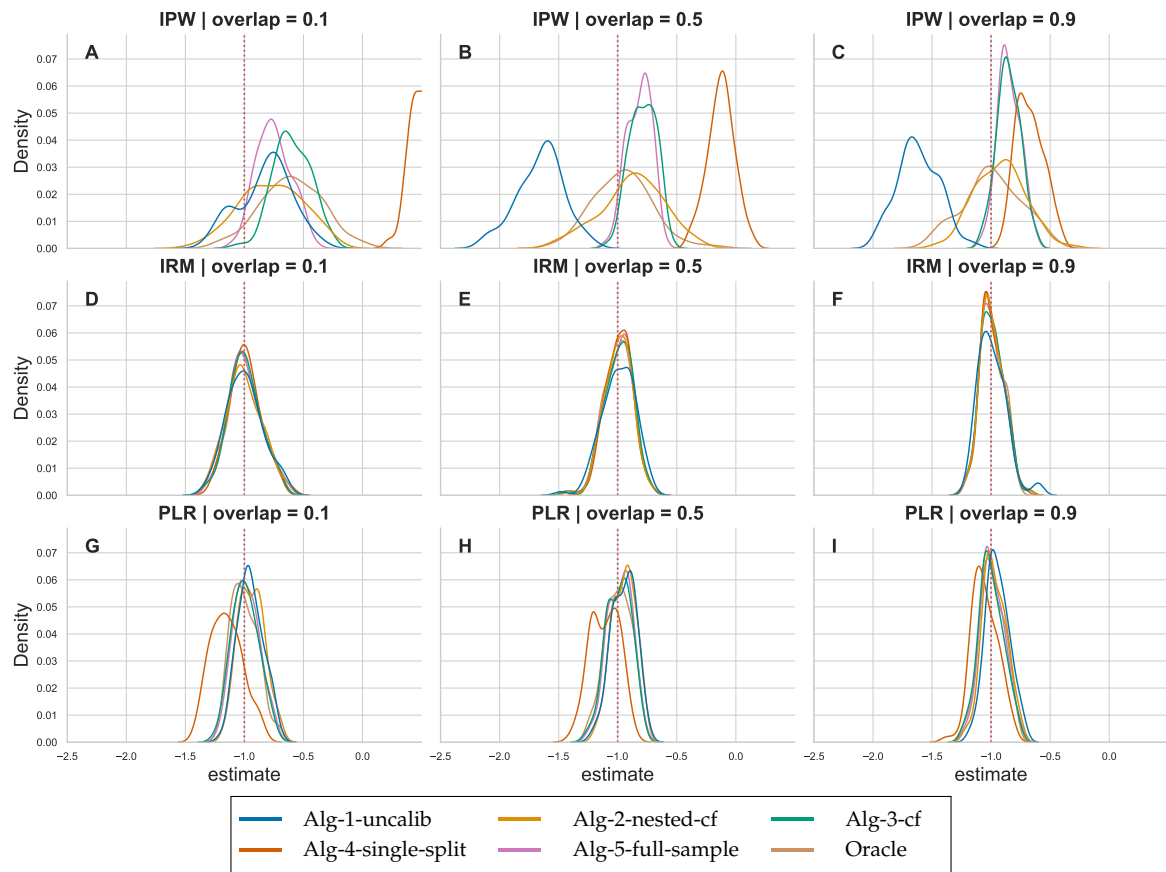


Figure 58: DGP 2 Drug, Overlap on ATE, $m = \text{LGBM}$, $g = \text{LGBM}$, $n = 2000$, $p = 3$, Calibration method for Algorithms 2-5: isotonic regression, $\text{Clip} = 0.01$

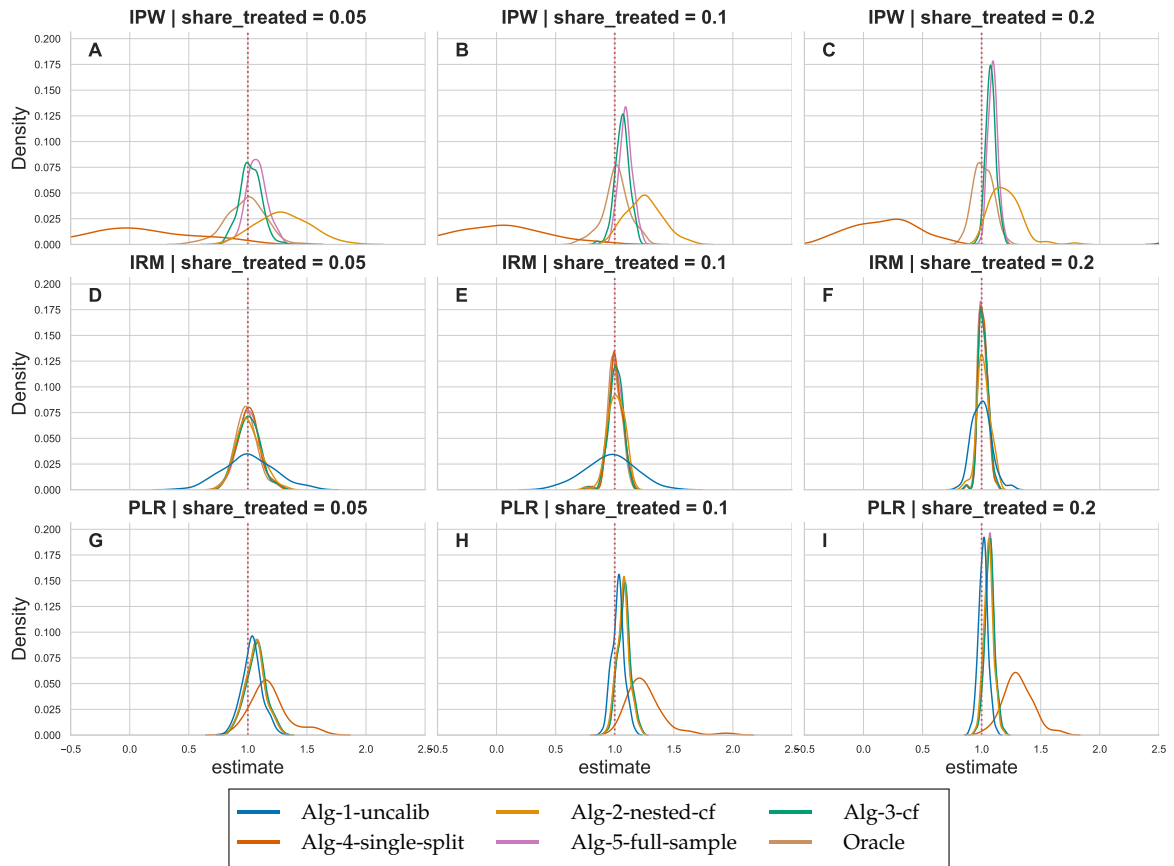


Figure 59: DGP 4 Unbalanced, Share.treated on ATE, $m = \text{LGBM}$, $g = \text{LGBM}$, $n = 4000$, $p = 20$, Calibration method for Algorithms 2-5: isotonic regression, $\text{Clip} = 0.01$